CONSTRUCTION OF RETINA SUBSTITUTE BY USING TISSUE ENGINEERING APPROACH

A THESIS SUBMITTED TO
THE GRADUATE SCHOOL OF NATURAL AND APPLIED SCIENCES
OF
MIDDLE EAST TECHNICAL UNIVERSITY

BY

AYLİN KÖMEZ

IN PARTIAL FULFILLMENT OF THE REQUIREMENTS
FOR
THE DEGREE OF MASTER OF SCIENCE
IN
BIOTECHNOLOGY

FEBRUARY 2015

Approval of the thesis:

CONSTRUCTION OF RETINA SUBSTITUTE BY USING TISSUE ENGINEERING APPROACH

submitted by **AYLİN KÖMEZ** in partial fulfillment of the requirements for the degree of **Master of Science in Biotechnology Department, Middle East Technical University** by,

Prof. Dr. Gülbin Dural Ünver _____
Director, Graduate School of **Natural and Applied Sciences**

Prof. Dr. Filiz Bengü Dilek _____
Head of Department, **Biotechnology**

Prof. Dr. Vasıf Hasırcı _____
Supervisor, **Biology Dept., METU**

Assoc. Prof. Dr. Erkan Türker Baran _____
Co-supervisor, **BIOMATEN, METU**

Examining Committee Members:

Prof. Dr. Meral Yücel _____
Biology Dept., METU

Prof. Dr. Vasıf Hasırcı _____
Biology Dept., METU

Prof. Dr. Kamil Can Akçalı _____
Biophysics Dept., Ankara University

Doç. Dr. Aysen Tezcaner _____
Engineering Sciences Dept., METU

Yrd. Doç. Dr. Salih Özçubukçu _____
Chemistry Dept., METU

Date: 03.02.15

I hereby declare that all information in this document has been obtained and presented in accordance with academic rules and ethical conduct. I also declare that, as required by these rules and conduct, I have fully cited and referenced all material and results that are not original to this work.

Name, Last Name: Aylin Kömez

Signature:

ABSTRACT

CONSTRUCTION OF RETINA SUBSTITUTE BY USING TISSUE ENGINEERING APPROACH

Kömez, Aylin

M.S., Department of Biotechnology

Supervisor: Prof. Dr. Vasıf Hasırcı

Co-Supervisor: Assoc. Prof. Dr. Erkan Türker Baran

February 2015, 103 pages

Millions of people are affected by retinal diseases such as age-related macular degeneration (AMD) and retinitis pigmentosa (RP, night blindness). Retinal tissue engineering has potential to become a valid therapeutic approach to regenerate retina. The aim of this study was to construct a biomimetic retinal tissue substitute by using biocompatible and natural polymers and in vitro techniques. For this purpose, a retinal pigment epithelial (RPE) cell monolayer was formed on an electrospun silk fibroin mesh to mimic Bruch's membrane. Results showed that RPE could proliferate and form a cell layer on the fibroin mesh. A HUVEC layer was constructed separately by microfabrication of a fractal tree design using photocrosslinkable methacrylated hyaluronic acid (HAMA) hydrogel to mimic the vasculature of choroid. To improve HUVEC adhesion in the design methacrylated collagen and methacrylated gelatin were immobilized in them using photolithography. It was seen that HUVEC could adhere only on the microchannels of the pattern and, form tubular structures at late culture periods. The co-culture studies in non-contact mode due to separation of the two cell types by the fibrous mat demonstrated that RPE cells on Bruch's membrane could change the cell morphology, proliferation and thickness of vascular pattern that was formed by HUVECs in microchannels.

Keywords: Retinal degeneration, hydrogel, photolithography, silk fibroin, hyaluronic acid.

ÖZ

DOKU MÜHENDİSLİĞİ YAKLAŞIMINI KULLANARAK YAPAY RETİNA YAPIMI

Kömez, Aylin
Yüksek Lisans, Biyoteknoloji Bölümü
Tez Yöneticisi: Prof. Dr. Vasıf Hasırcı
Ortak Tez Yöneticisi: Doç Dr. Erkan Türker Baran
Şubat 2015, 103 sayfa

Milyonlarca insan yaşa bağlı makula dejenerasyonu ve gece körlüğü gibi retina hastalıklarından zarar görmektedir. Bu şartlar altında, retina doku mühendisliği, retina yenilenmesi için geçerli olabilecek bir tedavi yoludur. Bu çalışmanın amacı, biyouyumlu doğal polimerler ve in vitro teknikleri kullanarak biyomimetik bir retina dokusu oluşturmaktır. Bu amaçla retina pigment epitel (RPE) hücre katmanı Bruk membranını taklit eden ve elektroeğirme ile oluşturulmuş ipek fibroin mat'ı üzerinde oluşturulmuştur. Sonuçlar RPE hücrelerinin fibroin mat üzerinde etkin şekilde çoğalarak bir katman oluşturabildiğini göstermiştir. Ayrıca, koroid damar tabakasını taklit etmesi için vasküler HUVEC katmanı foto çapraz bağlanabilir metakril hyaluronik asit (HAMA) jelinde bir fraktal ağaç şeklinde oluşturulmuştur. HUVEC'lerin mikrokanallara yapışmasını arttırmak için kanallar metakril kollajen ve jelatin ile işlenmiştir. HUVEC sadece yapışma faktörü ile kaplı fraktal ağaç mikrokanallarına yapışabilmiş ve böylelikle geç kültür periyotlarında tüp oluşumu göstermiştir. Kontaksız şekilde yapılan kokültür çalışması Bruk membranı üzerinde bulunan RPE hücrelerinin HUVEC hücre morfolojisini, çoğalmasını ve oluşan vasküler şeklin kalınlığını değiştirebildiğini göstermiştir.

Anahtar kelimeler: Retina dejenerasyonu, hidrojel, fotolitografi, ipek fibroini, hyaluronik asit.

Dedicated to my lovely family

ACKNOWLEDGEMENTS

I would like to express my special endless thanks and gratitude to my thesis supervisor, Prof. Dr. Vasıf Hasırcı for his continuous guidance, advice, support, encouragement and insight throughout my thesis. I feel very lucky to have had the opportunity to do my thesis research jointly in his laboratory and under his guidance.

I am also grateful to my co-supervisor, Assoc. Prof. Dr. Erkan Türker Baran for his studies, guidance and special suggestions during this study.

I wish to extend my thanks to Prof. Dr. Güngör Sobacı and Yrd. Doç. Dr. Üzeyir Erdem from GATA-OGEK Project.

I am very grateful to MD. Menekşe Ermiş for her helps in confocal microscopy and tissue culture studies and for her support.

I would like to thank to Dr. Arda Büyüksungur for his patience, support, helps and good advices throughout the research. I also thank to Gökhan Bahçecioğlu, Damla Arslantunalı and Esen Sayın for their encouragement, comments, valuable suggestions and helps in various parts of this study.

I would also like to thank my friends Deniz Sezlev Bilecen, Senem Heper, Gözde Eke, Büşra Günay and Onur Hastürk for their encouragement, support and all the great moments we shared.

I want to thank all of my friends that I met during my master study in BIOMATEN especially, Tuğba Dursun, Ezgi Antmen, Ayşe Selcen Alagöz, Sepren Öncü, Cemile Kılıç, Ayla Şahin and our technician Zeynel Akın.

I am also deeply grateful to my lovely friends Beliz Bediz, Gizem Güpür, Neşe Erdem and Sırma Damla User for their invaluable friendship, continuous support, encouragement and their presence in my life.

I would like to express my special thanks to Uluç Bilecen for his love, endless support, encouragement, patience and special advices.

Finally, I would like to express my deepest gratitude to my lovely family Anakadın Kömez, Seyfi Kömez, Güler Kömez, Aslıhan Kömez, Mesut Kömez and Ayşe Öztaş for their understanding, love, caring, support, patience and trust in me not only for this study, but for all my life.

TABLE OF CONTENTS

LIST OF TABLES

TABLES

LIST OF FIGURES

FIGURES

LIST OF ABBREVIATIONS

µm	micrometer
2D	Two Dimensional
3D	Three Dimensional
AAV2	Adeno-Associated Virus
ACh	Acetylcholine
AF	Area Fraction
AMD	Age Related Macular Degeneration
AR	Aspect Ratio
BM	Bruch's Membrane
BMSCs	Bone Marrow Mesenchymal Stem Cells
BMSF	*Bombyx mori* Silk Fibroin
BRVO	Branch Retinal Vein Occlusion
BSA	Bovine Serum Albumin
CNTF	Ciliary Neurotrophic Factor
CNV	Choroidal Neovascularization
CO_2	Carbon Dioxide
Col	Collagen
ColMA	Methacrylated Collagen
CRVO	Central Retinal Vein Occlusion
d	days
Da	Dalton
DAPI	4', 6-diamidino-2-phenylindole
DMEM	Dulbecco's Modified Eagle Medium
DMF	Dimethylformamide
DMSO	Dimethyl Sulfoxide
DPSCs	Dental Pulp Stem Cells
DR	Diabetic Retinopathy

DS	Degree of Swelling
ECM	Extracellular Matrix
EDTA	Ethylenediaminetetraacetic Acid
EGM-2	Endothelial Growth Medium
EL	Elastin Layer
ELM	External Limiting Membrane
ESCs	Embryonic Stem Cells
ESF	Electrospun Silk Fibroin Fiber Mat
FBS	Fetal Bovine Serum
FGF-2	Fibroblast Growth Factor
FITC	Fluorescein Isothiocyanate
FN	Fibronectin
g	gram
GA-1000	Gentamicin, Amphotericin-B
GABA	Gamma-Amino Butyric Acid
GCL	Ganglion Cell Layer
GDNF	Glial Cell Line-Derived Neurotrophic Factor
GEL	Gelatin
GelMA	Methacrylated Gelatin
Gly	Glycine
h	hour
HAc	Acetic Acid
hAM	Human Amniotic Membrane
HAMA	Methacrylated Hyaluronic Acid
hEGF	Human Endothelial Growth Factor
hESC	Human Embryonic Stem Cells
hFGF	Human Fibroblast Growth Factor
HFIP	Hexafluoro Isopropyl
HMEC-1	Microvascular Endothelial Cells
HUVEC	Human Umbilical Vein Endothelial Cells
HyA	Hyaluronic Acid
ICL	Inner Collagenous Layer

IGF-1	Insulin-Like Growth Factor
ILM	Inner Limiting Membrane
INL	Inner Nuclear Layer
IPL	Inner Plexiform Layer
iPSCs	Induced Pluripotent Cells
kDa	Kilo Dalton
kV	Kilovolt
M	Molarity
MeOH	Methanol
mg	milligram
min	minute
mL	milliliter
mm	millimeter
mM	millimolar
mRPCs	Mouse Retinal Progenitor Cells
Na_2CO_3	Sodium Carbonate
Na_2HPO_4	Sodium Phosphate Dibasic
NaCl	Sodium Chloride
NaH_2PO_4	Sodium Phosphate Monobasic
NaOH	Sodium Hydroxide
NFL	Nerve Fiber Layer
nm	nanometer
OCL	Outer Collagenous Layer
ONL	Outer Nuclear Layer
OPL	Outer Plexiform Layer
OsO_4	Osmium Tetroxide
PBS	Phosphate Buffer Saline
PCL	Poly(caprolactone)
PDMS	Poly(dimethylsiloxane)
PDT	Photodynamic Therapy
PEDF	Pigment Epithelium-Derived Factor
PEG	Polyethylene Glycol

Pen/Strep	Penicillin/Streptomycin
PEO	Poly(ethylene oxide)
PET	Poly(ethylene terephthalate)
PGA	Poly(glycolic acid)
PGS	Poly(glycerol-sebacate)
PHAs	Polyhydroxyalkanoates
PI	Polyimide
PIPES	Piperazine-N, N'-Bis(Ethanesulfonic Acid)
PLA	Poly(lactic acid)
PLCL	Poly(l-lactide-co-Ɛ-caprolactone)
PLGA	Poly(lactic acid-co-glycolic acid)
PLLA	Poly(l-lactic acid)
POS	Photoreceptor Outer Segments
RGD	Arginine, Glycine, Aspartic Acid Sequence
RHAMM	Hyaluronan-Mediated Motility Receptor
RP	Retinal Pigmentosa
RPCs	Retinal Progenitor Cells
RPE	Retinal Pigment Epithelium
RVO	Retinal Vein Occlusion
SEM	Scanning Electron Microscopy
SF	Silk Fibroin
SRD	Severe Retinal Detachment
TCPS	Tissue Culture Polystyrene
UV	Ultraviolet
v/v	volume/volume
VEGF	Vascular Endothelial Growth Factor
w	weight
w/v	weight/volume
wd	Dry Weight of HAMA Hydrogel
ws	Swollen Weight of HAMA Hydrogel
ZO-1	Zonula Occludens Protein

CHAPTER 1

INTRODUCTION

1.1. Structure and Function of the Retina

1.1.1. The Structure of Retina

The retina is a neural layer that coats the innermost of the eye. It is located between the choroid and vitreous (Fig. 1). It covers an important portion of the posterior pole and provides color vision and sharpest acuity, called as macula. The retina appears as a thin, transparent membrane although it is composed of millions of cell bodies and extensions (Remington, 2012).

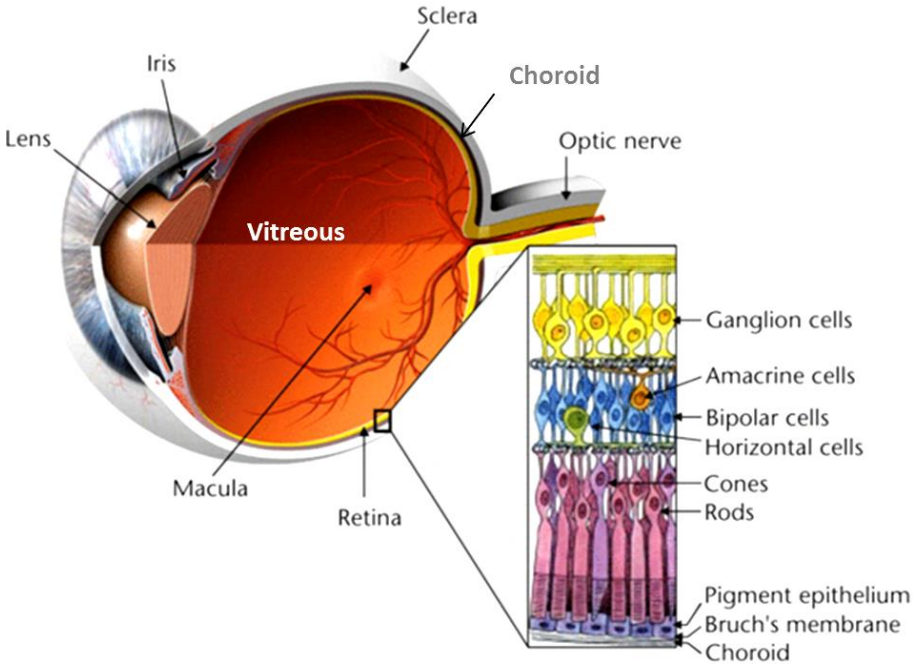

Figure 1. Schematic presentation of the anatomy of the human eye and detail of the retina (Bretillon et al., 2011).

Retinal pigment epithelium (RPE) and choroid are the support systems of the photoreceptors; the rods and cones. The retina has five important types of cells (photoreceptors, horizontal cells, bipolar cells, amacrine cells, and ganglion cells) in the visual pathway to transmit visual information from the environment to the brain (Fig. 1). Glial cells and Müller cells together with astrocytes and microglial cells are also distributed throughout the retina. These cells in the retina form ten different layers by spatial organization (Pikuleva & Curcio, 2014). The schematic presentation of these layers was shown in Fig. 2 and the existing cells and synaptic structures found in these distinct layers were given in Table 1.

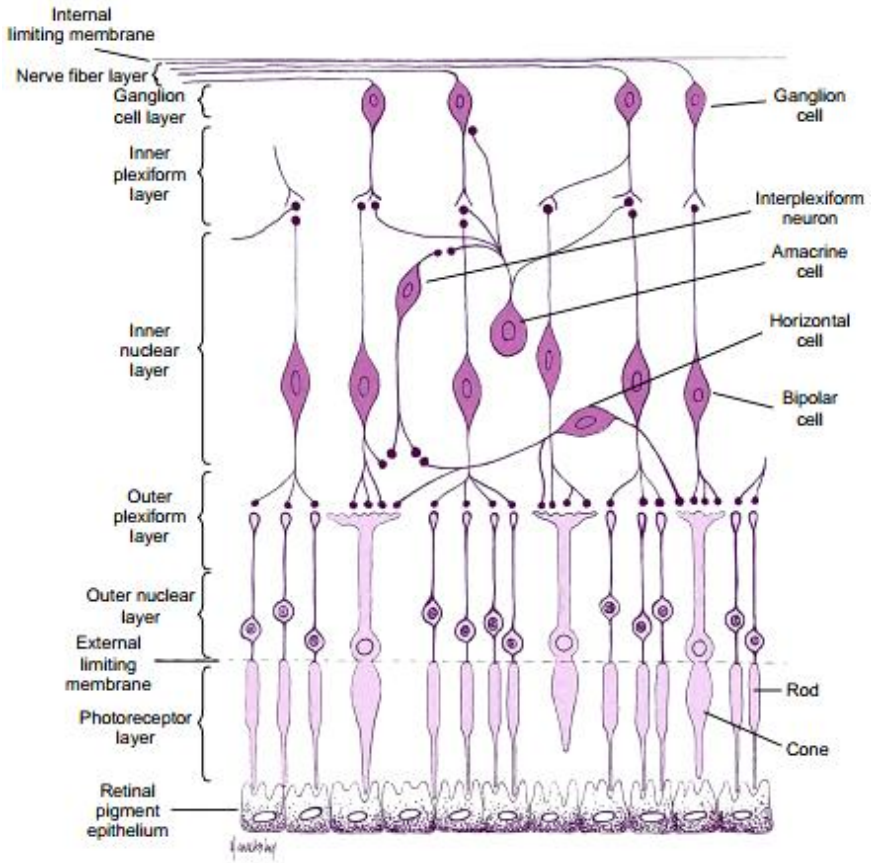

Figure 2. Schematic presentation of the 10 layers of retina. From top to bottom, Inner limiting membrane (ILM), nerve fiber layer (NFL), ganglion cell layer (GCL), inner plexiform layer (IPL), inner nuclear layer (INL), outer plexiform layer (OPL), outer nuclear layer (ONL), external limiting membrane (ELM), photoreceptor cell layer, and retinal pigment epithelium (RPE) (Remington, 2012).

Table 1. The layers of the retina and their contents.

LAYERS OF THE RETINA	CONTENTS
Inner limiting membrane	Basement membrane for Müller cells
Nerve fiber layer	Axons of ganglion cells
Ganglion cell layer	Nuclei of ganglion cells
Inner plexiform layer	Synapse between the bipolar cell axons and the dendrites of the ganglion and amacrine cells
Inner nuclear layer	Nuclei and surrounding cell bodies of the amacrine cells, bipolar cells and horizontal cells
Outer plexiform layer	Synaptic connection of photoreceptor, horizontal and bipolar cell
Outer nuclear layer	Cell bodies of rods and cones
External limiting membrane	Inner segments of the rods and cones
Photoreceptor layer	Rods and cones
Retinal pigment epithelium	Monolayer of pigmented cells

There is a center-to-peripheral gradient of the retina in terms of distribution and density of neural cells. This organization of neurons influences the modes of vision. While the central part plays role in bright light vision, peripheral part is involved in low-light vision. Fovea is the rod-free region of the retina (Nag & Wadhwa, 2012; Remington, 2012)

1.1.1.1. Bruch's Membrane and Choroid

Bruch's membrane (BM) is a thin (2-4 μm), unique pentalaminar structured extracellular matrix that placed between the RPE and choriocapillaries of the eye and it provides substratum for RPE and choriocapillaries wall (Fig. 3A). According to Hogan's classification in the early 1960s (Hogan, 1961), BM contains five layers from RPE to choroid: the basement membrane of the RPE, the inner collagenous

layer (ICL), the elastin layer (EL), the outer collagenous layer (OCL) and, the basement membrane of the choriocapillaris (Fig. 3B).

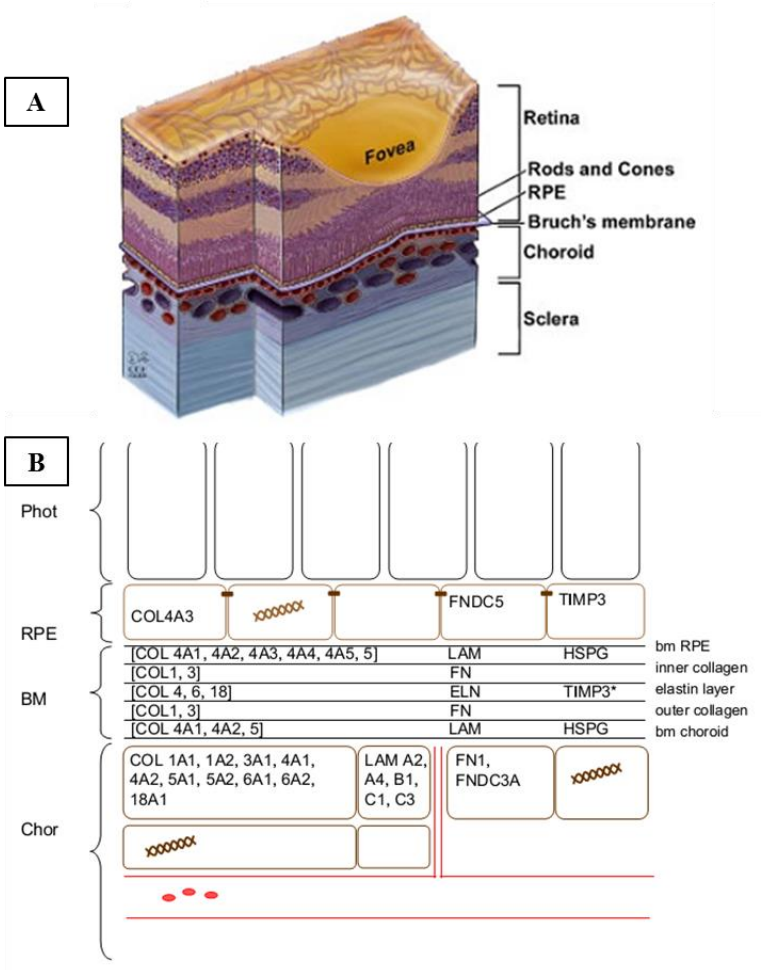

Figure 3. Schematic presentation of Bruch's membrane and its composition. (A) The cross section of the eye at the macular region that shows the Bruch's membrane position in the retinal tissue. (B) Proteins present in Bruch's membrane. Phot: Photoreceptors, RPE: Retinal Pigment Epithelium, BM: Bruch's Membrane, Chor: Choroid (Booij et al., 2010; Yuan et al., 2010).

The basement membrane of the RPE is approximately 0.14-0.15 µm in thickness and carries the features of typical basement membrane in the body. It mainly contains collagens type IV, laminin, fibronectin, heparan sulfate and chondroitin/dermatan sulfate. The inner collagenous layer (ICL) is 1.4 µm in diameter and it is composed of collagen type I, III, and V fibers that are formed collagen grid. This collagen grid

is embedded in the glycosaminoglycans such as chondroitin sulfate, dermatan sulfate and hyaluronic acid. The elastin layer (EL) of BM is approximately 0.8 μm thick and it includes the parallel elastin fibers. Besides elastin fibers, EL consists of collagen type VI, fibronectin and protein-associated substances. The roles of EL in the BM are to offer biomechanical features, vascular conformity and antiangiogenic barrier effects (Chong et al., 2005). The outer collagenous layer (OCL) is approximately 0.7 μm that is thinner than ICL, but the composition and structure of the outer collagenous layer (OCL) is same with ICL. The average thickness of the basement membrane of choriocapillaries is 0.07 μm. It is noncontinuous layer of BM because of the existence of the intercapillary pillars of the choroid. Its main composition is laminin, heparan sulfate and collagen type IV and V (Booij et al., 2010; Gregg et al., 2013).

There are three main functions of BM that are coordinating the diffusion of molecules between choroid and RPE cells, supporting RPE cell adhesion, migration and differentiation, and preventing both retinal and choroidal cell migration by providing a physical barrier. Since BM is acellular membrane, diffusion of biomolecules between RPE and choroid is performed with passive transport. Diffusion property of BM is affected by molecular composition that changes with age and location of the BM. While nutrients, lipids, pigment precursors, vitamins (vitamin A), oxygen, minerals, anti-oxidant components and race elements pass through the BM from the choroid to the RPE, CO_2, water, ions, oxidized lipids, oxidized cholesterol, and other waste products are transmitted from the RPE to the choroid through the BM. In addition to diffusion properties, BM provides a supportive material for RPE cell adhesion. The outer blood-retinal barrier is provided by RPE cells that are interacted to each other by means of tight junctions. BM supports the barrier function of RPE cells by acting role as a semipermeable membrane. The inner blood-retinal barrier is supported by the retinal vascular endothelial cells that are connected to each other by means of tight junctions like RPE cells (Booij et al., 2010).

The choroid is placed between the sclera and the retina (Fig. 1), and it provides nutrients to outer retinal layers. In human, the average thickness of choroid is approximately 200 μm. There are five layers that form the choroid. When starting from the retina, these layers are Bruch's membrane, the choroiocapillaris, the two vascular layers (Haller's and Sattler's), and the suprachoroidea (Fig. 4).

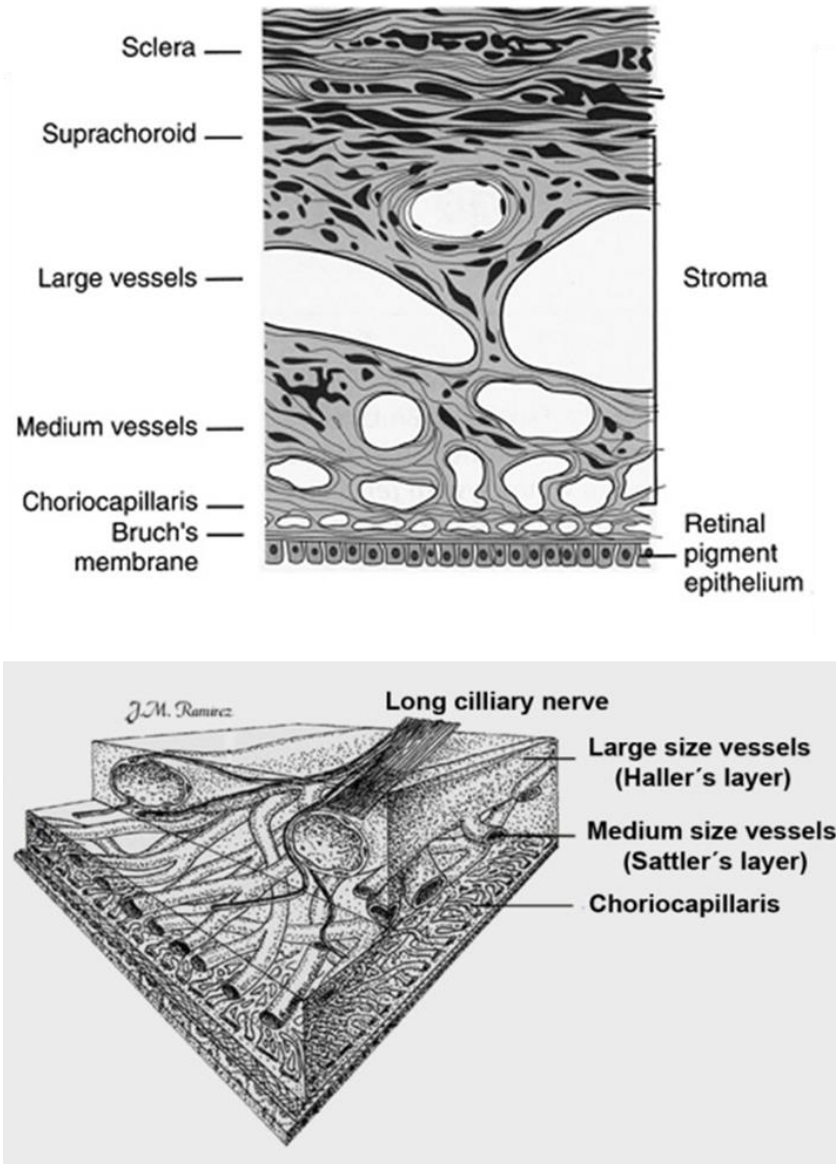

Figure 4. Schematic of the layers of the choroid (Ramírez, 2012).

The choroid performs several physiological functions. The choroidal vasculature is main supply of the outer retina. The blood flow from the choroid helps to cool and warm the retina. Moreover, the retina is moved forward and back by changing choroidal thickness to position the photoreceptor cells into the focus plane. The choriocapillaris is a network of capillaries that forms a sheet adjacent to the BM. The choroid vascular part contains the outer Haller's layer of large blood vessels and the inner Sattler's layer of medium and small arteries that supply the veins and capillaries (Nickla & Wallman, 2010).

1.1.2. The Function of Retina

The incoming light passes through the layers of the retina before stimulating the outer segments of the photoreceptors. Then, photoreceptors generate a neural signal and this signal is processed by complex synaptic pathway of retina through which it passes. After processing, the neural retina transmits the visual signal to the brain (Remington, 2012).

In the retina, like central nervous system, signal transmission is through chemical compound (chemical neurotransmission) and it is the major type of communication between neurons. Presynaptic neurons release the neurotransmitters such as the amino acids glutamate, gamma-amino butyric acid (GABA), acetylcholine (ACh), dopamine, and serotonin to the synaptic cleft to bind postsynaptic neurons. Depolarization or hyperpolarization of postsynaptic cells is achieved with opening or closing the ion channels of the receptors. In addition, many neurons are also bound via electrical synapses that are called the gap junctions (Gregg et al., 2013).

The rods and cones convert light energy into electrical signals in the process of phototransduction. The interneurons found in the retina convert the electrical signals to optic nerve impulses to be processed by brain as visual image. This visual pathway provides the recognition of shapes, colors, sizes and movements. Shortly, after photoreceptors absorb the incident light, phototransduction is initiated in their outer

segments that results in transmission of the electrical signals to the horizontal and bipolar cells. The dendrites of rod and cone bipolar cells establish synaptic contacts with the axonal terminal of the rods and cones at the outer plexiform layer. Then, amacrine and bipolar cells make synaptic connections with ganglion cell at the inner plexiform layer. Finally, the electrical signals is transmitted to the ganglion cells that send the electrical impulses thorough their long axonal extensions to the brain via optic nerves (Cuenca et al., 2014).

1.2. Retinal Diseases

The retinal tissue is vulnerable to changes caused by various pathological injuries due to its complex structure and resultant symptoms and these pathologies of the retina results in blindness and visual defects. The retinal diseases are generally divided into those involving photoreceptor death in the outer region of the retina and those influencing the neuronal cells in the inner retina (Hoon et al., 2014).

1.2.1. Age Related Macular Degeneration (AMD)

Age related macular degeneration (AMD) is the leading cause of blindness in older patients over the age 60. It is influenced by factors such as genetics, environmental factors and demographics. There are several risk factors included in the pathogenesis of AMD. These are cardiovascular disease, old age, high body mass index and high exposure to light (Bonnel et al., 2003).

AMD can be an early or a late form. An early form of AMD is generally asymptomatic, whereas late form of AMD can results in central vision loss. In the early stage, whitish-yellow deposits called as drusen is accumulated in the macula between the RPE and Bruch's membrane. Deposit is called as hard or soft drusen when it is small and distinct or large and confluent, respectively. It may also be placed between the RPE and the photoreceptors or within the photoreceptors (Sarks et al., 2011; Zweifel et al., 2010). The main composition of drusen is complement,

immunoglobulins, amyloid-β, phospholipids, cholesterol and apolipoproteins. Early dry AMD may turn into advanced dry or advanced wet AMD. The symptoms of the advanced dry AMD are death of RPE cells and choriocapillaries cells. On the other hand, an extension of abnormal choroidal vessels into subretinal space (choroidal neovascularization) is seen in the advanced wet AMD (Fig. 5C). Smoking is the strongest environmental reason for the progression of AMD. Oxidative stress is among the main causes of pathological AMD and especially aging, smoking and light exposure increase the oxidative stress (Brantley & Sternberg, 2013). Therefore, antioxidant and carotenoid supplements lower the risk of AMD.

1.2.2. Retinitis Pigmentosa (RP)

The retinitis pigmentosa (RP) is the most common retinal dystrophy. This disease is categorized in the pigmentary retinopathies that include the all retinal dystrophies resulted in the loss of photoreceptors and retinal pigment deposits. The RP is characterized by death of rods and cones. Initially rods are degenerated, after that the degeneration of cones is started. The other symptoms of the RP are the deposition of pigment in the peripheral retina and possibly, in some parts of the central retina and attenuation in retinal vessels (Fig. 5B).

In the early stage of the disease, mainly night blindness appears since rods are primarily degenerated. The disease seems stable at this stage and patients have normal life. In the mid stage, the night blindness is more obvious and peripheral visual field in day light is lost. In the mid-periphery, pigment deposits are observed and visual acuity is decreased. In the late stage of the RP, the peripheral vision is lost and patients cannot move autonomously. Also, pigment deposition is seen on the macula region (Hamel, 2006).

1.2.3. Diabetic Retinopathy (DR)

The diabetic retinopathy (DR) is among the most common complications of diabetes and is a leading cause of blindness. In the non-proliferative stage, DR leads to increase in vascular permeability, macular edema and visual deterioration. In the proliferative stage of DR, neovascularization through the surface of the retina is observed because of disrupted vascular function upon capillary occlusion. Newly formed vessels cause bleeding, hemorrhage (Fig. 5D) and detachment of the retina; thus, visual impairment or even blindness becomes inevitable (Usuelli & La Rocca, 2014).

Normal vision in the retina is a result of the interactions among many cells and diabetes damages the main retinal cells such as vascular cells (endothelial cells and pericytes), neurons (photoreceptors, bipolar, horizontal, amacrine and ganglions), glia (Müller cells and astrocytes), microglia, and pigment epithelial cells. Before any damage, the retinal cells are activated causing increased capillary permeability and blood flow. Consequently, proliferation of extracellular matrix and basal membrane thickening, modulation of cell turnover (apoptosis, proliferation, hypertrophy), formation of procoagulant and proaggregant patterns are observed leading to angiogenesis and tissue remodeling. The mechanism of damage that is caused by diabetes is directly associated with increased level of glucose, lipids, amino acids, hormones and inflammatory molecules. These molecules primarily activate the retinal cells and then effect of this activation causes cell damage in the retina (Ahsan, 2014).

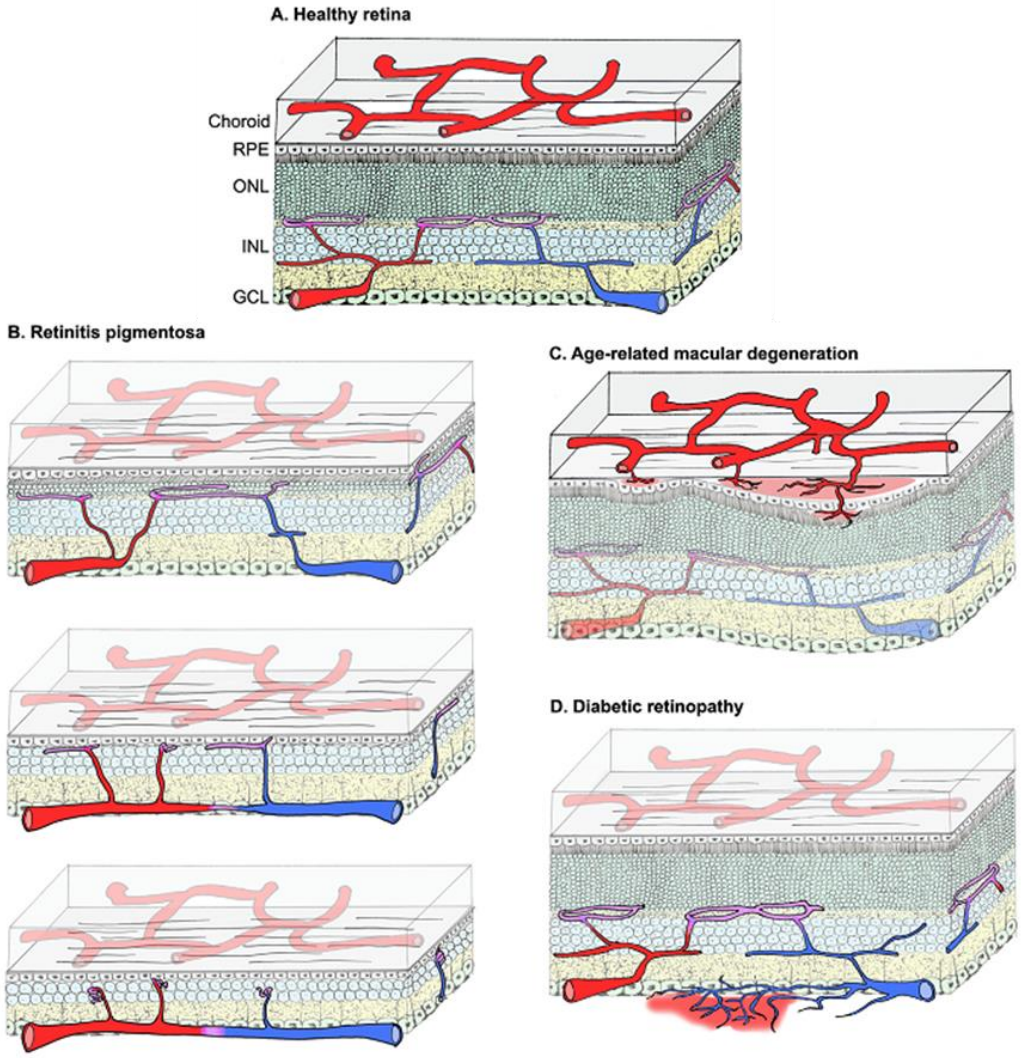

Figure 5. Vascular changes related with retinal disease. (A) Vasculature of the healthy retina and choroid. (B) Progressive degeneration of retinal vasculature associated with retinitis pigmentosa. (C) Changes in choroidal vasculature observed in age-related macular degeneration. New blood vessel growths from the choriocapillaris plexus and its entrance into the retina through Bruch's membrane. (D) Neovascularization of the inner retinal layers during diabetic retinopathy. RPE: Retinal pigment epithelium; ONL: outer nuclear layer; INL: inner nuclear layer; GCL: ganglion cell layer (Cuenca et al., 2014).

1.2.4. Retinal Vein Occlusion (RVO)

Following the DR, the retinal vein occlusion (RVO) is the next common retinal vascular disease. Branch retinal vein occlusion (BRVO) is encountered approximately three to four more times higher than central retinal vein occlusion (CRVO). The main risk factors of RVO are age, hypertension, hyperlipidemia, diabetes, glaucoma, hyper-homocysteinemia, systemic inflammatory conditions, and thrombophilic conditions. In the pathology of RVO, vessel wall compression results in endothelium damage that causes the formation of thrombus. Besides the ischemia caused by the occlusion, vision loss results from the necovascularization and macular edema raising hemorrhage of vitreous and glaucoma (Voleti & Hubschman, 2013). In addition, there is a relation between RVO and severe retinal detachment (SRD). Mainly, the retinal detachment is the separation of retina from RPE leading to the vision loss and blindness. SRD can be shown in approximately 80% of CRVO patients with cystoid macular edema. It is demonstrated that SRD is more common in major BRVO than macular disease. SRD results in deposition of macular hard exudates and this causes poor vision (Ozdemir et al., 2005; Tsujikawa et al., 2010; Yamaguchi et al., 2006).

1.3. Current Methods for the Treatment of Retinal Degeneration

Neurodegeneration is a widespread process seen in the various retinal diseases. Neuroprotective treatments are one of the basic therapeutic options regardless of the degeneration etiology. The main aim of neuroprotective treatment is to offer a proper environment to retinal cell for prolonged viability. This is established by providing neurotrophic factors to retina, preventing pro-apoptotic pathways or delivering some viability factors. In addition, retinal diseases are treated with gene and cell-based therapy and retinal transplants according to severity and type of the diseases (Cuenca et al., 2014).

Various approaches have been taken to protect the healthy neurons and the neurons that are susceptible to damage by slowing the retinal degenerations (Hoon et al., 2014). For example, the amino acid taurine supplement has been demonstrated to slow the degeneration of retinal ganglion cell (Froger et al., 2012, 2013) and to enhance the resistance to hypoxia in retinal cell cultures (K. Chen et al., 2009). Neuroprotection of photoreceptors has been achieved with the application of neurotrophic factors such as CNTF (ciliary neurotrophic factor). The main role of CNTF is to control phototransduction and regenerate the outer segments of the photoreceptor cells (Li et al., 2010). Moreover, there are active agents that have antioxidant and anti-inflammatory effects which can be used in the treatment of retinal diseases. For example, quercetin is a flavonoid that has anti-inflammatory and anti-oxidative functions found in black and green tea. Recently, studies on human RPE cell line ARPE-19 have showed that quercetin has protective effects against oxidative stress by inhibiting the intrinsic apoptosis pathway and pro-inhibitory molecules (Cao et al., 2010).

Advanced therapies of retinal diseases involve different approaches unlike conventional chemical or protein dependent therapies. Advanced therapies were classified into three main groups as: gene therapy, cell therapy and tissue engineering. Gene therapy with anti-angiogenic proteins enables the suppression of neovascularization and vascular leakage in the eye. In a mouse model that simulates the human DR, gene transfer of anti-angiogenic PEDF by help of AAV2 (adeno-associaated virus) in the vitreous has been proved to have positive effects. PEDF production provided inhibition of intravitreal neovascularization, normalization of retinal capillary density, prevention of retinal detachment, and reduction in the intraocular levels of vascular endothelial growth factor (VEGF). In addition, reduction in the VEGF level caused down-regulation of angiogenesis effectors like matrix metalloproteinases 2 and 9 and the content of connective tissue growth factor that have roles in the angiogenesis, effectively (Haurigot et al., 2012). In the case of RP disease, the gene-targeted therapy is an inapplicable approach due to genetic heterogeneity and thus, the finding of mutation-independent treatment is needed to

prevent photoreceptor cell death. One encouraging approach for the neuroprotection of photoreceptor is the utilization of neurotrophin secretion from Müller cell that is the primary retinal glia. Müller glial cells are promising targets for neurotrophin secretion by gene transfection since they are found in the entire tissue and interact with all neuronal cells. An AAV (adeno-associated virus) serotype (ShH10) has been designed which efficiently and selectively transfects glial cells with intravitreal injection. Transfected cells showed glial cell line-derived neurotrophic factor (GDNF) secretion that leads to recover over 5 months in the retinitis pigmentosa rat model (Dalkara et al., 2011).

The cell therapy is another advanced strategy in the treatment of retinal degeneration. Human cells like somatic, adult stem or embryo-derived cells are the main sources for cell therapy. Recently, the reprogramming of adult cells into 'pluripotent cells' has become a promising method (Mason & Dunnill, 2008). The retinal tissue is located at one of the best sites in the body to treat with cell based therapy like gene therapy because of immune privilege, easy access and relative isolation from the rest of the body. Cell therapy is used for patients that suffer incurable eye disease or severe visual impairments due to irreversible vision loss like RP, AMD, DR, ischemic retinopathy and glaucoma. In these situations, photoreceptors and RPE cells are the targets for replacement therapy. The therapy should, however, not need immunosuppression or cause side effects. The cells should proliferate adequately with a low harvest amounts and not have ethical issues. Moreover, the cost should be low and the transplantation technique must be easy to apply (Ramsden et al., 2013).

Cells used in the cell-based therapy for retinal degenerations are
a) eye derived progenitor cells (ciliary body-derived progenitor cells, iris pigmented epithelial cells, retinal progenitor cells),
b) trans-differentiating stem cells (pigmented epithelial cells, Müller glia), and
c) non-eye derived stem/progenitor cells (embryonic stem cells, bone marrow stem cells, neural progenitor cells and adipose-derived stem cells) (Fig. 6) (Bi et al., 2009).

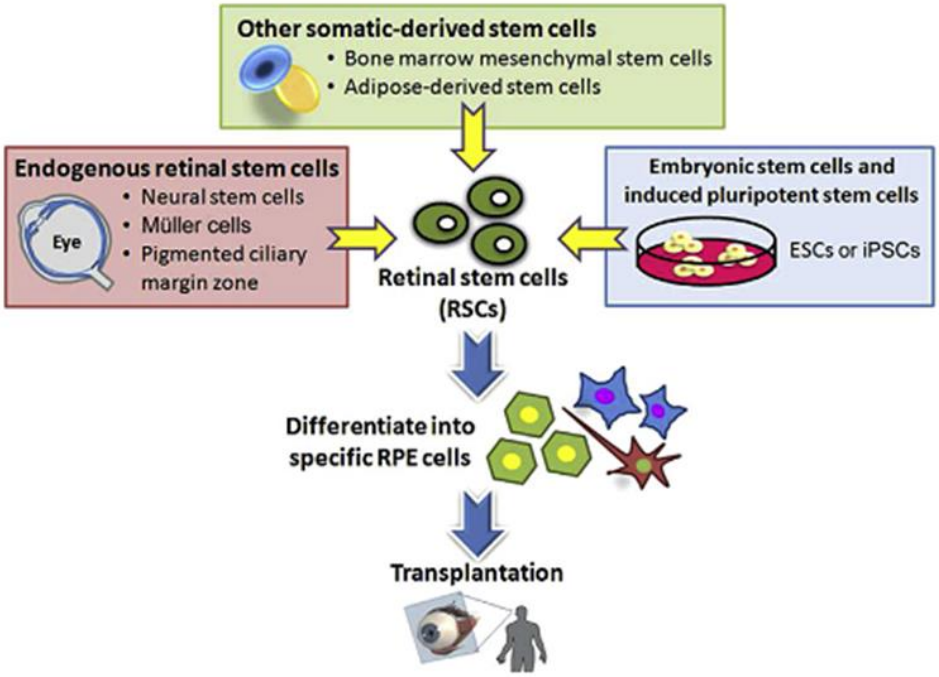

Figure 6. Cell sources for stem cell treatment of retinal diseases (Lin et al., 2014).

Eye derived progenitor cells have the capability to differentiate into retina-specific cells in a proper culture environment. Even though they show multipotent differentiation, they are not called progenitor cells because they need spatial cellular interactions and lack self-renewing features. Some of the cells isolated from adult mammalian ciliary body have some characteristics of neural progenitors and stem cell properties such as differentiating into retinal neurons. It was shown that these cells can proliferate in vitro by means of FGF-2 in culture medium and express nestin which is a neuroectodermal marker (Ahmad et al., 2000).

Müller cells are the main type of glial cells in the retina, and are considered as one of the eye-derived progenitor cells. They provide homeostatic and metabolic support to the retinal neurons. The Müller cells are distributed through the whole retinal layer from vitreous to the subretinal space. The main function of these cells is to control transportation of ions, and water. Since the Müller cells have the capability to generate neural stem cells, they are thought as a potential source for use in cell based therapies for retinal degenerations. In some studies, transdifferentiated Müller cells

could be cultured from Müller cells to use in mature human retina, human retinal cell line and epiretinal membrane of proliferative vitreoretinopathy patients. After transplantation of these cells into subretinal space or vitreous, Müller cells migrate to the retina and express neuronal markers (Johnsen et al., 2012; Lawrence et al., 2007).

Stem cells are totipotent before generating blastocysts and then they become pluripotent. They have the ability of regenerating into different cell types with selective induction. When certain stem cell populations are transformed to a specific lineage, they are called progenitor cells. In trans-differentiation process, a differentiated somatic cell dedifferentiates to lose the features of the original tissue, and then differentiates into another cell type. These stem cells are called tissue-specific and local cells. Since the characteristics of non-local stem cells are suitable to trans-differentiate, they are called trans-differentiating stem cells (Bi et al., 2009). Pigmented epithelial cells constitute a potential source for cell based therapies because of their capability of trans-differentiation into retinal cells in vitro (Amemiya et al., 2004) Adult retinal pigment epithelium cells can trans-differentiate into retinal neurons in a proper environment and they can be used in the treatment of retinal degenerations (Susaki & Chiba, 2007).

Pluripotent embryonic stem cells, as non-eye-derived stem/progenitor cells, have yielded the best results among all the retinal cells in cell based therapies. Embryonic stem cells (ESCs) are extracted from the cell mass of blastocyst, and have the ability to differentiate into retinal cells. They preserve the typical karyotype and differentiation capability for long periods. It has been shown that mouse, monkey and human ESCs can form retinal cells by use of growth factors, retinal co-cultures and genetic modifications (Pearson, 2014). In a study, Lamba et al. (2009) showed that human ESC could adapt a retinal fate that resembles that of the natural retinal cells in terms of morphology and function when injected into the subretinal space of Crx-deficient mice. The human ESC-derived photoreceptors could have markers that demonstrate differentiation to rod and cone and their morphology is similar with the

host photoreceptors. Moreover, transplanted cells of ESC derived photoreceptors could respond to light and transmit signals to the bipolar cells (Lamba et al., 2009).

The stem cells with their capability to differentiate to retinal cells are very promising for their use in clinical applications. It is important that the recipient retina must accept cells from another source and the microenvironment of retina must support the maintenance of cells from an external source under certain conditions. These are the important points before applying a type of cell source into a specific retinal degeneration. For example, immunological and tumorigenic considerations can limit the effective use of ESCs. Although BMSCs (bone marrow stromal cells) are free from ethical concerns, they can be obtained in very low numbers and proliferate with difficulty.

Induced pluripotent cells (iPSCs) can be an alternative approach to sustain cells that are undifferentiated for long time, to increase cell numbers, to enhance differentiation to a specific lineage, and to avoid tumorigenicity. However, it is difficult to direct clinical setting toward iPSCs since disease and patient specific iPSC transplantation need more efforts (Lin et al., 2014). If reprogramming, differentiation and cell characterization protocols continue to develop, stem cell technology could be used more widely. It is clear that a customized approach will be required to treat any retinal disease effectively (Cuenca et al., 2014).

In brief, delivery of retinal cells in the subretinal space, both in suspension and as transplanted tissue is being widely studied. These studies aim to find the most appropriate cell types for a treatment of retinal degeneration. Mature cell types have shown limited survival and integration with host tissue. Embryonic or neonatal donor tissue is not promising because of limitations in the supply and ethical issues. Tissue and cell transplantations are prone to immune rejection, although graft survival may be enhanced with the injection into the vitreous or administration of immunosuppressive drugs. Progenitor cells induce low immune responses, can be adult derived and could be cultured for a long time which provides a continued

presence of cell source. Neural progenitor cells may repair photoreceptors and are easily differentiated in vitro. RPCs also have progenitor cell priority and the capability of differentiating into the retinal cell types. RPCs are a promising cell type to replace damaged photoreceptors and are a proper cell type for attaching to a scaffold for transplantation into the subretinal space. However, photoreceptor replacement provides only partial retinal regeneration. The co-transplantation of RPCs with RPE cells may be a good method to increase cell survival and be important to maintain function. Recently, human iPSCs derived-RPE cells are functional and excellent cell type for retinal transplantation (Hynes & Lavik, 2010).

The studies also showed that the bolus injection of stem and progenitor cells into the subretinal space causes disorganized and poorly localized grafts. Thus, low cell survival is seen because of poor integration of donor cells into host tissue with the injection reflux. Therefore, slow degrading biocompatible polymers can be used as a support material for cells and the donor cells can produce their own extracellular matrix on polymer supports and a transplantable healthy donor tissue can be generated. At this point, tissue engineering appears as a promising approach for retinal regenerations (Trese et al., 2012)

1.3.1. Retinal Tissue Engineering

Tissue engineering combines the principles of cell transplantation, materials science, and bioengineering to develop new biological substitutes that may restore and maintain normal organ function (Atala, 2012). It involves isolating cells from the host and seeding them into 3D scaffolds or tissue substitutes that naturally mimic the structure and composition of the tissue, and finally implanting the cell seeded construct into the patient. After implantation, the natural tissue regeneration begins and blood vessels infiltrate the scaffold while it slowly degrades and the new tissue is formed (Liu et al., 2007).

Scaffolds used in tissue engineering are defined as 3D constructs that are used to repair the function of the damaged tissue. These scaffolds should provide mechanical support, facilitate cell seeding, regulate cell behavior and enhance the delivery of drugs or trophic molecules. Scaffolds are created by using a various natural and synthetic materials that support tissue survival and repair. A natural scaffold is isolated from a biological tissue. These constructs are obtained with the decellularization of donor tissue. Natural membranes that have been used for subretinal implantation are human amniotic membrane (hAM), human lens capsule, and Bruch′s membrane. These membranes can mimic the natural mechanical properties of the target tissue and they are also biocompatible structures. However, there are some limitations about these natural scaffolds such as disease transmission from donor to host and low availability of donor tissue. At this point, both natural and synthetic polymers are considered for a range of scaffold design. Some examples of natural polymers are collagen, alginate, hyaluronic acid, and fibrin. The synthetic polymers that can be used in the fabrication of scaffolds in retinal tissue engineering are poly(lactic-co-glycolic acid) (PLGA), poly(lactic acid) (PLLA), poly(glycerol-sebacate) (PGS), poly(caprolactone) (PCL) as well as many others (Hynes & Lavik, 2010).

The ideal polymer used in the fabrication of the scaffold for retinal tissue engineering must be biocompatible, not provoke immune reactions, porous to enable the infiltration of choriocapillaries, thin (less than 50 μm thick) and biodegradable by means of hydrolysis. In addition, its Young's modulus should match with the sensory retina and also it should have enough mechanical strength to provide good surgical manipulation (Trese et al., 2012).

Cells used in the retinal degenerations were explained under the cell-based therapy. Those cells are also included into the retinal tissue engineering component as cell source. Now, materials used in the fabrication of scaffolds for retinal tissue engineering will be reviewed.

1.3.1.1. Materials

1.3.1.1.1. Natural Polymers

1.3.1.1.1.1. Collagen

The most well known natural polymers used in retinal tissue engineering are collagen, alginate, hyaluronic acid, fibrin and silk fibroin. Collagen is primary component of the extracellular matrix, especially in basement membrane. It is a natural protein biopolymer composed of amino acids. It provides an ideal matrix for cell culturing. Collagen membranes can be robust structures for cell proliferation. It is suitable for attachment of RPE cells since the inner collagenous layer of Bruch's membrane, the natural support of RPE cells in the retina is composed mainly of Collagen I. It was shown that a thin collagen membrane (approximately 5 μm) enhance the RPE cell attachment, proliferation, nutrient transportation through the membrane and formation of monolayer epithelium with desired cell morphology. This cell seeded construct can be used in therapy of age-related macular degeneration (AMD) (Lu et al., 2007).

1.3.1.1.1.2. Gelatin

Gelatin is obtained by partial hydrolysis of collagen under acidic or alkaline conditions. It is a biocompatible material and has low immunogenicity. It is biocompatible when transplanted into the anterior chamber and subretinal space of the eye. Gelatin constructs have been used to deliver ocular cells or tissues, such as cultured corneal endothelial cell and sheets, cultured RPE cells, photoreceptor sheets and retinal sheets. Since ocular cells and tissues are delicate in nature, their transplantation into the damaged tissue is a challenging process. Previously, crosslinked gelatin matrix was used as a retinal sheet and it was shown that the retinal sheet integrated with the Bruch's membrane (Lai & Li, 2010).

1.3.1.1.1.3. Silk Fibroin

Silk fibroin is another natural material used in retinal transplantations. Collagen that is the major ECM protein may seem more appropriate than silk fibroin as it is present naturally in the eye. However, constructs fabricated from collagen lack mechanical strength unless they are not modified by crosslinking or blended with other materials (Deng et al., 2010). Scaffolds obtained from silk fibroin stronger than collagen counterparts. Therefore, the use of fibroin presents an advantage in the fabrication of scaffolds for retinal cell delivery (Altman et al., 2003). The biodegradation profile of fibroin may also be advantageous for the eye. Formed by the assembly of glycine and alanine repeats fibroin makes stable β-sheet, it is hydrophobic and is one of the strongest organic material in nature. Fibroin based constructs degrade more slowly than those with collagen, fibrin and polylactides. Degradation rate of fibroin scaffolds can be controlled with fraction of β-sheet in the structure. Other advantage of fibroin compared with synthetic materials is the nature of the degradation products; leads to smaller local variations in tissue osmolarity and pH than degradation products of aliphatic polyesters (Harkin et al., 2011).

1.3.1.1.1.4. Fibrin

Fibrin is another appropriate natural polymer used in retinal tissue engineering. Fibrin network is produced by the conversion of fibrinogen to fibrin by the action of thrombin in the presence of excess calcium ion. This leads to spatially organized clots that mimic the natural wound healing process. Fibrin is highly biocompatible and elastic. It promotes cell migration and it is suitable for cell entrapment and provides mechanical support. In a study, a 3D construct was developed by mixing fibrin network. Dental pulp stem cells (DPSCs) were differentiated into retinal ganglion-like cells after entrapping in fibrin to treat neurodegenerative disease of the eye. Differentiation of DPSCs into a multipolar neuronal cells was shown with the changes in morphology and neuronal marker (MAP2 and GFAP) expression (Roozafzoon et al., 2014).

1.3.1.1.1.5. Hyaluronic Acid (HyA)

Hyaluronic acid (HyA) is the only non-sulfated glycosaminoglycan that is found in the extracellular matrix (ECM) of many parts of the body. Its physical and biochemical properties, solution or hydrogel form, is appropriate for tissue repair. HyA is suitable as a scaffold because it is natural, biodegradable and biocompatible. It is a major component of the connective tissue and so it enhances lubrication, cell differentiation and cell growth. HyA has functional groups like carboxylic acids and hydroxyls on its backbone that facilitates the integration of functional domains or to fabrication of hydrogels by crosslinking. Since HyA plays role in every step of wound healing, exogenous HyA is promising material to provide faster and better healing (Collins & Birkinshaw, 2013). It is involved in many biological functions, such as cell proliferation and migration, morphogenesis, inflammation, angiogenesis, and tumor growth. Moreover, HyA oligosaccharides stimulate secretion of cytokines and proliferation and migration of endothelial cells, new vessels formation, and leucocyte recruitment (Genasetti et al., 2008). Photopolymerizable methacryloyl groups can be conjugated to HyA to obtain a photocrosslinkable polymer (Zawko et al., 2009).

1.3.1.1.2. Synthetic Polymers

Synthetic polymers can have a large variety of changes in their properties with changes in their composition (i.e., contact angle, Young's modulus, surface topographies, degradation rate, etc.) (Lee et al., 2001). One of the most widely used synthetic polymers used in scaffold fabrication is poly(lactic acid-co-glycolic acid) (PLGA). This polymer degrades with hydrolysis and its degradation products like lactic and glycolic acids can be further metabolized in the body. Their degradation rate can be altered by changing the ratio of lactic acid-to-glycolic acid subunits (Gunatillake et al., 2006). In addition, PLGA can be blended with poly(L-lactic acid) (PLLA) to create more rigid scaffolds. These constructs may be particularly reliable for subretinal applications (Lavik et al., 2005). Poly(caprolactone) (PCL) is another

synthetic biodegradable polymer like PLGA. Its degradation rate is lower than PLGA because of its more hydrophobic and semi-crystalline structure (Coombes et al., 2004). Poly(glycerol sebacate) (PGS) is a recently developed biodegradable and flexible polymer. It shows low swelling profile when crosslinked and that prevents its high water retention (Wang et al., 2002). The PGS is also appropriate for subretinal transplantations in terms of its mechanical properties (Neeley et al., 2008). Polyhydroxyalkanoates (PHAs) are also polyesters derived from bacteria (Page et al., 1992). These polymers have been used for in vivo applications due to their degradation products, D-3-hydroxybutyrate, a ketone that is normally present in the blood (Tezcaner et al., 2003).

Liu et al. (2014) used biostable poly(ethylene terephthalate) (PET) and biodegradable poly(L-lactide-co-ε-caprolactone) (PLCL) separately to construct polymeric scaffolds to culture RPE cells. Their aim was to obtain a functional RPE monolayer that could be placed under the retina. Films and electrospun fiber mats of both PET and PLCL (fiber diameters ranging from 200 to 1000 nm) were cultured with human fetal RPE cells and transplanted subretinally in rabbits. The scaffolds with fiber diameter of 200 nm supported the highest RPE cell densities, formation of monolayers pigmentation and uniform hexagonal tight junctions. Histology results showed RPE migration on the nanofibers and some photoreceptor generation. Consequently, 200 nm fibers improved RPE cell culture and increased subretinal biocompatibility (Liu et al., 2014).

Subrizi et al. (2012) constructed a substrate by using biopolymer (laminin, collagen and heparan sulfhate) coated polyimine (PI) membranes to support differentiation and maturation of hESC (human embryonic stem cells) toward RPE phenotype. They chose synthetic polymer polyimide (PI) because its biocompatibility was clinically confirmed when used in various ophthalmic applications such as PI-based intravitreal implant (Kane et al., 2008). In this study, they constructed a thin (24 μm), porous PI membrane coated with some adhesive compounds to mimic the natural Bruch's membrane and laminin coated membranes gave the best results. They showed that

the cells took a distinctive hexagonal, cobblestone morphology with high pigmentation. In addition, expression of RPE specific genes and proteins and phagocytosis events in photoreceptor outer segments (POS) were shown after co-culture with rat retinal explants. Transepithelial electrical resistance and permeability measurements also demonstrated the barrier function of hESC-derived RPE (hESC-RPE) monolayers (Subrizi et al., 2012).

Redenti et al. (2009) used poly(glycerol sebacate) (PGS) as a scaffold for subretinal cellular delivery. They preferred PGS because of its processability into thin structures (45 μm), ease of surface modification and good mechanical properties that enable implantation. In addition, it has an important advantage during surgery; a cell seeded PGS substitute can be made into a scrol, loaded into a syringe and injected subretinally. After the injection the polymer unrolls and cells are integrated with the desired regions of the retinal tissue. Mouse retinal progenitor cells (mRPCs) were cultured on PGS scaffolds and high levels of survival, adherence and proliferation were demonstrated in vitro. mRPC differentiation toward mature phenotypes was shown with the changes in mRNA and protein levels. Transplanted substitutes also showed long term mRPC survival like in vitro. Moreover, cells migrated from the tissue engineered substitute displayed mature marker expressions in the host retina. These results indicate that PGS scaffolds seeded with mRPCs is a viable approach for retinal tissue engineering (Redenti et al., 2009).

1.3.1.2. Scaffold Processing Techniques

The most promising techniques used in the fabrication of scaffolds for the subretinal space are solvent casting and microfabrication. Solvent casting is a conventional method used for the simple formation of polymer films and scaffolds. Briefly, a polymer is dissolved in a solvent and poured into a desired mold. The solvent is evaporated leaving behind a thin, nonporous polymer film. Porous films are obtained after adding porogen to the polymer solution and then leaching the porogen. This method is called as particulate leaching. These methods cannot generate complex

predetermined architectures, which may be an important component in the design and fabrication of a subretinal scaffold (Hynes & Lavik, 2010). Electrospinning is another method used to fabricate subretinal scaffolds. It forms nanofibrillar structures that facilitate cell adhesion, proliferation and differentiation, while they provide efficient transport of nutrients and metabolites through the nanofibers (Ito et al., 2005; Harkin et al., 2011). In the recent days, electrospun nanofibers are used to mimic the natural basement membranes for retinal tissue engineering applications. For example, electrospun nanofibers closely mimic the nanofibrous architecture of BM (Xiang et al., 2014). In electrospinning, a high potential is applied to a polymer solution to eject it as a thin jet towards the oppositely charged plate. The fiber diameter, porosity and morphology can be controlled by changing the parameters such as polymer solvent and concentration, potential, distance from the collector plate, and conductivity of the polymer solution (Chen et al., 2011). Microfabrication techniques can also be used to control the architecture of a material. Photolithography and/or soft lithography are common microfabrication techniques. Photolithography is a method used to create micro/nano-structures with high precision by exposing a material to UV through a patterned mask. Briefly, a silicon wafer or glass is used as etchable or unetchable substrate, respectively. A photoresist is coated on the wafer as a thin layer. The photoresist which is a light sensitive polymer can be crosslinked or degraded with exposure to UV through a mask to etch the desired 2D pattern on the photoresist layer. Finally, depending on the photoresist material, wet or dry etching was used to develop the photoresist. Then, this pattern can be used to create a mold that is used in micromolding or microcontact printing. In soft lithography, an elastomeric stamp that is generally made up of from PDMS is used to transfer the desired 3D pattern to polymer (Falconnet et al., 2006; Truskett & Watts, 2006).

1.3.2. Bruch's Membrane and/or Choroid Substitutes

A Bruch's membrane (BM) substitute should allow attachment, proliferation and development of a typical RPE cell phenotype such as apical and basal polarity. One

of the important requirements about this substitute is permeability since RPE cell transportation across BM is not desirable phenomena for retinal tissue functions. Optical transparency is not required since the material would not be located in the pathway of the incoming light. However, the BM substitute should integrate with the choriocapillaris. The basal surface of the substitute might support the attachment of the thin 3D scaffold to allow ingrowth of capillaries from the choroid. An alternative approach is the seeding microvascular endothelial cells on the basal surface of the prosthetic BM that could reconstruct components of the choriocapillaris in vitro before implantation. Since engineered substitute will be in contact with sensitive layer of photoreceptors, it is critical that the potential toxic effects of degradation products to be taken into consideration (Harkin et al., 2011).

Recently, some studies have reported the implantation of BM and RPE seeded artificial constructs to the subretinal space. Mainly, aim was the treatment of age-related macular degeneration (AMD) since BM exposed to a variety of biochemical and it loses adjacent RPE cells with age, and consequently it leads to AMD. Several types of materials and RPE (cell lines, stem cell derived RPE cells, etc.) were used on these constructs in the treatment.

Treharne et al. (2012) designed a BM from methyl methacrylate and (ethylene glycol) methacrylate copolymer. They fabricated BM as fibers of a methacrylate copolymer into which PEG chains were incorporated to improve hydrophilicity, decrease nonspecific binding of protein, and provide a spacer arm between the cell adhesion ligand and the polymer chain. PEG chains were then functionalized with a succinimidyl carbonate end group to enable the conjugation of various cell attachment factors, such as laminin and short peptides (GRGESP (Gly-Arg-Gly-Glu-Ser-Pro), GRGDSP (Gly-Arg-Gly-Asp-Ser-Pro), YIGSR (Tyr-Ile-Gly-Ser-Arg) and RGD (Arg-Gly-Asp)). ARPE-19 RPE cells were seeded on electrospun fibers of functionalized copolymer and they showed survival and proliferation on the scaffolds. SEM micrographs of cells suggested that cells attached on the surface as a monolayer like natural retinal pigment epithelium (Treharne et al., 2012).

Warnke et al. (2013) produced an ultrathin 3D nanofibrous membranes from collagen type I and PLGA by using an advanced, needle-free electrospinning method. The nanofibrillar mat closely resembled the fibrillar structure of the inner collagenous layer of BM. They cultured human primary RPE cells on the nanofibrous membranes and showed that cells possessed impressive similarity to native human RPE. SEM showed that the cultured cells were organized as a monolayer in a typical polygonal shape and showing sheet-like microvilli on their apical surfaces. Cells formed tight junctions and expressed RPE65.

Silk fibroin is another material to fabricate Bruch's membrane. In a study, Shadforth et al. prepared ultrathin (3 μm) membranes from *Bombyx mori* silk fibroin (BMSF) and showed that enhanced cell attachment. Both ARPE-19 RPE and human RPE cells showed cobble-stoned morphology. Tight junctions were demonstrated with staining of the zonula occludens protein (ZO-1) (Shadforth et al., 2012). In another study, Xiang et al. (2014) prepared an ultrathin porous nanofibrous film (3-5 μm) of wild Antheraea pernyi silk fibroin (RWSF), PCL and gelatin to mimic BM. Gelatin (GEL) was introduced into nanofibrous film to increase hydrophilicity and support cell attachment and proliferation. Culture of human RPE cells on these structures had high cell growth and expressed RPE specific gene. After long culture periods, RPE cells showed typical polygonal morphology and apical microvilli. Moreover, the cells on the RWSF/PCL/GEL films functionally secreted polarized PEDF and phagocytosed porcine photoreceptor outer segments (POS) that demonstrate the functionality of RPE. Furthermore, RWSF/PCL/GEL membranes that were transplanted subsclerally indicated high biocompatibility and no inflammation or immune response. This type of composite matrix provided a favorable environment for growth of RPE cells and resulted in improved cytocompatibility in vitro and biocompatibility in vivo (Xiang et al., 2014).

In literature, no study has been reported about development of choroid substitute. Although vascularized tissue engineered construct can be considered as a choroid substitute, it still cannot be considered as a tissue engineered choroid construct.

When the choroid is disrupted, RPE and the other retinal cells are damaged and cell transplantation can be the only solution. Choroid tissue can be transplanted together with the RPE/Bruch's membrane complex since the damaged cells in the retinal degenerations are generally photoreceptors, RPE cells, and also underlying BM. Some researchers reported construction of RPE/BM/choroid substitute as a model construct by co-culturing RPE cells and endothelial cells. In these studies, the major aim was to construct a trilayer RPE/BM/choroid construct as an outer blood-retinal barrier and to study the interaction of cells and pathomechanisms of some diseases such as AMD. For example, Shadforth et al. (2013) cocultured the human ARPE-19 RPE cells and microvascular endothelial cells (HMEC-1) on opposing sides of a BM substitute (3 μm) made of silk fibroin to mimic the natural relationships between the RPE and choriocapillaris. The fibroin membranes were coated with vitronectin (for ARPE-19 cells) and gelatin (for HMEC-1 cells) to enhance cell attachment. The RPE cells of the 3D model showed cobblestone morphology and a good barrier. In addition, phagocytic activity of RPE cells demonstrated with cytoplasmic uptake of vitronectin-coated microspheres. HMEC-1 also attached well on the modified fibroin membrane and achieved physical separation from the underlying RPE layer. In another study, Hamilton et al. (2007) constructed a viable human in vitro model for the outer blood–retina barrier by of using the trilayer RPE/amnion/HUVEC. Amnion membrane was used as a BM and HUVECs were used to mimic choriocapillaries of the eye. RPE and HUVECs were seeded on opposite sides of the membrane. In the model trilayer substitute, RPE cells formed a continuous monolayer, and they showed polarity by forming apical microvilli and tight junctions while endothelial cells designated fenestration. In addition, permeability studies demonstrated that in vitro model trilayer substitute resembles in vivo model in terms of its barrier features (Hamilton et al., 2007).

In a study, surgery of eyes with foveal choroidal neovascularization (CNV) in AMD patients, which did not respond to laser, photodynamic therapy (PDT) or intravitreal medication and anti-VEGF therapies (Binder et al., 2007). RPE transplantation was made with suspension technique (n=8) or with the full-thickness RPE-choroid flap

method (n=8). They observed a better performance of the transplanted flap, when placed it near the edge of healthy RPE in the donor tissue. A slow improvement in visual acuity and formation of pigmented cell bridges were observed in the implanted retinal tissue (Binder et al., 2007).

1.4. The Aim and Novelty of the Study

The aim of the study is to construct a bilayer of Bruch's membrane and Choroid for use in the repair of retinal degenerations. Electrospun silk fibroin membranes were used as a substitute for Bruch's membrane and RPE cells were seeded onto it to generate a continuous monolayer. Silk fibroin was used instead of collagen to fabricate fibrous Bruch's membrane because of the good mechanical properties. The choroid layer of the substitute was created by using methacrylated collagen (ColMA) modified methacrylated hyaluronic (HAMA) acid hydrogel with a vascular pattern. HUVEC were seeded on hydrogels patterned in the form of a tree to mimic a vascular network. The major novelties of the study are the use of the silk fibroin in the fabrication of electrospun membrane as BM, the fractal tree patterned hyaluronic acid hydrogel and its modification with ColMA to enhance the cell adhesion and form a vascular network. Permeable silk fibroin mats provided a mechanically and structurally strong support for the RPE cells. In this way, RPE cells could organize in a form to be transplanted at the damaged site. Choroid layer was created to provide cellular cross-talk with the RPE cells without allowing the cells physically cross the mat. Vascularized tissue together with functional RPE cells is a novel approach for the use in treatment of the retinal degenerations. Moreover, this bilayer substitute can serve as a model of the outer blood-retinal barrier which can be used to study the interaction of the RPE and endothelial cells. Some drug release studies can be done to observe the changes of the morphology and functions of cells upon testing with new drugs.

CHAPTER 2

MATERIALS AND METHODS

2.1. Materials

Dulbecco's Modified Eagle Medium (DMEM)-high glucose (glucose concentration: 4.5 g/L), DMEM-low glucose (glucose concentration: 1.0 g/L), DMEM-high glucose colorless, fetal bovine serum (FBS), Trypsin-EDTA (0.25%), and Snake Skin dialysis tubing were obtained from HyClone, Thermo Scientific (USA). *Bombyx mori* silk threads were gift from Prof. Dr. Esra Karaca, Uludag University Textile Engineering Department (Turkey). Penicillin/streptomycin (100 units/mL-100 μg/mL) and bovine serum albumin (BSA) were purchased from Fluka (Switzerland). Dimethyl sulfoxide (DMSO) and Triton X-100 were bought from AppliChem (USA). Nano^{TM} XP SU-8 100 (Negative Radiation Sensitive Resist) and its developer were purchased from MicroChem (USA). Alamar Blue, Alexa Fluor ® 532 Phalloidin was purchased from Invitrogen Inc. (USA). Sodium phosphate monobasic and dibasic, sodium chloride (NaCl), ethanol, acetic acid (HAc), acetone, and Tween-20 were purchased from Merck Millipore (Germany). NucleoCasette was obtained from ChemoMetec (Denmark). DRAQ5 was purchased from Abcam (UK). Alexa Fluor® 488 anti-mouse CD31 Antibody was bought from BioLegend (USA). Hyaluronic acid sodium salt (from *Streptococcus equi)*, 2-hydroxy-4′-(2-hydroxyethoxy)-2-methylpropiophenone, methacrylic anhydride (94%), sodium benzoate, 1,1,1,3,3,3-hexafluoroisopropanol (HFIP), glutaraldehyde, paraformaldehyde, N,N-dimethylformamide anhydrous, 99.8%, 4‟,6-diamidino-2-

phenylindole, dihydrochloride (DAPI) were purchased from Sigma (USA and Germany).

2.2. Methods

2.2.1. Preparation of Scaffolds

2.2.1.1. Preparation of Electrospun Silk Fiber Mats

2.2.1.1.1. Isolation of Silk Fibroin from Silk Threads

Silk fibroin was isolated from silk threads obtained from *Bombyx mori* cocoons as described by Schneider et al, 2008. Briefly, silk threads were cut into small pieces (20 g) and washed with Na_2CO_3 (0.02 M) to remove sericin for 30 min. Sericin removed silk threats were washed with distilled water and dried at room temperature. Silk fibers (19 g) were dissolved in LiBr solution in a flask (9.3 M, 475 mL) at 60˚C and incubated for 3 h with mixing on a magnetic stirrer. Silk fibroin solution was filtered with filter paper and dialyzed against distilled water for three days. Dialyzed silk fibroin solution was frozen at -80˚C and then lyophilized (Labconco Freezone 6, USA) until completely dry. The dry fibroin was stored at +4˚C.

2.2.1.1.2. Electrospinning of the Silk Fibroin

Regenerated silk fibroin-based fiber mats were prepared by using electrospinning. Silk fibroin solution was prepared at various concentrations (10-20%) in hexafluoro isopropyl (HFIP) and transferred to a 10 mL plastic syringe with blunt ended metal needle. The flow rate of the silk fibroin solution was controlled by a syringe pump (New Era Pump Systems Inc., UK) and set to 5 µL/min. The metal needle tip was attached to a power supply (Gamma High Voltage Research, USA) providing a voltage (10-20 kV) with an air-gap distance of 10 cm between the needle and the metal plate. Electrospun silk fiber mesh was collected on a metal flat wire for 3 h.

Silk fibroin mat was separated from metal wire, put in a sealed container with aqueous methanol (80%) and stored in methanol vapor overnight at room temperature for fibroin self-assembly.

2.2.1.2. Preparation of Fractal Tree-Patterned Methacrylated Hyaluronic Acid (HAMA) Hydrogels

2.2.1.2.1. Methacrylated Hyaluronic Acid (HAMA) Synthesis

The synthesis of methacrylated hyaluronic acid was prepared as described by Messager et al., 2012 (Fig. 7). Briefly, hyaluronic acid was dissolved in distilled water at a concentration of 0.5 w/v %. DMF (dimethylformamide) was added to achieve a ratio of 3:2 (distilled H_2O:DMF). Methacrylic anhydride (1%) was added dropwise on the solution while stirring the mixture on magnetic stirrer at +4˚C. During the initial 4 h the pH was adjusted to ca. 8- 9 by adding NaOH (0.5 M). Then, it was incubated overnight at +4˚C with continuous stirring on a magnetic stirrer. After this reaction period, methacrylated hyaluronic acid (HAMA) solution was dialyzed against distilled H_2O for 3 days with daily changes of water. After dialysis, the solution was frozen at -80˚C and then lyophilized in a freeze drier (Labconco Freezone 6, USA) until complete dryness. Dry methacrylated hyaluronic acid was stored at -20˚C until use.

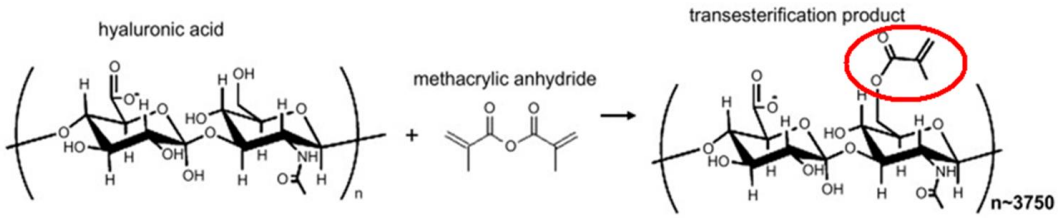

Figure 7. The conjugation of methacrylate group with the hydroxyl groups of hyaluronic acid.

2.2.1.2.2. Preparation of Fractal Tree-Patterned Photoresist (SU-8) by Photolithography

To create patterned hydrogel vascular, a photoresist layer was coated on a glass substrate and a fractal tree pattern was etched by using photolithographic techniques (Fig. 8). A photomask with fractal tree was designed and printed on a transparency film to create a patterned surface on the photoresist. All steps of photolithography process were done in darkness. Photoresist layer preparation process includes substrate (glass) cleaning, dehydration, photoresist coating and soft baking. In substrate cleaning step, a glass slide was cleaned for 5 minutes in acetone in an ultrasonic bath. Substrate was soaked in methanol for 1 min and rinsed with isopropyl alcohol. Cleaned substrate was then dried under nitrogen gas. In the dehydration step, the glass substrate was baked at 200 ˚C for 5 min on a hot plate and cooled with N_2 gas. In photoresist coating step, SU-8 photoresist liquid (Nano^{TM} XP SU-8 100 Negative Radiation Sensitive Resist) was coated on the cleaned glass substrate with spin coating. SU-8 photoresist was put on glass substrate and a spun for 30 s. SU-8 coated glass substrate was put on a hot plate at 65˚C for 2 min. for pre-baking. Then, it was put on hot plate at 95˚C for 5 min for soft baking. After completing soft-bake, the coated substrate was cooled slowly to room temperature. A photomask with the pattern was placed on the substrate in such a way that printed or toner side of the mask was faced to photoresist layer and UV-A was applied for 35 s. After UV exposure, the substrate was baked at 65˚C for 1 min and 95˚C for 2.5 min for post exposure baking. In the development step of photolithography process, the substrate was immersed in SU-8 developer for 5 min. Then, the exposed photoresist was soaked into isopropyl alcohol bath for 30 s for pattern etching.

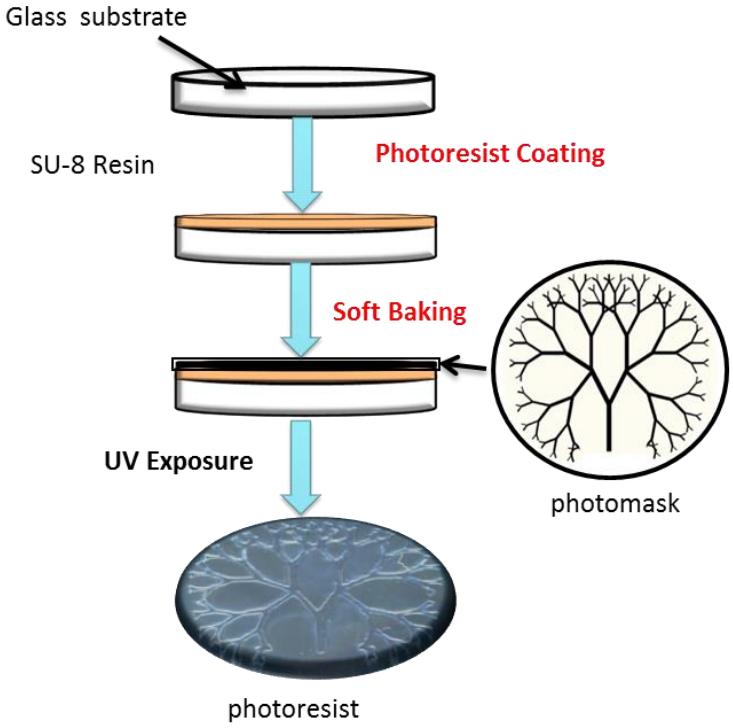

Figure 8. Schematic presentation of photoresist preparation.

2.2.1.2.3. Preparation of Fractal Tree-Patterned Polydimethylsiloxane (PDMS) Mold for Soft Lithography

The replica of fractal tree pattern was obtained by casting and curing of silicone pre-polymer on the etched pattern in photoresist that was made by photolithography. Poly(dimethylsiloxane) (PDMS) prepolymer was prepared by mixing Sylgard 184 silicone polymer and Sylgard 184 Curing agent (Dow Corning Company, UK) in a ratio of 10:1 (w/w). Care was taken not to capture bubbles during mixing. The mixture was cast onto the developed photoresist in a glass petri plate. Vacuum was applied to remove bubbles and then the prepolymer mixture was cured at 50˚C for 5 h. The cured PDMS mold was peeled off carefully and a negative copy of the vascular pattern was obtained from the etched pattern on the photoresist (Fig. 9).

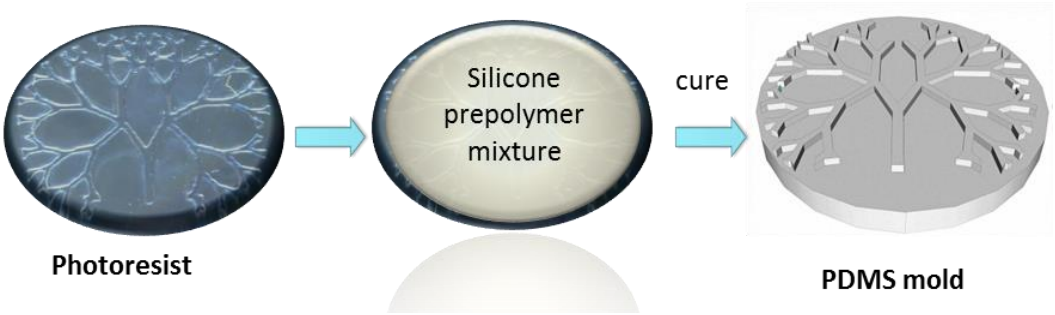

Figure 9. Schematic presentation of PDMS mold preparation.

2.2.1.2.4. Preparation of Fractal Tree-Patterned HAMA Hydrogels

Methacrylated hyaluronic acid polymer solution was prepared by dissolving HAMA (1.5%) and photoinitiator (0.5%) in distilled water. The polymer solution was cast on the fractal tree-patterned PDMS mold and N_2 gas was applied for 5 min in a chamber with gas inlet and outlet. The fractal tree-patterned hydrogel was obtained after UV exposure (0.120 Joule/cm^2) in a UV crosslinker chamber (BIO-INK-UV Crosslinker BLX-365) for 4 min. The gelled and pattern transferred membrane was then peeled off from PDMS mold and washed in distilled water to remove the impurities (Fig. 10).

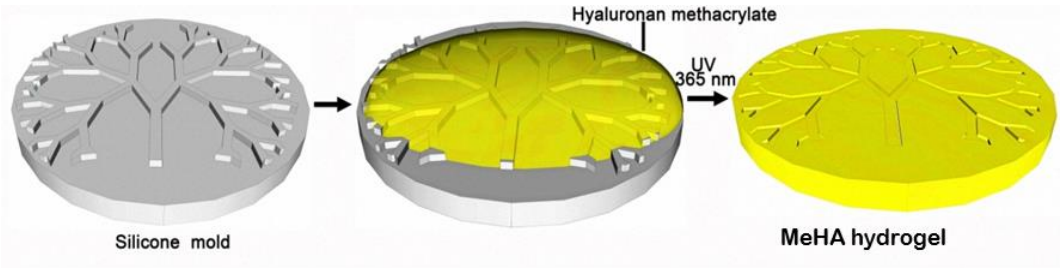

Figure 10. Schematic presentation of HAMA hydrogel preparation.

2.2.1.2.5. Photoimmobilization of Cell Attachment Factors on to Microchannels of HAMA Hydrogel

2.2.1.2.5.1. Methacrylated Gelatin (GelMA) Synthesis

The synthesis of methacrylated gelatin was previously reported by Nichol *et al.*, 2010 (Fig. 11). Briefly, a solution was prepared by dissolving gelatin (10%, w/v) in phosphate buffer (10mM, pH 7.4) at 50˚C with magnetic stirrer until completely dissolved. Methacrylic anhydride was added into the solution and the reaction was maintained for 1 h at 50˚C. After the reaction was complete, the mixture was diluted 5 fold with warm phosphate buffer and dialyzed against distilled H_2O for 3 days. The dialyzed solution of was lyophilized (Labconco Freezone 6, USA), a white porous foam was obtained and stored at +4˚C for further studies.

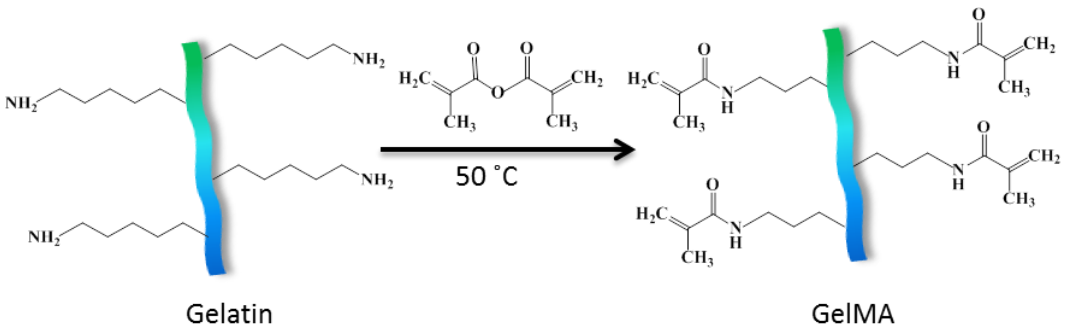

Figure 11. Schematic presentation of GelMA synthesis showing conjugation of methacrylic groups with the primary NH_2 groups of gelatin.

2.2.1.2.5.2. Methacrylated Collagen Type I (ColMA) Synthesis

2.2.1.2.5.2.1. Collagen Type I Isolation

Collagen type I was isolated Spraque-Dawley rat tails as reported previously (Kinikoglu et al., 2001). Briefly, tendons of the rat tails were dissolved in 0.05 M cold acetic acid solution (+4˚C), the solution filtered through glass wool and dialyzed with a dialysis tubing (MWCO = 10,000 Da) against phosphate buffer (12.5 mM NaH_2PO_4, 11.5 mM Na_2HPO_4, pH 7.2) at 4˚C for 1 week with daily changes buffer. After dialysis, collagen was centrifuged (1,600 g x 10 min) at +4˚C. The pellet was dissolved in 0.15 M acetic acid at +4˚C, precipitated with NaCl solution (5% w/v) and centrifuged (16,000 g, 10 min). The pellet was dissolved in 0.15 M acetic acid and dialyzed. Collagen precipitate was obtained after centrifugation and stored in ethanol (70%) with stirring. The precipitate was centrifuged, the resulting pellet was lyophilized and the collagen was stored at +4˚C until use.

2.2.1.2.5.2.2. ColMA Synthesis

Acetate buffer was prepared for dissolving collagen by using acetic acid (0.5 M) and sodium acetate (0.5 M) by adjusting pH to 2.5 by adding HCl (10 M). Isolated collagen type I (1%) was dissolved in acetate buffer overnight at 40˚C. Then, methacrylic anhydride (3% v/v) was added dropwise on the collagen solution and maintained at 60 ˚C in a water bath with magnetic stirring for 1 h. The solution was dialyzed (MWCO 10,000 Da) against distilled water at +4˚C. The methacrylated collagen solution was lyophilized and stored at +4˚C until use.

2.2.1.2.5.3. Photoimmobilization of GelMA, ColMA and Fibronectin on to Microchannels of HAMA Hydrogels

GelMA solution was prepared by dissolving GelMA (0.1 mg/mL) and photoinitiator (0.5%) in distilled H_2O. ColMA solution was prepared by dissolving ColMA (0.5 mg/mL) and photoinitiator (0.5%) in 0.05 M acetic acid. Fibronectin solution was prepared by dissolving fibronectin (1.0 mg/mL) and sodium benzoate (7.5 mg/mL) in distilled H_2O. GelMA (6 μL), ColMA (6 μL) or fibronectin (6 μL) solution was put on patterned HAMA hydrogel surface. Photoimmobilization of GelMA in the channels was achieved by superimposing the mask with the tree pattern with the pattern of hydrogel and exposing UV through the mask for 4 min (Fig. 12). In this way, UV passed through the transparent regions of the photomask and immobilized the cell adhesion factors while opaque regions of photomask blocked the crosslinking. The, immobilization of cell attachment factors on the microchannels of the tree pattern was achieved. Modified hydrogels were washed with sterile PBS to remove unbound cell adhesive factors on the unexposed regions.

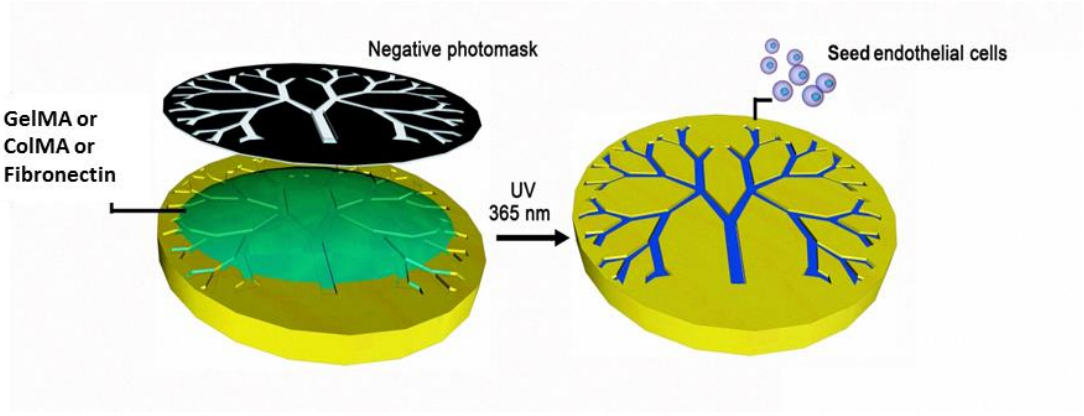

Figure 12. Schematic presentation of photoimmobilization of cell attachment factors on microchannels of HAMA hydrogels.

2.2.2. Characterization of Scaffolds

2.2.2.1. Characterization of Electrospun Silk Fiber Mats

2.2.2.1.1. ATR-FTIR

The FT-IR spectra of silk fibroin was obtained in solid state in the region 4000–400 cm^{-1} using Perkin Elmer FT-IR Spectrometer (USA), at room temperature, with a spectral resolution of 4.0 cm^{-1} and averaging of 32 scans.

2.2.2.1.2. Measurements of Mat Thickness and Fiber Diameter

Thickness of the electrospun silk fiber mats were measured with a micrometer (Erste Qualitat, Germany) to a sensitivity of 0.1 μm with ca. 10 measurements per sample (n=3).

SEM micrographs were used to measure the fiber diameters and to study scaffold morphology. The electrospun silk fiber mats (1 cm^2) were placed on carbon tapes over SEM stubs. The mats were coated with Au-Pd under vacuum and analyzed with a scanning electron microscope (JEOL, JSM-6400, USA) equipped with NORAN System 6 X-ray Microanalysis System and with SEM (QUANTA, 400F Field Emission SEM, USA) at 5-20 kV. SEM micrographs were analyzed with ImageJ (NIH, USA) was used to calculate the average fiber diameters making around 100 measurements.

2.2.2.2. Characterization of Micropatterned Hydrogels

2.2.2.2.1. Swelling Test

Photocrosslinked HAMA hydrogels were washed in distilled water and dried by lyophilization. They were then weighed and immersed in PBS (10 mM, pH 7.4) at 37˚C for 24 h. Swollen hydrogels were weighed and the degree of swelling (DS) was calculated according to the following equation;

$$DS\ (\%) = \frac{W_s - W_d}{W_s} \times 100 \quad (1)$$

where,

DS (%): Degree of swelling (%, w/w)
W_s: swollen weight of HAMA hydrogel (mg)
W_d: dry weight of HAMA hydrogel (mg)

2.2.2.2.2. SEM Analysis

The hydrogel morphology was investigated by SEM analysis using dried hydrogels which were sectioned horizontally and vertically with a razor blade. The preparation, observation and calculation were according to Section 2.2.2.1.2.

2.2.2.3. Characterization of PDMS Mold

2.2.2.3.1. Non-Contact, 3D Optical Surface Profile Measurement

The pattern morphology and pattern transfer efficiency on PDMS mold was studied by using an optical profilometer (Contour GT-K, Bruker Corp.) under white light illumination with 5X objective.

2.2.3. In vitro Cell Culture Studies

2.2.3.1. Culture of D407 (RPE) Cells

D407 cell line of retinal pigment epithelium (RPE) (P18-21) was used in the cell culture studies on ESF. The RPE cells, stored frozen at -80˚C in a mixture of their medium and DMSO (15%), were thawed and allowed to proliferate in T-flasks in an incubator (37˚C, 5% CO_2). The cells were plated in Dulbecco's Modified Eagle Medium high glucose, supplemented with fetal bovine serum (FBS) (10%), penicillin (100 UI/mL), and streptomycin (100 µg/mL). The growth medium of cells was replaced with fresh medium every 2 days. Cells at 70-80% confluency were then used for seeding onto scaffolds.

2.2.3.2. Culture of RPE Cells on Electrospun Silk Fiber Mats

For cell culture on electrospun silk fibroin fiber mats, tissue culture inserts were used to the mats and manipulate them. The electrospun silk fibroin fiber mats were inserted into cell crown holders in 12 well plates. For sterilization, mats were inserted into the sterile holders and inserted into ethanol (70%) in 12 well plate for 15 min. After ethanol treatment, membranes were dried in laminar hood and immersed into PBS (10 mM, pH 7.4) for 1 h to wash off residual ethanol. Later, the mats were washed twice shortly with PBS before use.

For seeding, plated cells were detached with trypsin (0.05%, 5 min, 37˚C) in an incubator. After detachment, growth medium was added to inactivate trypsin and cells were collected by centrifugation (3000 g, 5 min). Following this the pellet was suspended in the culture medium and cells counted using Nucleocounter (ChemoMetec, Denmark). 30,000 cells in 70 µL medium were seeded on mats. The inner surface area of tissue culture insert was 1.54 cm^2 and consequently the adhesion area of cells on silk fibroin fiber mats was considered 1.54 cm^2 (cell seeding density 20,000 cells/cm^2). After seeding, scaffolds were incubated at 37˚C for 30 min to allow the cells to attach, then 15 µL medium was added to prevent drying and incubated for another 30 min. Finally, growth medium was added into the inserts on wells and cultured in the humidified CO_2 incubator. During in vitro studies growth media were replaced with fresh medium every other day.

2.2.3.3. Culture of HUVEC

HUVEC (P38-41) was used in the cell culture studies on HAMA hydrogels. The cells were stored frozen at -80˚C in a mixture of their medium and DMSO (15%). After thawing, they were plated in T-flasks in an incubator (37˚C, 5% CO_2). Low glucose Dulbecco's Modified Eagle Medium supplemented with fetal bovine serum (FBS) (10%), penicillin (100 UI/mL), and streptomycin (100 µg/mL) was used in the culture. The growth medium of cells was changed every other day.

2.2.3.4. Culture of HUVEC on Vascular Patterned HAMA Hydrogel

No specific sterilization method was applied for HAMA hydrogels since these hydrogels were exposed to UV (4 min) during crosslinking and photoimmobilization steps. After crosslinking and photoimmobilization, the gels were washed with plenty of PBS prior to cell seeding. Cells were detached from T-flasks and suspended with trypsin (0.05%) solution for 5 min at 37˚C and 5% CO_2. Centrifugation and cell counting steps were done as described previously for RPE cells. Cell seeded on the hydrogels at a density of 15,000 cells/cm^2. After seeding, hydrogels were incubated

at 37˚C for 20 min, then 15 µL medium was added and to prevent drying. After further incubation for 20 min at 37˚C (5% CO_2), 3 mL medium was added to hydrogel membrane in wells of plates. The plates were incubated at 37˚C in a humidified 5% CO_2 incubator and mediums were replaced with fresh medium every second day. In addition, EGM-2 medium that contains hEGF (human endothelial growth factor), hydrocortisone, GA-1000 (Gentamicin, Amphotericin-B), FBS (Fetal Bovine Serum), VEGF (vascular endothelial growth factor), hFGF-B (human fibroblast growth factor), R3-IGF-1 (insulin-like growth factor), ascorbic acid, heparin was also used as angiogenic medium to induce vascularization of seeded HUVECs on microchannels.

2.2.3.5. Co-culture Studies of RPE and HUVEC

In the co-culture studies, only ColMA modified hydrogels were used as ColMA gave the best results in terms of cell adhesion and growth. For co-culture, initially, HUVECs were cultured on ColMA modified HAMA hydrogels and RPE cells were cultured on electrospun silk fiber mats separately for 2 days. In co-culture studies, a Teflon ring (inner area is 2 cm^2) was placed at the bottom of 12 well plate. Hydrogels were put at the center of the ring to be immobilized. Cell crown holders into which electrospun silk fiber mats were inserted were placed on top of HUVEC cultured hydrogel. These stacked, cell seeded scaffolds were cultured together with EGM-2 medium at 37˚C and 5% CO_2. DMEM high glucose was also used in co-culture studies in order to study the effect of medium composition on attachment and morphology of HUVEC and RPE cells by using confocal microscopy.

2.2.3.6. Cell Proliferation on Scaffolds

Cell proliferation on scaffolds was quantified by the Alamar Blue cell viability assay. The cell viability assay was performed for only D407 cells. Cell seeded and unseeded scaffolds were washed with PBS two times and incubated in Alamar Blue solution (1 mL 10% in DMEM-high glucose colorless supplemented with penicillin

(100 U/mL), streptomycin (100 µg/mL)) for 1 h at 37˚C and 5 %CO_2 condition. After incubation, the Alamar Blue solution (200 µL) was transferred into 96 well plates. The absorbance of transferred solution was determined at both 570 nm (λ_1) and 595 nm (λ_2) with Elisa plate reader (Molecular Devices, USA). The absorbance values were converted to 'percent reduction' by using the following equation:

$$\text{Reduction (\%)} = \frac{\left((\varepsilon_{ox})_{\lambda_2} x\, A_{\lambda_1}\right) - \left((\varepsilon_{ox})_{\lambda_1} x\, A_{\lambda_2}\right)}{\left((\varepsilon_{red})_{\lambda_1} x\, A'_{\lambda_2}\right) - \left((\varepsilon_{red})_{\lambda_2} x\, A'_{\lambda_1}\right)} x\ 100 \qquad (2)$$

where,

λ_1= 570 nm λ_2=595 nm

$A_{\lambda 1}$ and $A_{\lambda 2}$= Absorbance of test well,

$A'_{\lambda 1}$ and $A'_{\lambda 2}$= Absorbance of negative control well (blank)

Molar Extinction coefficients

$(\varepsilon_{ox})_{\lambda 2}$= 117.216 $(\varepsilon_{red})_{\lambda 1}$= 155.677

$(\varepsilon_{ox})_{\lambda 1}$= 80.586 $(\varepsilon_{red})_{\lambda 2}$= 14.652

A calibration curve was constructed to determine the number of cells on the scaffolds by applying the same experimental procedure with known cell numbers.

2.2.3.7. Microscopy Studies

2.2.3.7.1. Light Microscopy

HUVEC seeded hydrogels were observed with an inverted light transmission microscope (Olympus IX70, Japan) at x40 magnification. Micrographs of cells in the vascular pattern were obtained with the digital camera of the microscope.

2.2.3.7.2. Fluorescence Microscopy

HUVEC seeded on both glass coverslip and HAMA hydrogel were washed with PBS (10 mM, pH 7.4) and fixed with paraformaldehyde (4% w/v) for 15 min at room temperature. Cell membranes were permeabilized with the treatment of Triton X-100 (0.1% v/v in 10 mM Tris-HCl buffer) for 5 min at room temperature. After washing step with PBS, cells were incubated in BSA (1% w/v in PBS) at 37˚C for 30 min to prevent non-specific binding. Then, they were incubated in Alexa 488-labelled Phalloidin (1:50 dilution in 0.1% BSA in PBS) or Alexa 594-labelled Phalloidin (1:50 dilution in 0.1% BSA in PBS) for 1 h. at 37˚C and incubated with DAPI (1:500 dilution in 0.1% BSA in PBS) for 15 min at room temperature. Scaffolds were washed twice with PBS and stored in PBS solution and light protected by wrapping aluminum foil around the plate at 4˚C until analysis with a fluorescence microscope (Zeiss Axio Imager M2, Germany).

2.2.3.7.3. Confocal Laser Scanning Microscopy

HUVEC seeded hydrogels and D407 seeded silk fibroin fiber mats were stained for confocal microscopy analysis. The fixation and blocking were done as described in Section 2.2.3.7.2. After incubation in blocking solution (1% BSA in PBS), HUVECs were incubated Alexa488-labelled Phallodin, whereas; D407 cells were incubated in Alexa532-labelled Phalloidin at 37˚C for 1 h. Since silk fibroin is an autofluorescence material and give fluorescence signal around 488 nm, Alexa532-labelled Phalloidin was used to stain the cytoskeleton. Then, scaffolds were washed twice with PBS and incubated in DRAQ5 (1:1000 dilution in 0.1% BSA in PBS) for 30 min at room temperature to stain cell nucleus. After staining, cell seeded hydrogels and mats were washed with PBS and stored in PBS at 4˚C until analysis with a confocal laser scanning microscope (Leica DM2500, Germany).

2.2.3.7.4. SEM Analysis of Cells Cultured on Scaffolds

D407 seeded electrospun silk fiber mats were removed from cell culture media and washed twice with PIPES (piperazine-N, N'-bis(ethanesulfonic acid)) buffer. The scaffolds were fixed with 4% paraformaldehyde solution for 5 min at room temperature. After fixation, the samples were stained with 1% osmium tetroxide (OsO_4) and washed twice with PIPES buffer and dehydrated with ethanol series. After that, samples were coated with Au-Pd under vacuum and analyzed with a scanning electron microscope.

2.2.3.8. Immunocytochemistry Studies

2.2.3.8.1. Anti CD31 Staining of HUVEC

HUVEC seeded hydrogels that were co-cultured with D407 on fibroin mats and HUVEC seeded hydrogels (mono-cultured, control) were stained with antiCD31. The fixation and permeabilization steps were done as described in Section 2.2.3.7.2. Cell seeded hydrogels were washed with PBS and incubated in blocking solution (10% BSA in PBS) for 1 h at 37˚C. After incubation in blocking solution, samples were incubated in Alexa Fluor 488-labelled Anti Human CD31 (1:4 dilution in 1% BSA in PBS) at 37˚C for 1 h and again they were put in blocking solution (1% BSA in PBS) for 30 min at 37˚C. Then, scaffolds were incubated in Alexa532-labelled Phalloidin for 1 h at 37˚C and then in DRAQ5 for 30 min at room temperature. After all staining steps, scaffolds were washed with PBS and analyzed with a confocal laser scanning microscope (Leica DM2500, Germany

CHAPTER 3

RESULTS AND DISCUSSION

3.1. Characterization of Scaffolds

3.1.1. Characterization of Electrospun Silk fibroin Mat

3.1.1.1. ATR-FTIR Analysis of Silk Fibroin Mat

ATR-FTIR analysis was used to study the secondary structure of silk fibroin (SF) in terms of conformation and crystallinity. Basically, FTIR measures the transmission differences in vibration of the bonds such as the amide bonds (α-helix, β-sheet, or random coils). SF has characteristic vibration bands around 1641 cm^{-1}, 1514 cm^{-1}, 1230 cm^{-1}, 1445 cm^{-1}, and 670 cm^{-1} were assigned to the absorption bands of the peptide amide I (C=O stretching), amide II (N-H bending), amide III (C-N stretching), and amide IV, respectively. These characteristic peaks demonstrate the presence of a hydrogen-bonded N-H group (Zhang et al., 2012; Zhou et al., 2010). In Fig.13 the FTIR of silk fibroin strong peaks were observed at 1641, 1514 and 1230 cm^{-1}. According to the literature strong characteristic bands at 1622 cm^{-1}, 1515 cm^{-1} and 1232 cm^{-1} show β-sheet conformation of the SF after methanol vapor treatment (Das et al., 2015). After methanol vapor treatment, the Amide I peak of the SF spectra moved from 1641 cm^{-1} to 1622 cm^{-1} probably due to the conversion of random coil conformation to β-sheet of SF. MeOH vapor treatment was used to induce crystallization of SF. In this way, mechanical strength of mats was increased.

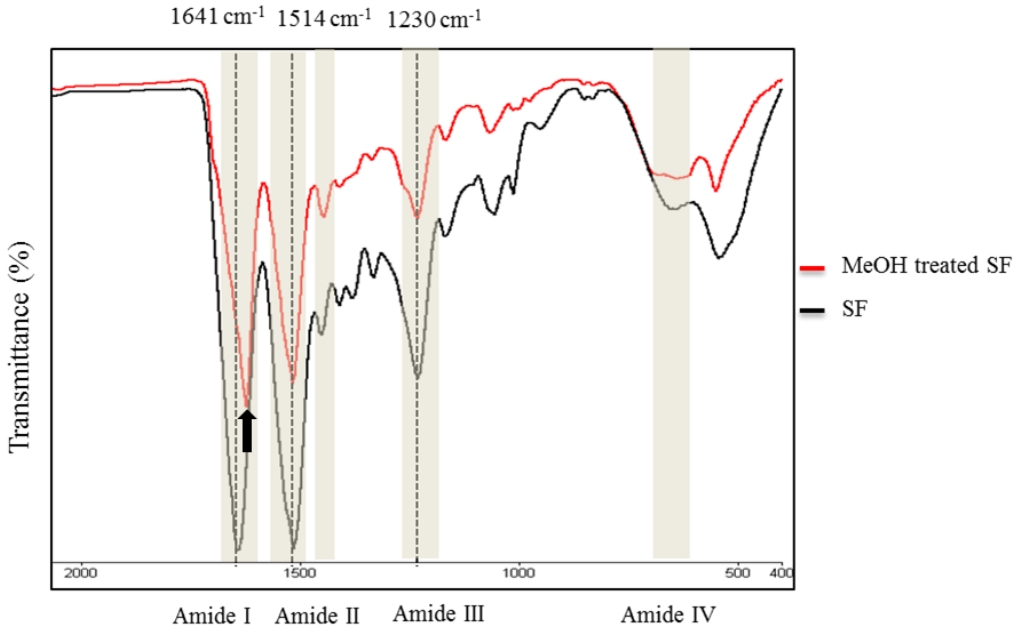

Figure 13. FTIR-ATR spectra (2000 cm^{-1} and 400 cm^{-1}) of untreated and methanol vapor treated silk fibroin mat. The bands around 1641 cm^{-1}, 1514 cm^{-1} and 1230 cm^{-1} indicate characteristic amide bands of SF.

3.1.2. Scanning Electron Microscopy (SEM) of Silk Fibroin Mat

In this study, electrospun silk fibroin fiber mat (ESF) was used as scaffold to mimic Bruch's membrane of the retina structure. ESF was used to mimic natural Bruch's membrane due to its fibrillar structure which serves as a molecular sieve between RPE and choriocapillaris. The SEM of electrospun silk fibroin fiber mat was analyzed with NIH ImageJ for the fiber alignment, fiber thickness and morphology (Fig. 14A and Fig. 14B). As expected a random deposition of SF fibers was observed on the mats collected on a smooth copper collector.

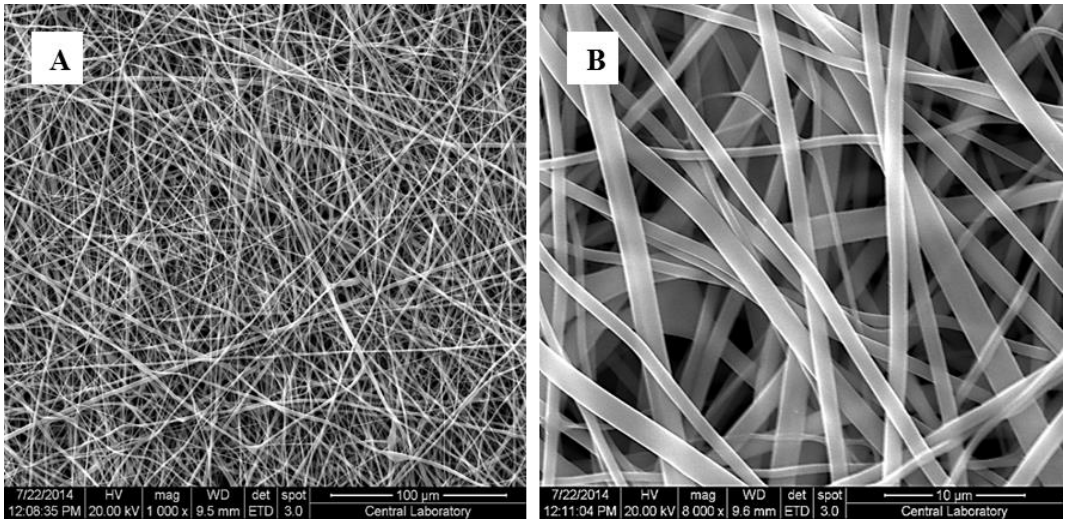

Figure 14. SEM micrographs of electrospun silk fibroin fiber mats (ESF). x1000 and x8000. Micrographs show random fiber orientation and a mean fiber diameter size of about 1 µm.

Similar data was generated using SEMs of silk fibroin fiber mats (ESF) produced with various fibroin concentrations and potentials (Table 2).

Table 2. The fiber diameters of silk fibroin mats produced by electrospinning. (Solvent: HFIP, Distance: 10 cm and 5 µL/min flow rate)

	Fibroin Concentration (% in HFIP)	Potential (kV)	Fiber thickness (µm)
SF Batch I	20 %	20 kV	0.87 ± 0.22
		15 kV	0.88 ± 0.52
		10 kV	0.84 ± 0.20
	15 %	20 kV	1.41 ± 0.24
		15 kV	0.51 ± 0.12
		10 kV	0.85 ± 0.20
SF Batch II	10 %	15 kV	1.00 ± 0.30

Batch differences were observed in the isolation of fibroin and these affected the morphology and thickness of formed fibers. These batch differences might be due to freeze drying conditions as the water removal from frozen fibroin solution might

induce self-assembly and can change water solubility. For the Batch I, the obtained mats were not as strong as the mats that were produced by Batch II. Batch II, which can be solubilized completely in hexafluoroisopropanol (HFIP), at 10% concentration and 15 kV voltage gave the best results in terms of homogenous fiber formation and the optimum mat strength. Therefore, the electrospun fibroin mats from those conditions were employed through the in vitro cell culture studies. The average fiber diameter and the average thickness of the ESF (n=4) from these conditions were measured as 1 μm and 25 μm, respectively (Table 1).

3.1.4. Characterization of Methacrylated Hyaluronic Acid (HAMA)

Methacrylate group was bound to the chain of hyaluronic acid to be able to photocrosslink it later. Thus, HAMA would be crosslinked by UV irradiation and hydrogels could be prepared in the desired shape. The synthesized HAMA was analyzed with FTIR-ATR to confirm the methacrylation of the hyaluronic acid (Fig. 15). The absorption band observed around 1730–1690 cm^{-1} corresponds to the C=O group of the methacrylate introduced in the chain. It can come from the methacrylate group. In addition, the shoulder peak of HAMA around 1640 cm^{-1} that corresponds the C=C double bond indicates the incorporation of methacrylate group in the HA chain (Coutinho et al., 2010). These show that the introduction of methacrylate group into the HyA was successful.

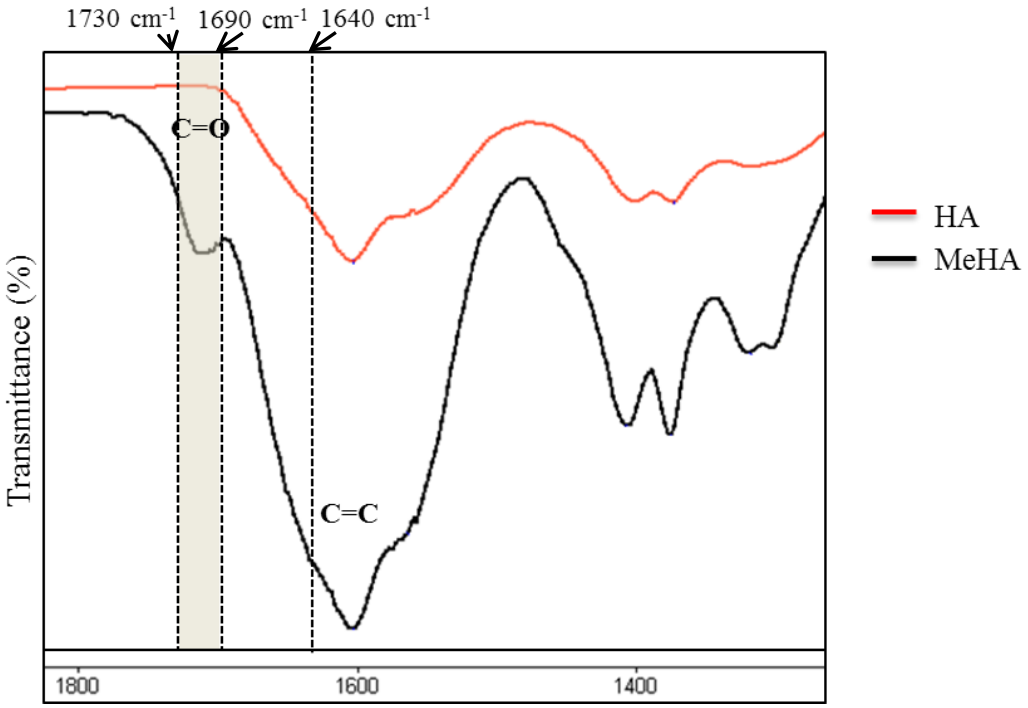

Figure 15. FTIR-ATR spectra of hyaluronic acid (HA) and methacrylated hyaluronic acid (HAMA). The absorption band present around 1730–1690 cm^{-1} corresponds to the C=O group of the acrylate ester introduced in the chain. The shoulder peak around 1640 cm^{-1} indicates C=C double bond of methacrylate group.

3.1.5. Characterization of Micropatterned Methacrylated Hyaluronic Acid Hydrogel

3.1.5.1. Swelling of HAMA

The degree of the swelling of HAMA hydrogels was calculated by using Equation 1 (see section 2.2.2.2.1). Ideally, slight or no significant swelling is desired to protect the fidelity of micropatterns in the hydrogel during in vitro testing. After immersing into PBS at 37˚C, weights of the dried hydrogels increased abruptly in 4 h and leveled off at 24 h. After 2 h no significant degree of swelling change was observed

(Fig. 16). The swelling degree of hydrogels reached 97% within 2 h and it reached equilibrium and water content of them did not change after 2 h incubation.

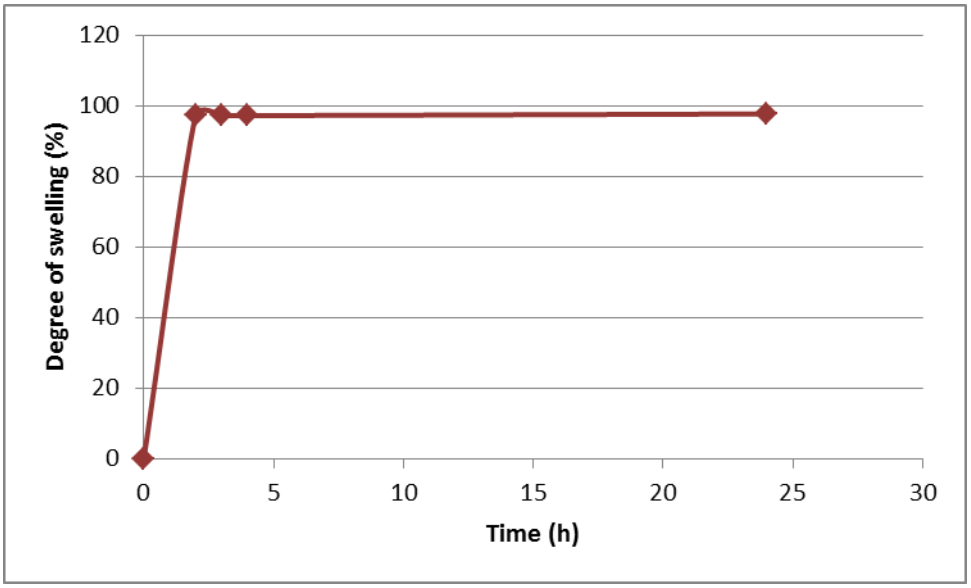

Figure 16. Degree of swelling of freeze dried HAMA hydrogel in PBS at 37˚C (average was taken from three gels).

3.1.5.2. Morphology of HAMA Membrane

In the design, the UV crosslinked hydrogel sheets were used to serve as the choroid layer. SEM micrographs show a porous internal structure (Fig. 17A) and a smooth surface (Fig. 17B). The micrographs clearly show that hydrogels have open and interconnected pores. Irregular pore size distribution was obtained upon freeze-drying because the pore size distribution is determined by freezing kinetics (Verhulsel et al., 2014). These results showed that the photocrosslinked hydrogel layer could transfer nutrients, waste products and other bioactive factors in the culture medium.

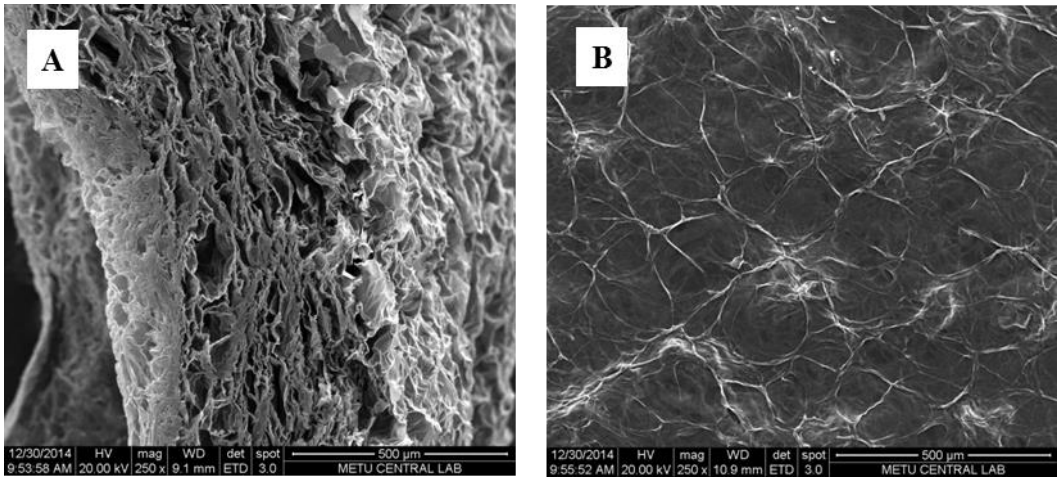

Figure 17. SEM micrographs of freeze dried HAMA hydrogels. (A) SEM micrograph showing vertical cross-section and, (B) surface of the freeze dried HAMA hydrogel. (x250). Scale bar: 500 µm.

3.1.5.3. Characterization of Micropatterned HAMA Membrane

3.1.5.3.1. Stereomicroscopy

Initially, a fractal tree pattern was created on template (PU-8 photoresist) by using photolithography mimicking the vascular layer on hydrogel according to section 2.2.1.2.2. Stereomicrograph of the photoresist with sharp contours and smooth surface is shown in Fig. 18. The pattern fidelity or regularity on the photoresist is an important parameter to create desired shape in hydrogel since photoresist is a master mold for silicone replica, and in turn, for hydrogel micromolding. Adequate pattern transfer from the template generates a proper PDMS mold, thus a vascular pattern can be produced in hydrogel accurately. In the present case, microchannels were successfully formed as a fractal tree pattern on the photoresist.

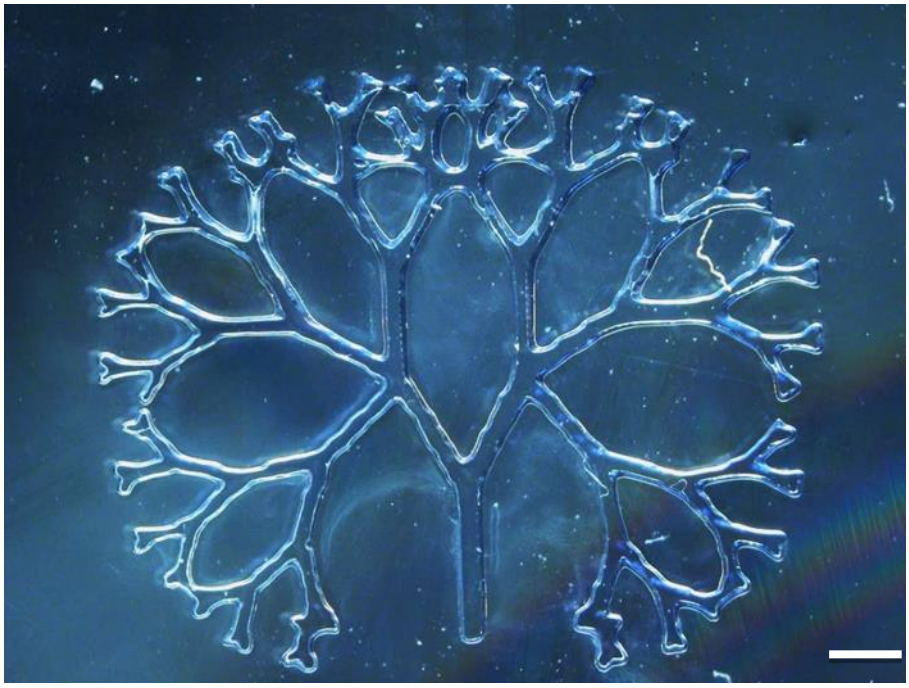

Figure 18. The stereomicrograph of PU-8 photoresist template for PDMS mold preparation. Vascular pattern on the template was clearly seen as grooves. Scale bar: 100 μm.

3.1.5.3.2. Surface Profilometry of PDMS Mold

The pattern fidelity of PDMS mold was investigated by using Non-Contact, 3D Optical Surface Profilometer. Fig.19 shows the tree pattern on the PDMS mold in the form of a continuous network without any defects and discontinuities.

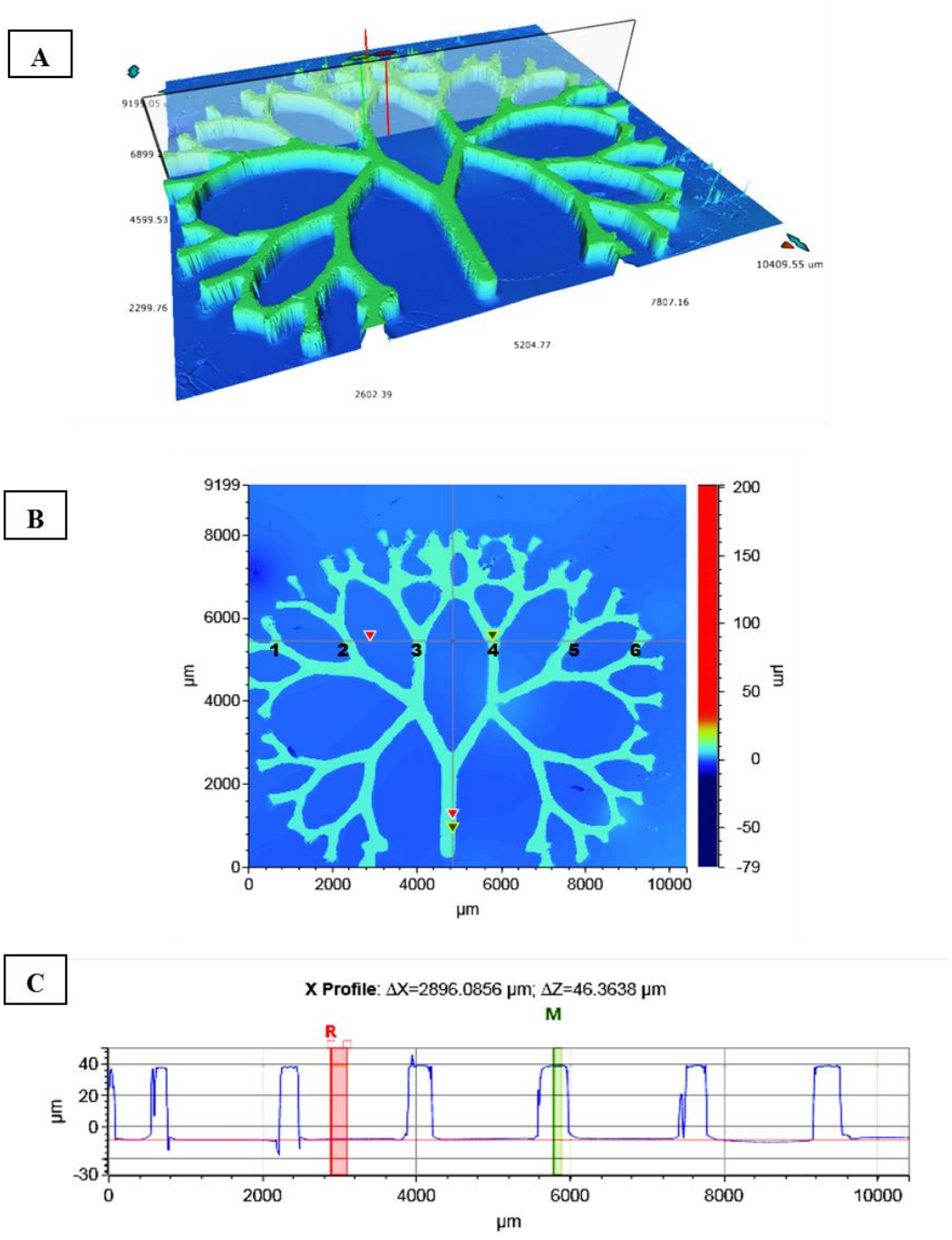

Figure 19. Non-contact, 3D optical surface profile measurement of PDMS mold. (A) 3D scanned micrograph of PDMS mold, and (B) top view are shown with X and Y scan. (C) Profiler also shows the depth of microchannels at the z-stack (50 µm scan).

Table 3. The pattern dimensions on PDMS mold measured by profilometry. Channel numbers (1, 2, 3, 4, 5 and 6) refer to the channels of Fig.19B.

Channel No	**1**	**2**	**3**	**4**	**5**	**6**
Channel Diameter (μm)	260	301	387	453	412	405

Fig. 19A represents 3D scanned micrograph of PDMS mold and Fig. 19B shows the top view image of the mold with X and Y scans. Fig. 19C shows the depth of microchannels at the z-stack. Since only 50 μm of the ridge was scanned, they are equal to each other. The widths of the patterns were found to decrease from trunk to branches of fractal tree (320-450 μm). The decrease in pattern diameter towards the tip of branch is clearly seen. The width of the patterns from perimeter to center of fractal tree (numbers 1-3) were 387 μm, 301 μm and 260 μm, respectively (Fig. 19A) (Table 2).

3.3. In Vitro Experiments

In the in vitro studies, the cell lines D407 retinal pigment endothelial cells (RPE) and human umbilical vein endothelial cells (HUVEC) were used to assess cell behavior like adhesion, proliferation and expression of differentiation markers on the structures.

3.3.1. RPE Culture on Bruch's Membrane

3.3.1.1. Cell Proliferation Assay

D407 RPE cell line was used in the in vitro studies to examine cell attachment and proliferation on the electrospun silk fiber mats. Electrospun silk fibroin fiber mats served to mimic Bruch’s membrane of eye. This type of structure not only mimics the fibrous extracellular matrix ECM but also allows transport of cellular signals but

prevents crossing of the cells. Proliferation of the RPE cells seeded on these fibrous scaffolds was determined with Alamar Blue Assay. The cell number on Day 1, 3, and 7 were calculated (Fig. 20) by using a calibration curve prepared with known cell numbers (Appendix Fig. 41). The cell number on the fibroin mats increased in the first seven days, however, it decreased in the next week. This result was obtained probably because the cells reached confluency on day 7 and prohibited cell proliferation. On the other hand, the tissue culture poly styrene surface (TCPS) control showed a gradual increase in the cell number during the first week and it did not change significantly (or decreased slightly) in the second week. This probably was due to the confluence of the cells in the first seven days and limited space for the attachment of cell. When the trends on TCPS and ESF are compared it is realized that TCPS had a large area (4 cm^2) than the surface of ESF (1.54 cm^2). Therefore cell number on silk fibroin decreased significantly; whereas cell number on TCP remained stable at second week since TCPS surface area is 2.5 times higher than ESF.

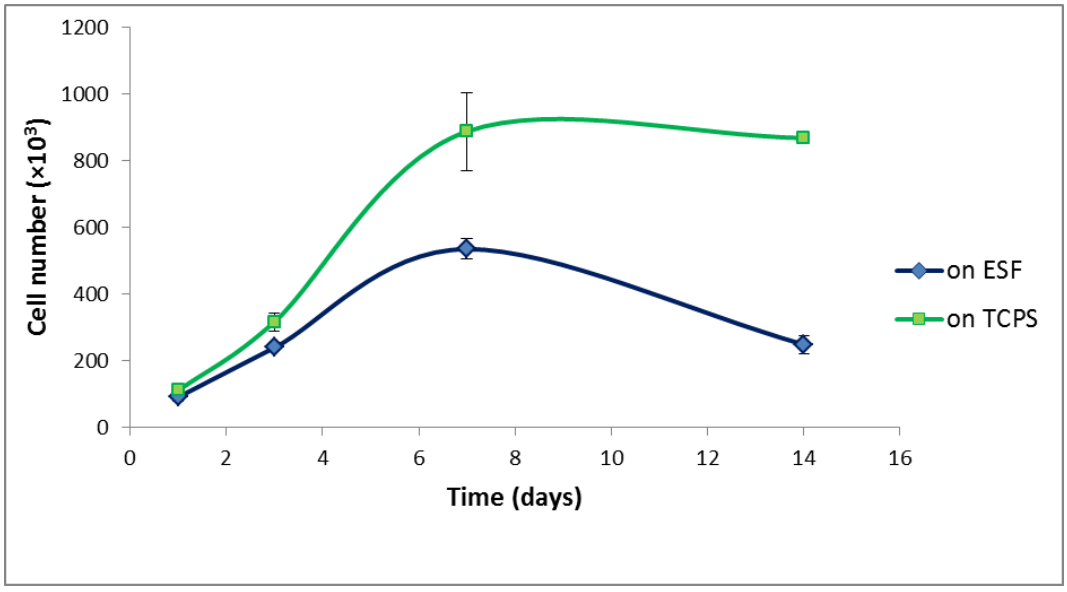

Figure 20. Cell proliferation of retinal pigment epithelial cells (RPE) on ESF and TCPS (cell seeding density: $3x10^4$; DMEM-high glucose medium).

3.3.1.2. SEM Analysis

The SEM micrographs of the RPE cells on ESF are presented in Fig.21. The cells adhered on the surface and cell protrusions through the fibers are clearly seen.

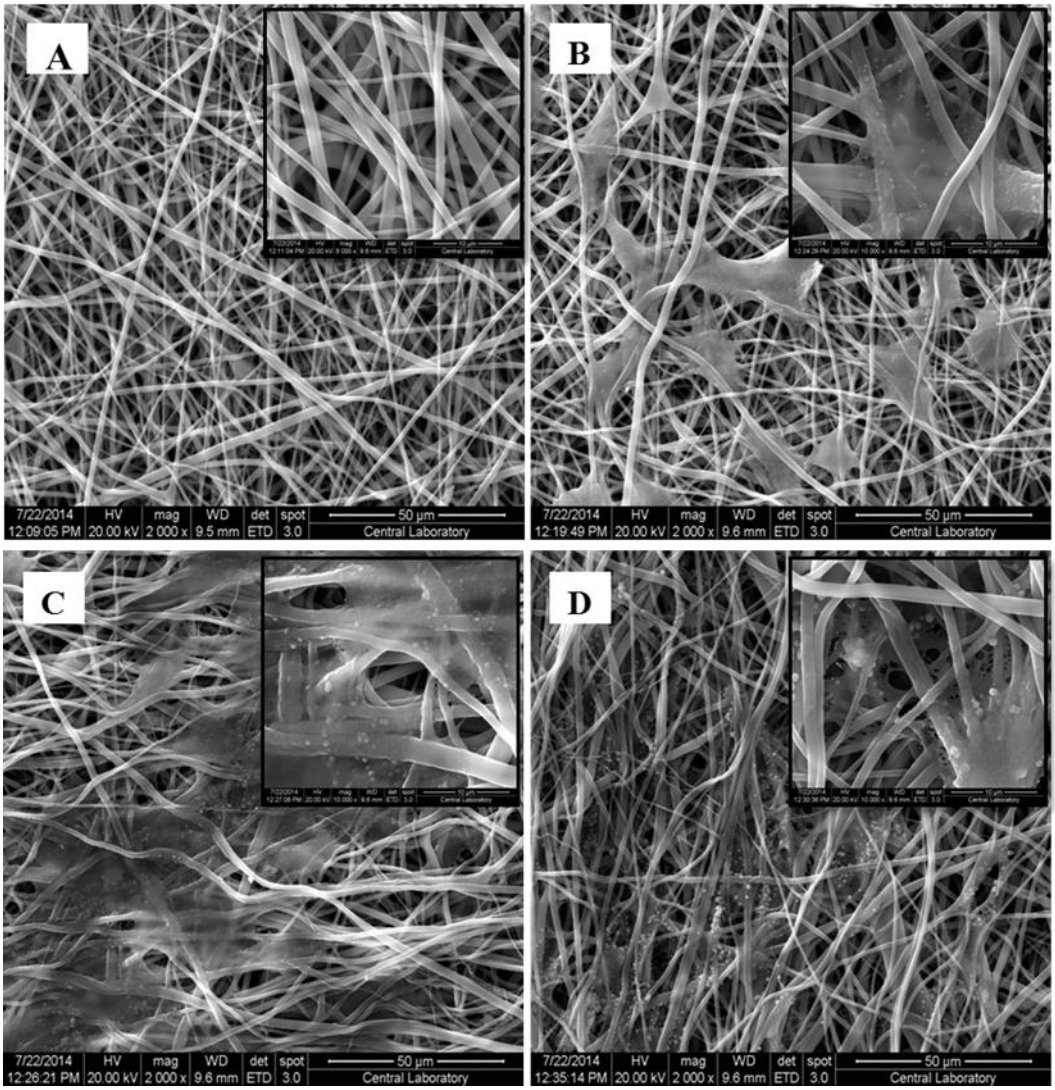

Figure 21. SEM micrographs showing the surfaces of ESF structures. (A) Cell free and (B-D) RPE seeded on Days 1, 3 and 7. Cell seeding density: $3x10^4$, DMEM High medium. Scale bar: 50 µm.

On day 1 (Fig. 21B), cells were seen attached and spread on the fibers individually. During later days, the cells came together and formed a partial cell sheet on some

regions of the ESF as seen on day 3 (Fig. 21C). During this stage cells were seen as thin sheet and fibers could be seen behind cell membrane. On day 7 (Fig.21D), intracellular vesicles of RPE cells increased by compared with day 3. Retinal pigment epithelial (RPE) is one of the most active phagocytic cells and can eliminate photoreceptor fragments actively (Mao et al., 2013). Therefore, this event shows that RPE cells started their normal physiology on fibroin mat. Also, RPE began to die after seven days because of limitation in surface area for cell attachment. Therefore, RPE cells might show phagocytic activity against cell debris and increase their vesicle formation. After 7 day culture, they started to migrate between the fibers, but it is an undesired situation. In our case, the main aim is to form an epithelium and so that they can form a confluent cell layer. Since retinal pigment epithelium separate photoreceptors from the choriocapillaries and provide a barrier between them, a distinct cell layer of RPE is desirable. RPE cells monolayer provides blood-retinal barrier by forming tight junctions. In this case, the average fiber diameter of ESF (1 μm) may be thick and they created large pores between fiber that allow the proliferation of cell between the fibers. Migration of cell through the scaffold is normally preferred in the tissue engineered constructs, but single cell layer of RPE can only perform its typical functions in retina. Thus, fiber diameter can be decreased in the range of 100-500 nm to provide small pores on the ESF.

3.3.1.3. Confocal Laser Scanning Microscopy

Confocal micrographs of RPE cells seeded scaffolds are shown in Fig. 22. Cytoskeleton of the cell was stained with Alexa Fluor® 532 Phallodin and cell nuclei were stained with DRAQ5. Since SF is auto-fluorescent, it can be detected clearly without staining. The images show that cell numbers increased over time this is agreement with Alamar Blue cell proliferation results obtained in Fig. 20. On the ESF surface, characteristic hexagonal shape of RPE is seen which covered the surface on Day 7 extensively. Thus, results showed that SF fibers are suitable for both attachment and proliferation of RPEs.

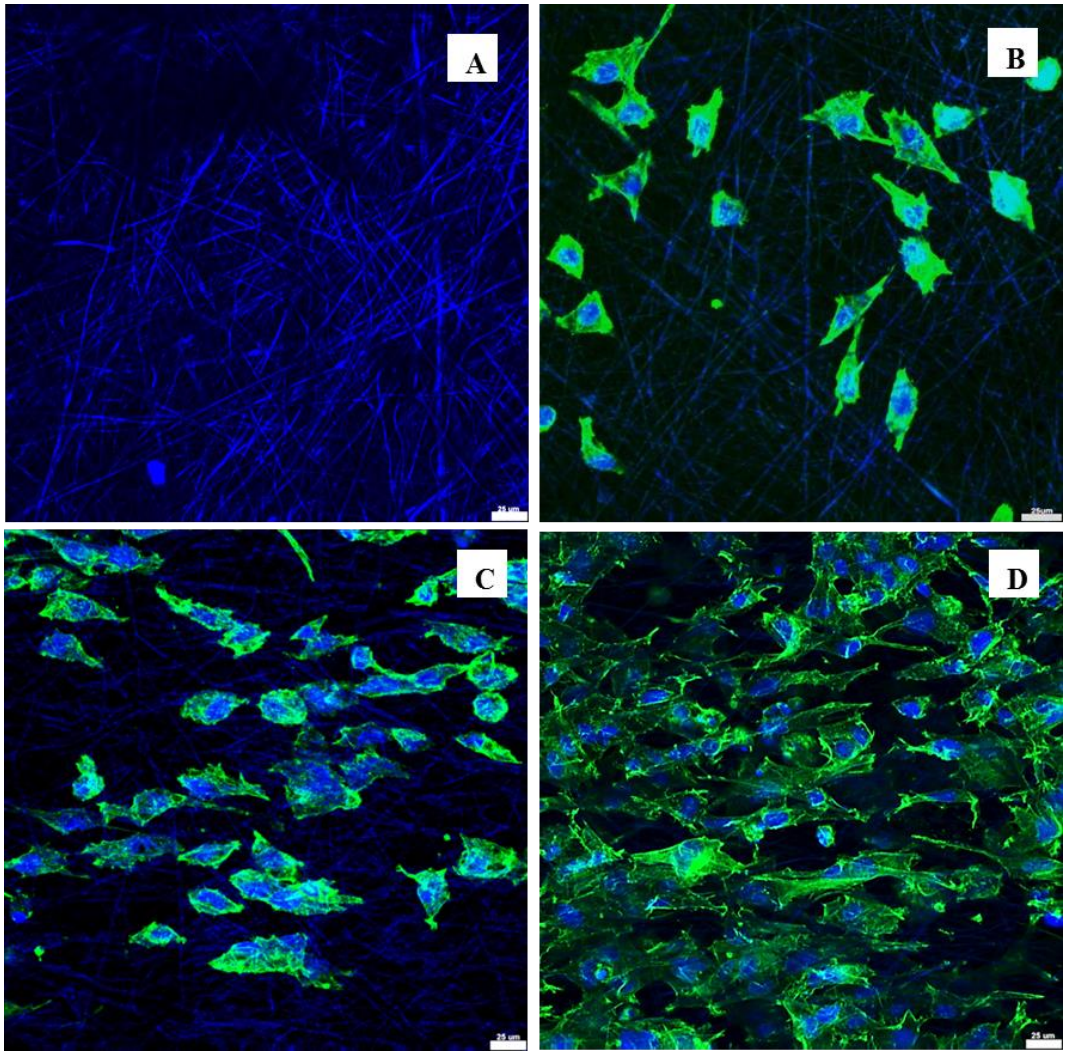

Figure 22. Confocal micrographs of ESF and RPE-seeded ESF surfaces. (A) Cell free and (B-D) RPE-seeded ESF surfaces on Day 1, 3 and 7, respectively. Alexa Fluor® 532- Phalloidin (green) and DRAQ5 (blue) were used for actin and nucleus staining, respectively. SF fibers were seen blue by autofluorescence behind the cells. Cell seeding density: $3x10^4$, DMEM-high glucose medium. Scale bar: 25 µm. Magnification (x200).

In a recent study, RPE cells were cultured on solvent-cast Bombyx mori silk fibroin (BMSF) membranes (Shadforth et al. 2012). In this study, poly(ethylene oxide) was added in the fibroin aqueous solution to create pores into BMSF membranes. ARPE-19 RPE cell line were seeded on membranes and they demonstrated validity of silk

fibroin in the culture of RPE cell in terms of permeability of membranes and cell proliferation (Shadforth et al., 2012).

3.3.2. HUVEC Culture on Microchannel Network as Choroid Layer

HUVEC cell line was used to seed on HAMA hydrogels membrane to mimic the choriocapillaries to serve as a supporting layer for Bruch's membrane. Micropatterning technique was used to guide endothelial cells to form vascular network. Cell morphology, attachment, and proliferation were studied with various hydrogel compositions and surface modifications using various cell attachment molecules.

3.3.2.1. Microscopy

3.3.2.1.1. HUVEC on HAMA Hydrogel

Fluorescence micrographs of HUVECs seeded on HAMA hydrogel membrane and glass substrates (positive control surface) on day 2 are seen in Fig. 23. It was observed that cells did not spread well on the hydrogel (Fig. 23B) while they attached and spread well on the glass substrate (Fig. 23A). Cell protrusions and cytoskeleton of the cells were clearly seen in the cell seeded on the glass substrate. HUVECs were seen to have characteristic flat, cobblestone morphology with large nuclei inside the cell on the glass substrate. Whereas, on the hydrogel they had a round shape and aggregated. It is known that cells cannot adhere on very hydrophilic surfaces. Hyaluronic is known for its poor cell adhesiveness and its modification with some cell adhesive compounds, such as collagen (Suri and Schmidt, 2009), fibronectin (Seidlits et al., 2011) and RGD peptide (Lei et al., 2011; Park et al., 2003) were tested to improve cell attachment.

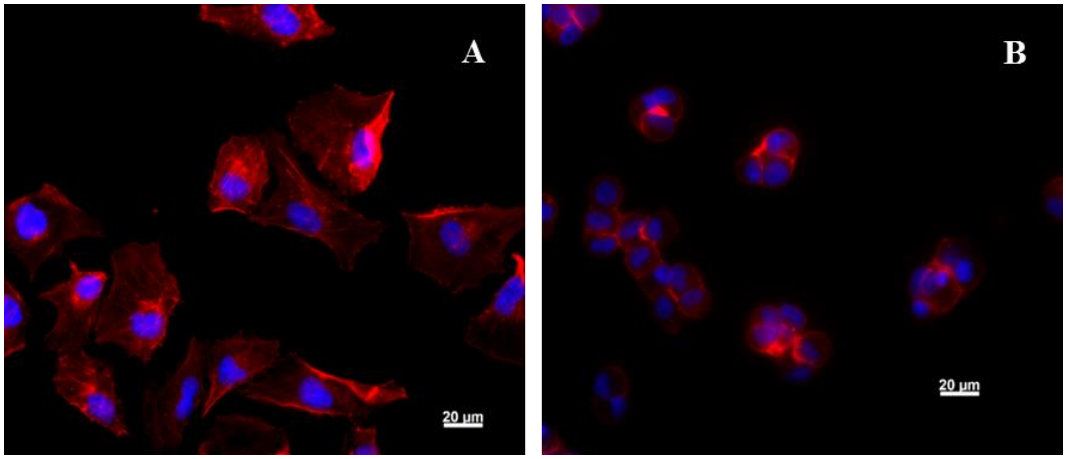

Figure 23. Fluorescence micrographs of HUVEC. (A) On glass substrate and (B) HAMA hydrogel. Day 2. DAPI stain nucleus (blue) and Alexa Fluor® 594 Phallodin stain cytoskeleton (red).

Cell culture studies on unmodified HAMA hydrogels did not yield satisfactory results in the following vascularization studies. It was observed that cells did not adhere to the surface and could not proliferate to form vascular structures. In order to improve cell adhesion and vascularization of HUVEC, cell attachment factors were used on the hydrogel. For this purpose, the hydrogel surfaces were modified with cell adhesive molecules fibronectin, gelatin and collagen.

3.3.2.1.2. HUVEC on GelMA:HAMA Hydrogel

Fig. 24 represents phase contrast micrographs of HUVEC on methacrylated gelatin:methacylated hyaluronic acid (2:3) hydrogel on Day 16. GelMA was blended with HAMA and then the mixture was crosslinked with UV to generate a 3D hydrogel scaffold. Gelatin is a natural protein that is obtained from hydrolysis of collagen and its bioactivity resembles collagen. Arginine, glycine, aspartic acid (RGD) sequence, which is an essential attachment factor of fibronectin, presents on the gelatin. Lysine residues on the chain of gelatin provide chemical modification like methacrylation to enable crosslinking with UV. GelMA is a promising material

to culture cell on and encapsulate into it in terms of its high cellular compatibility, enzymatic degradability and photocrosslinking property (Hutson et al., 2011).

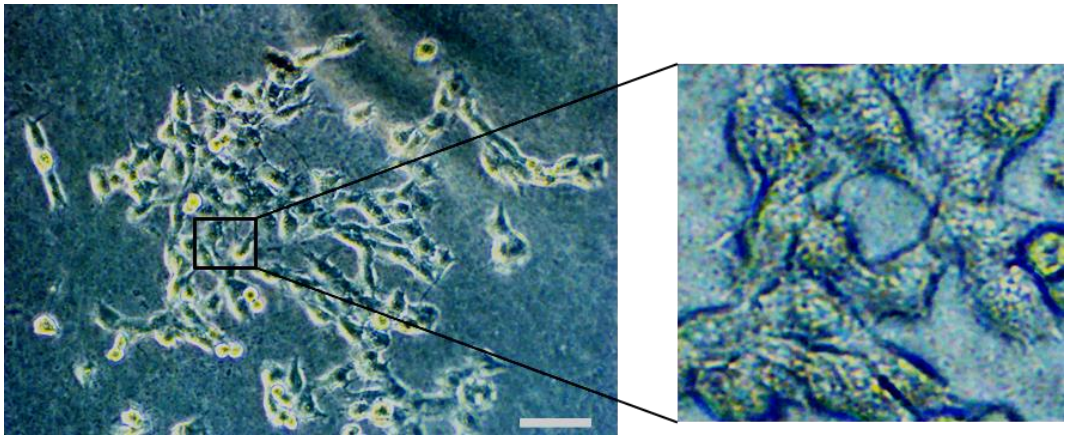

Figure 24. Phase contrast micrographs of HUVEC on GelMA:HAMA (2:3) blend hydrogel on Day 16. Scale bar: 100 μm.

Unlike HAMA hydrogel, on the GelMA:HAMA cells were seen to elongate and adopt the typical cobblestone morphology. This increased cell attachment was due to the protein content of GelMA. GelMA has advantage over gelatin since it can be easily photocrosslinked with UV and allows photolithographic processes. HAMA and GelMA can form interpenetrating and crosslinked polymer network (IPN) since both are photocrosslinkable. If gelatin and HAMA was used to generate a hybrid construct, only gelatin would be entangled in the HAMA network and it creates semi-IPNs (SIPN). IPN increases the mechanical strength of final 3D construct with increasing crosslinking groups of the two polymers as both polymers have methacrylate groups. In addition, GelMA composition in the GelMA-HAMA hydrogel does not erode fast with degradation since it is crosslinked covalently via methacrylate group. In a recent study, Camci-Unal et al. (2013) designed a similar hydrogel that composed of GelMA and HA methacrylate (HAMA) and HUVEC were seeded on the construct. They used hybrid hydrogel since hyaluronic acid alone does not support cell adhesion and gelatin has low mechanical strength due to their fast degradation. By blending both biopolymers they created a promising hybrid

hydrogel structure for the application in cardiovascular tissue engineering. HUVECs were both cultured as 2D on the surface and as 3D by encapsulating in IPN hydrogels. They found that cell attachment and spreading increased with addition of GelMA. When UV exposure was increased, the hydrogel stiffness and cell spreading increased on the 2D. In the 3D, cell spreading decreased with increasing gel stiffness probably because excess crosslinking prevented cell penetration and stretching (Camci-Unal et al., 2013).

3.3.2.1.3. HUVEC on FN Modified HAMA Hydrogel

In our study, initially fibronectin (FN) was used to modify microchannels of hydrogel because fibronectin interacts with the endothelial cells via the integrins on the cell surface and this interaction is necessary for angiogenesis. In order to immobilize fibronectin on the hydrogel, sodium benzoate was used to create free radicals by exposure to UV, then fibronectin was bound the parts exposed to UV through a photomask were activated. Then, HUVECs were seeded on the hydrogel membrane expecting to see the HUVEC at the exposed channels. Fig. 25 shows confocal micrographs of HUVECs cultured on fibronectin modified parts of the hydrogel on day 8. Fig. 25A, B and C show that cells attached in the microchannels. Fig. 25D shows z-stack of cells that fill the channel. It was observed that cells attached on the surface but did not extend. This may be the result of the insufficient amount of FN immobilized in the microchannel. Besides, sodium benzoate might not have been an effective photoinitiator. Acryloyl groups can be attached to fibronectin in order to provide effective immobilization by crosslinking on the channel of the hydrogel.

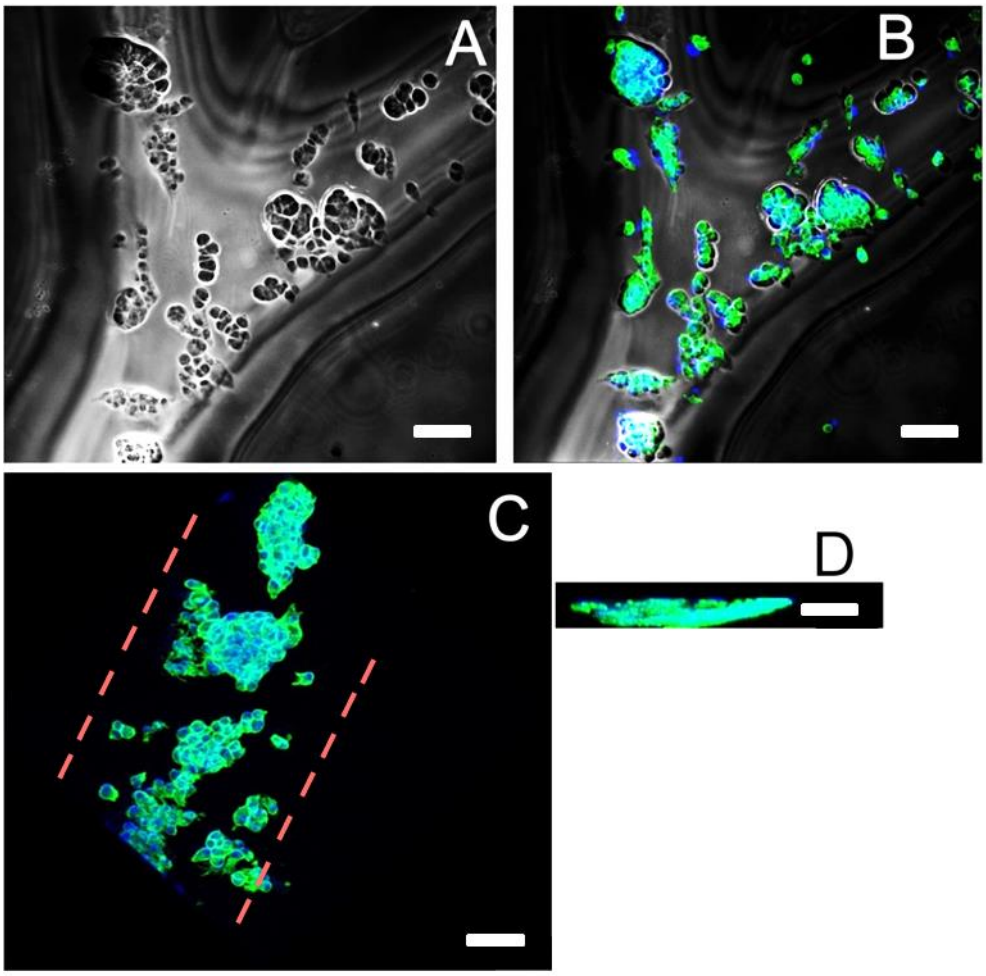

Figure 25. Confocal micrographs of cultured HUVEC on fibronectin modified HAMA hydrogel. (A) Light reflection image of microchannel of hydrogel seeded with HUVEC, (B, C) confocal merged image of actin and nucleus staining of HUVEC in the FN modified micro channels, (D) cross section of a channel with HUVEC. Actin (green)-Alexa Fluor® 488 Phallodin and nucleus (blue)-DRAQ5. Scale bar: 75 μm.

Seidlits et al. (2011) also used photocrosslinkable fibronectin attached on methacrylated hyaluronic acid hydrogel surface by UV illumination. In another study, they modified HA hydrogel with RGD peptide instead of FN to promote endothelial cell adhesion and to initiate angiogenesis. However, they observed that RGD sequences can interact with several integrins that cause signals to induce

specific phenotype. On the other hand, RGD sequences within tertiary structure of fibronectin can provide more efficient binding to specific integrins for initiating angiogenesis (Leach et al., 2004). Therefore, they encapsulated HUVEC in the FN-HA composite hydrogels and observed cell attachment, proliferation and migration in the 3D hydrogel constitute. In this composite scaffold, both HA and FN promoted angiogenic phenotype of HUVEC by binding of FN to angiogenesis specific integrins and interaction of HA with cell surface proteins like CD34 and RHAMM (hyaluronan-mediated motility receptor) (Seidlits et al., 2011).

In our case, alternatively, the method of FN immobilization may be changed. However, since modification is desired only in the microchannel, cell attachment factor should be a photosensitive material to provide immobilization with UV through negative photomask. For example, a photosensitive group like acryloyl can be incorporated on the FN. In this study, instead of FN, GelMA and ColMA were tested to modify the microchannels as they are both photosensitive and support the cell attachment effectively.

3.3.2.1.4. HUVEC Culture on GelMA Modified HAMA Hydrogel

After observing improved cell attachment with GelMA, masked photoimmobilization of HAMA in the microchannels was tried. In this way, both physical (microchannels) and chemical (cell attachment factor-GelMA) cues were provided to HUVEC in the process of vascularization. Fig. 26 shows phase contrast micrographs of HUVEC on GelMA modified HAMA hydrogel. Since GelMA was immobilized only in the channels, cell attachment was confined into the channels. Cells took spindle-like shape, elongated through channels and extended protrusions. It showed the success of gelatin immobilization in the microchannels and increased cellular compatibility with GelMA.

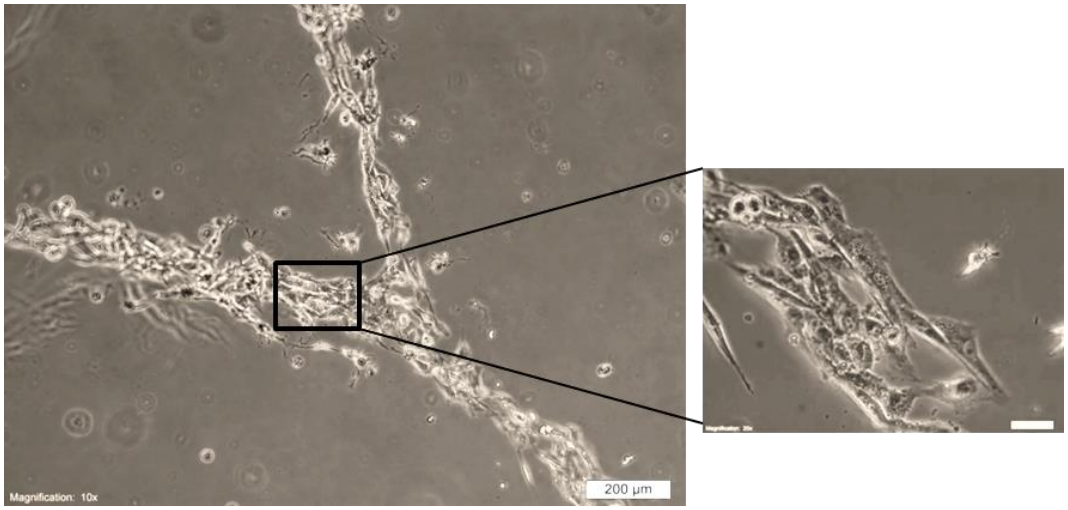

Figure 26. Phase contrast micrographs of HUVEC cultured on the fractal tree pattern that was photoimmobilized with GelMA within HAMA membrane on Day 5.

HUVEC seeded on GelMA modified hydrogels were also analyzed with confocal laser scanning microscopy to see the cytoskeleton organization and morphology of cells clearly (Fig. 27). HUVEC spread extensively on the modified region of the gel unlike on the FN modified hydrogels where limited extension was observed. Cell interactions were also clearly seen.

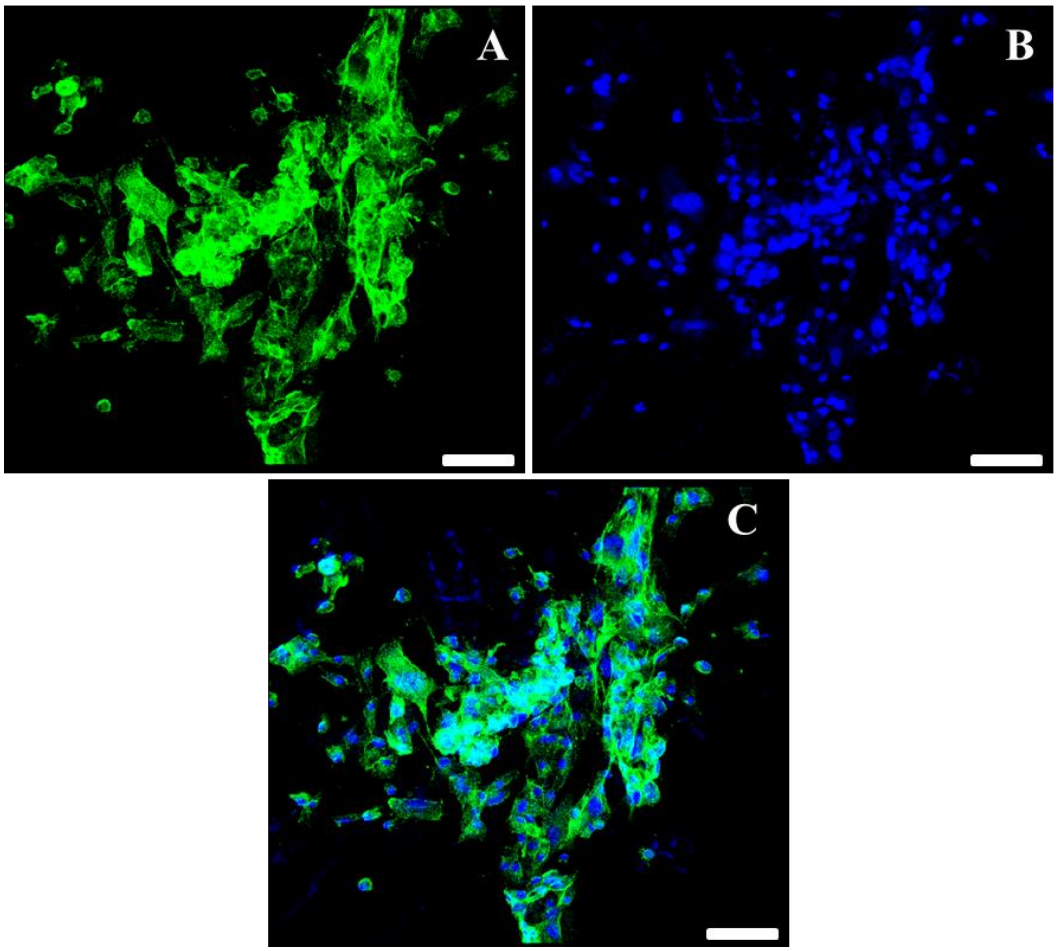

Figure 27. Confocal micrographs of HUVECs on GelMA modified HAMA hydrogel membrane on Day 8. (A) Actin, (B) nucleus and (C) merged image of HUVECs in microchannel of the hydrogel. Alexa Fluor® 488 Phalloidin (green) for actin and DRAQ5 (blue) for nucleus. Scale bar: 100 μm.

3.3.2.1.5. HUVEC on ColMA Modified HAMA Hydrogel

In this study, collagen type I was also used to modify the surface of the microchannels of HAMA hydrogel. Collagen molecule has a triple helix structure which was expected to increase cellular interactions compared with randomly folded gelatin molecule. As was observed with GelMA, cells attached only to the microchannels (Fig. 28). Few dead cells were seen on the unmodified regions on the gel. Cells showed the characteristic cobblestone shape within the microchannels.

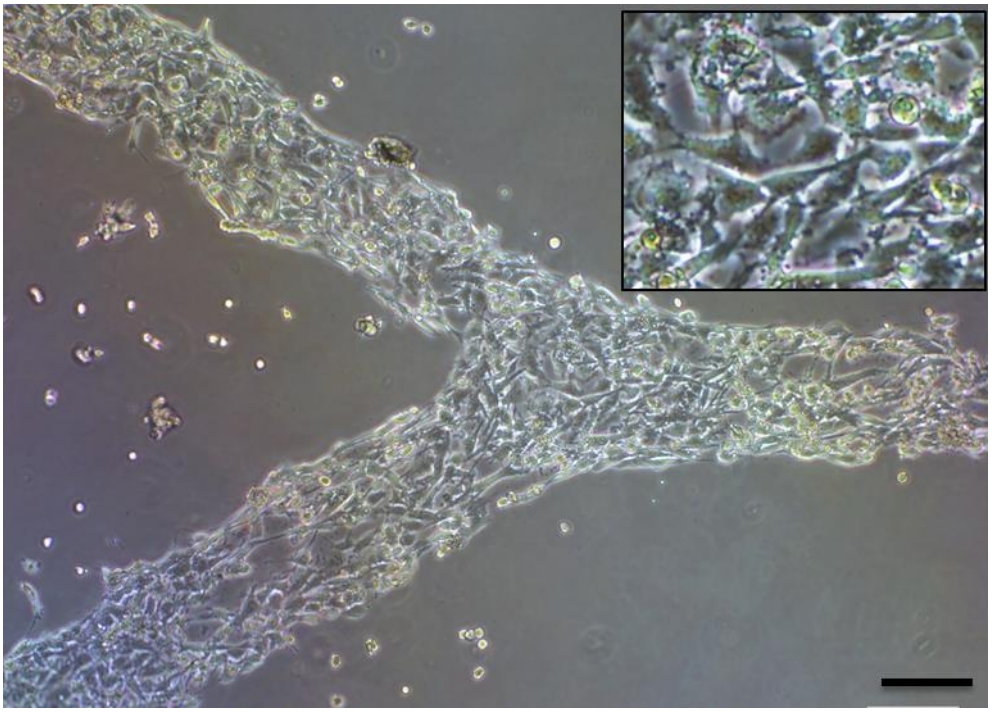

Figure 28. Phase contrast micrographs of HUVEC on the ColMA-modified tracks within HAMA hydrogel membrane on day 3 (in angiogenic EGM-2 medium). Inset: Magnified version of micrographs shows HUVEC morphology. (x40) Cell seeding density: 2×10^4, scale bar: 200 μm.

Similar to phase contrast micrographs, confocal micrographs of HUVEC were shown that cells adhered only on the microchannels and increased in number with time (Day 10) (Fig. 29). More cells adhered on microchannels and cell guidance was better on ColMA modified hydrogel when compared with GelMA and FN modified hydrogel. Fig. 29A shows the combined images of cells stained for actin and nucleus. Cells completely filled the microchannels of the hydrogel during the 10 days of culture. CD31 staining for cell marker of HUVEC showed the marker positive cells filling the microchannel track (Fig. 29B). Light reflection imaging also confirmed this (Fig. 29C-D).

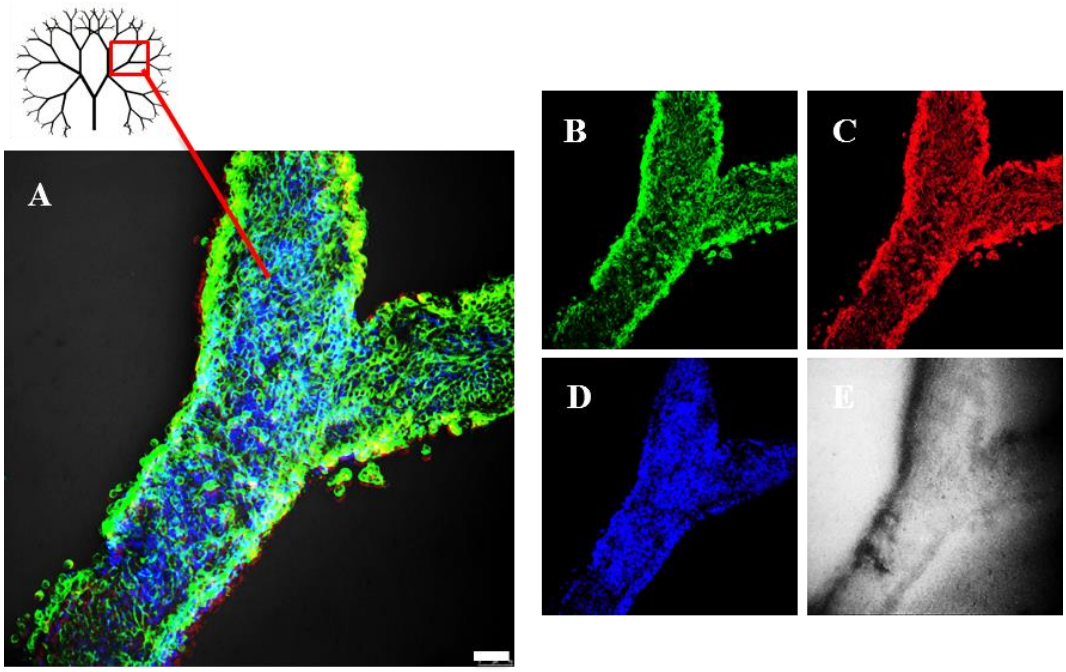

Figure 29. Confocal micrographs of HUVEC cultured on ColMA modified HAMA hydrogel membrane on day 10 (in angiogenic EGM-2 medium). Micrographs show (A) merged, (B) CD31, (C) actin, (D) nucleus, (E) light reflection images of HUVEC in microchannel of hydrogel. Alexa Fluor 488 anti-human CD31 (green) for CD31, Alexa Fluor® 532- Phalloidin for actin (red) and DRAQ5 (blue) for nucleus. Scale bar: 75 µm. Cell seeding density: 2×10^4.

Fig. 30 also shows confocal micrographs from a small section of pattern filled with HUVEC. Fig. 30A, B and C represents CD31, actin and nucleus staining on day 10, respectively. Z-stack images of the channel (Fig. 30D and E) demonstrated the formation of tube-like structure since z-stacked images appear like a hollow circle. Occasionally, incomplete tubular formation was also observed in microchannel and the lumen of vascular-like structure could be differentiated clearly (Fig. 30 F, G).

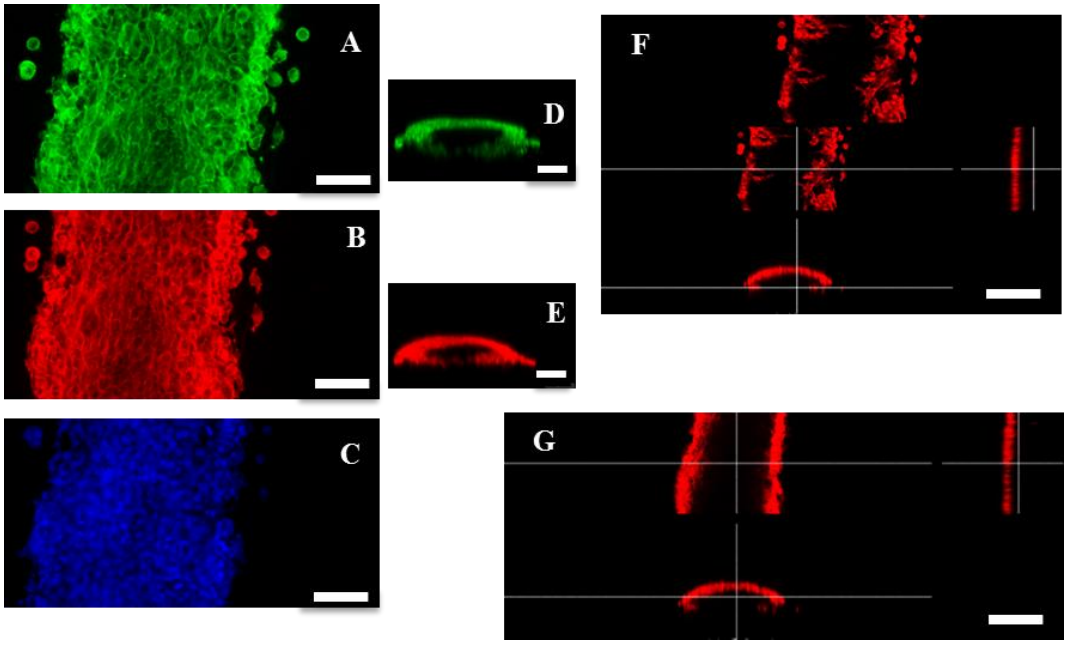

Figure 30. Confocal micrographs of HUVEC cultured on ColMA modified HAMA hydrogel on Day 10. (A) CD31, (B) actin, (C) nucleus staining of HUVEC in the microchannel, (D, E) z stack of HUVEC in microchannel (F) confocal image of HUVEC with incomplete tubular formation, (G) confocal images of lumen of the tubular structure. Alexa Fluor® 488 anti-human CD31 Antibody (green) for CD31, Alexa Fluor® 532- Phalloidin for actin (red) and DRAQ5 (blue) for nucleus. Scale bar: 75 µm. Cell seeding density: 2×10^4.

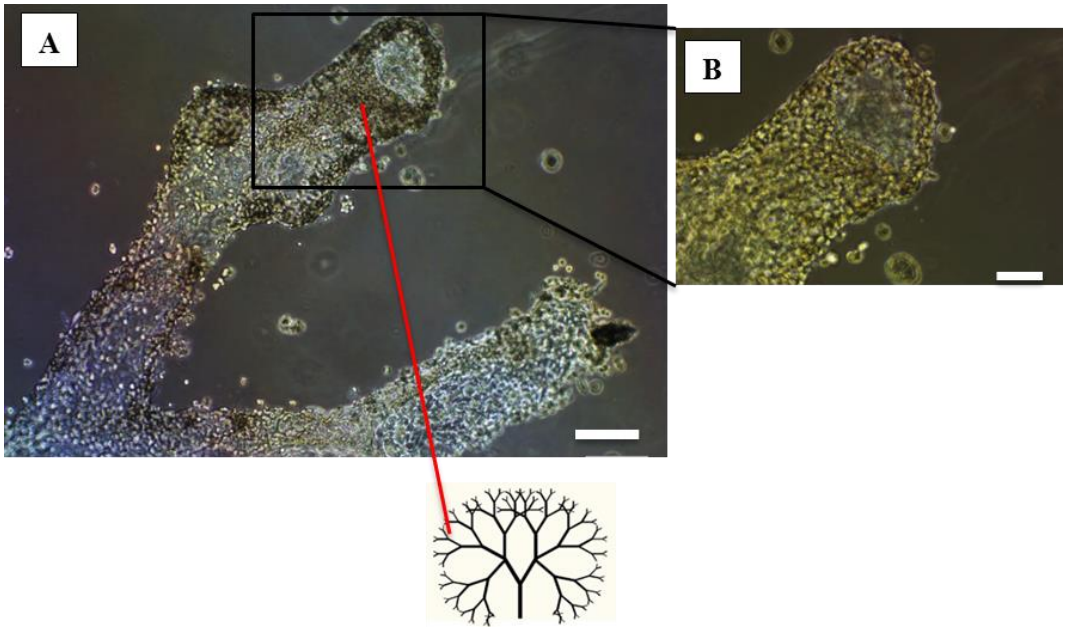

Figure 31. Phase contrast micrographs of HUVEC on ColMA modified HAMA hydrogel on Day 6. Micrographs show HUVECs in the microchannel forming a tubular structure (A, B). Scale bar (A) 200µm and (B) 100 µm. Magnification (A) x40 and (B) x100. Cell seeding density: 2×10^4. Cell cultured in EGM-2 Medium.

Actually, the fundamental aim of the construction of fractal tree-patterned network with cell adhesion factors in hydrogel membrane was to guide HUVECs to form vascular network. By immobilizing cell adhesive compounds in the desired pattern, cells were directed toward tubular formation. In Fig. 31, phase contrast micrographs tube-like formation of HUVEC on ColMA modified HAMA hydrogel were illustrated. On day 6, they began to generate tube-like structures. Since the tip of the branches was narrower than the main body of the pattern, the vascularization started from tips. The formation of 3D tube-like structure was easier for thin microchannels as cells can span only narrow spaces. In the following days, it would be expected that tube formation can progress along the pattern network.

3.3.2.2. Proliferation of HUVEC on ColMA Modified Hydrogel

Cell proliferation of HUVEC adhered on microchannel of HAMA hydrogel was measured by using an indirect method. Phase contrast micrographs of cells on different days were taken and images were processed by using image analysis software (ImageJ). Since HUVEC do not adhere on unmodified HAMA hydrogel, analysis was made only for modified hydrogel. ColMA modified hydrogel was chosen to examine cell proliferation since cells on ColMA modified hydrogels showed consistent and reproducible results. 3 micrographs for specified day of culture were calculated according to the ratio between total area and area used for cells. In this calculation, the cell number was not counted directly, because phase contrast micrographs of 3D cell seeded constructs cannot give the desired image resolution to enable the program to distinguish cell peripheries separately. Consequently, area fraction of cells on hydrogel was measured quantitatively. Fig. 32 shows phase contrast micrographs that were converted to binary image by ImageJ and used to calculate total area of adhered cell on the hydrogel for day 1, 2, 4 and 7. Cell proliferation of HUVEC on ColMA modified hydrogel, which was calculated by using the software measurement, was presented in Fig. 33. Although exact cell number cannot be said for a specific time point, the proliferation profile of cells on the microchannel of hydrogel can be demonstrated. Such as, by this area fraction (AF) comparison the confluence of cell can be determined. With the increase of AF values, the rate of confluency of cell, and so cell number expected to be increased. The AF value was three times higher on day 7 when compared to day 1 and cells reached to confluence at that time point. Based on AF change, there was a little change in the cell covering area on day 4 compared with day 7.

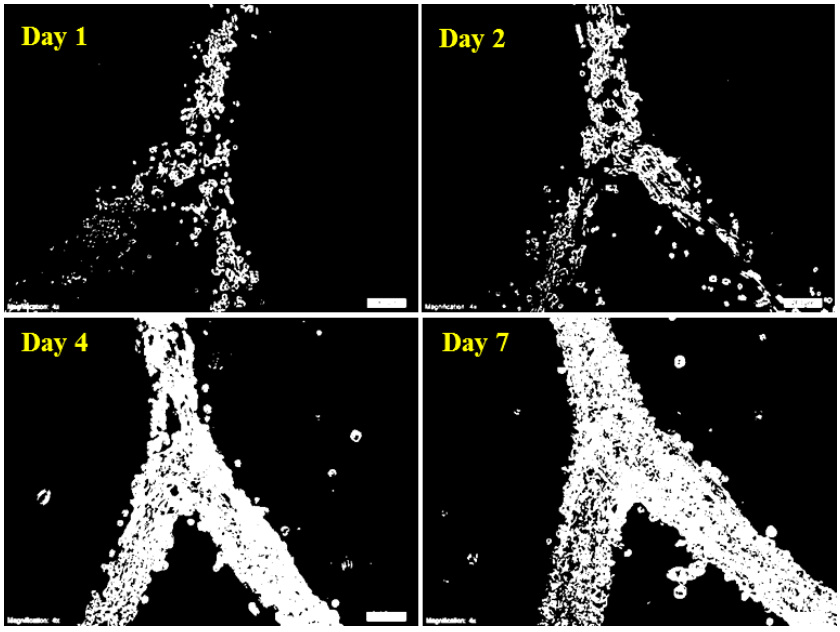

Figure 32. ImageJ software converted binary black and white phase contrast micrograph images of HUVECs that were cultured on ColMA modified HAMA hydrogel membrane.

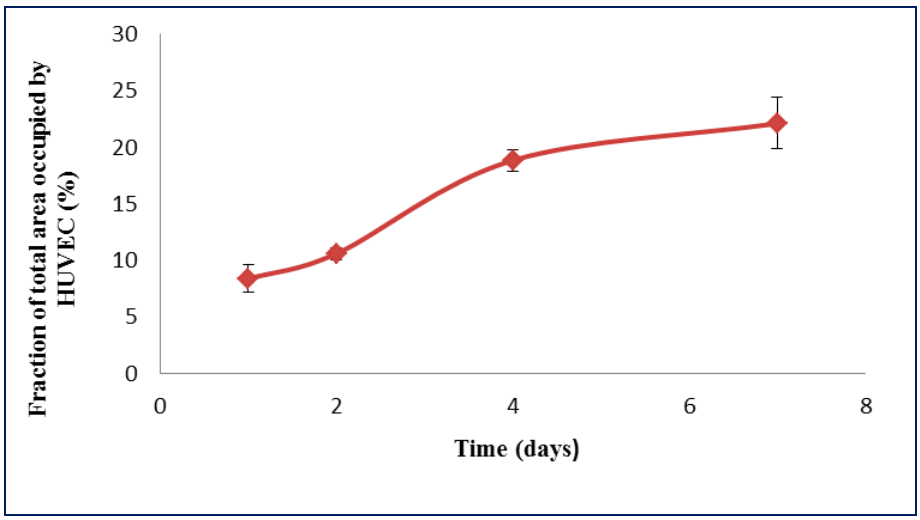

Figure 33. Cell proliferation profile of HUVECs cultured on ColMA modified HAMA hydrogel membrane (n=3). It presents the fraction of the total area covered with cells phase contrast micrographs by using NIH ImageJ.

3.4. Co-Culture with RPE on Bruch's Membrane and HUVEC in the Microchannels

Bilayer culture model was used to mimic the retinal pigment epithelium monolayer on the Bruch's membrane and the capillaries of the choroid generated in the microchannels. In this bilayer model, proliferation, changes in cell morphology and expression of surface markers were studied. HUVEC populated hydrogel was placed at the bottom and on top ESF with RPE cells was placed. For co-culture studies, ColMA surface was chosen because it gave the best cell adhesion and morphology. Before assembly, the layers were separately cultured for 2 days to achieve cell attachment and some proliferation. Analysis was performed with confocal and SEM microscopy. The cell number of HUVEC was determined in an indirect manner by using ImageJ.

3.4.1. Cell Proliferation Estimation by Image Analysis

In the previous method, Area Fraction Output was given as measure of confluence for growing adherent cells. There is also another method that offer approximate cell number from acquired micrographs of cell by using AF method that is measured by ImageJ program (Busschots et al., 2015). In this method, cell number can be determined on a certain area of the image. Confocal micrograph of cell nuclei was used as they are separate from each other and the software can discriminate their perimeters. Cell proliferation of HUVECs in noncontact culture with RPE in ColMA modified hydrogel and singly cultured HUVECs were measured. Fig. 34A was given as an example of confocal micrograph of monoculture of HUVECs nuclei, and it is an original image. Fig. 34B shows a digital image generated after analysis in the ImageJ to count cell from the analysis of original image. Red dots on the image represent the counted cells.

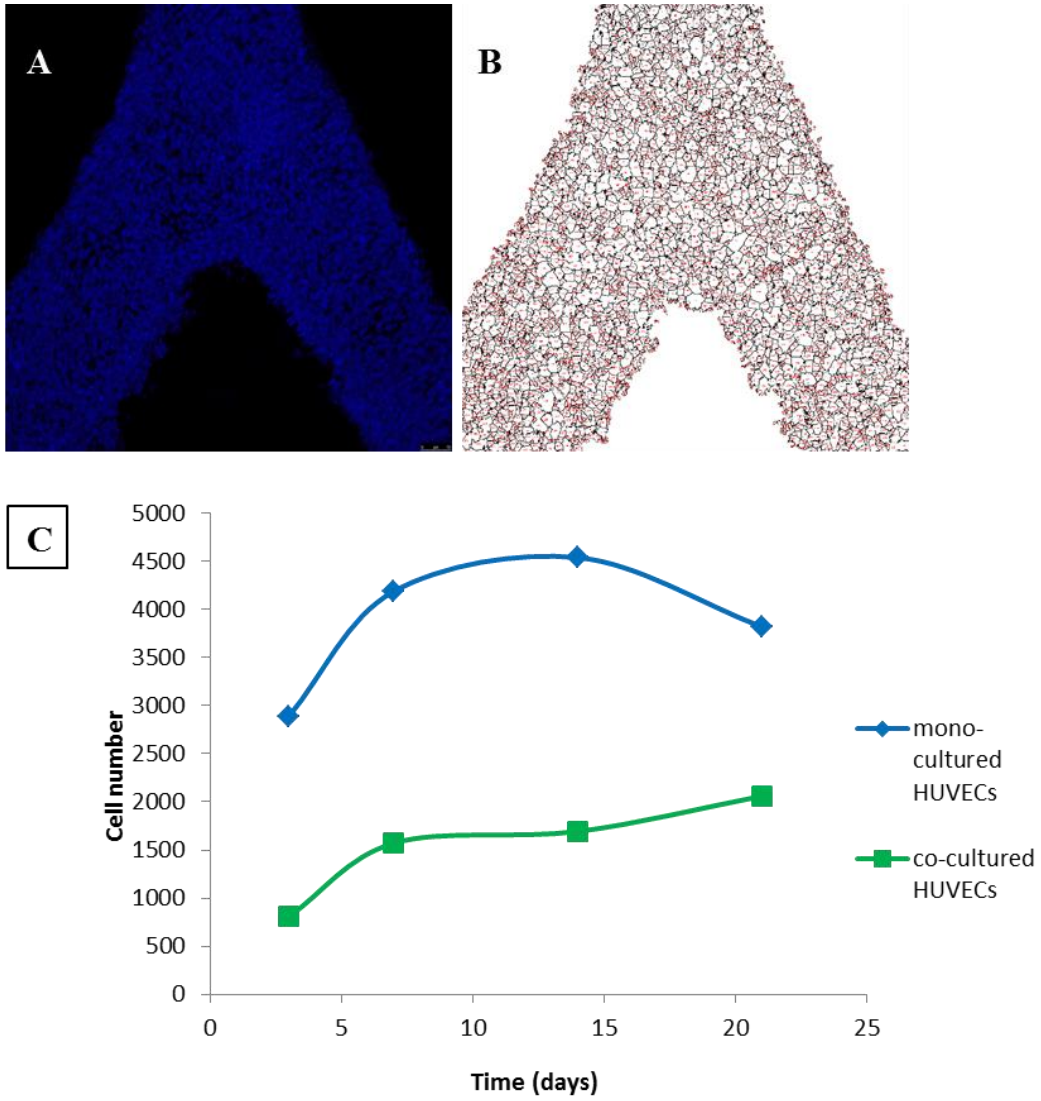

Figure 34. Cell proliferation assessment by using Area Fraction (AF) calculation method (ImageJ program). (A) Original confocal micrograph of HUVEC nuclei on ColMA modified HAMA hydrogel, (B) Image generated after processing with ImageJ to convert the original micrograph to digital image, (C) Proliferation profile of HUVEC monoculture and in co-culture with RPE obtained after image processing.

As seen in the Fig. 34C, monoculture of HUVECs' cell number is more than co-culture of HUVECs with RPE cells on days 3, 7, 14 and 21 despite the same number of cells were seeded at the beginning of the cell culture. Although the cell growth was slower, there was a gradual increase in the number of co-cultured HUVEC cells

during 3 weeks. On the other hand, without co-culture, HUVECs reached confluence on day 14 and then their number decreased until day 21. That result might be due to the contact inhibition of cells which covered all microchannel surface (Fig. 35). Relatively low cell number of co-cultured HUVEC in the channel is explained with the anti-angiogenic effect of RPE cells on HUVEC by cross-talk events through permeable Bruch's membrane.

3.4.2. Immunocytochemistry of Co-cultured Cells

Besides determining cell proliferation, study of cell morphology and cell distribution on the scaffolds is also important to specify the quality of adhesion. The RPE cells and HUVECs were grown in co-culture system for 21 days, which allow bidirectional diffusion of soluble factors while physical interaction was not allowed. To investigate the effect of co-culture, the bilayer components were examined separately. Co-culture studies were performed in culture mediums which can affect growth and morphology of HUVECs and RPE cells. Therefore, EGM-2 medium and DMEM High Glucose was used for HUVEC and RPE cells.

Confocal micrographs of HUVECs on ColMA immobilized HAMA hydrogel are shown in Fig. 35. Both co-cultured (Fig. 35A-C) and mono-cultured HUVECs (Fig. 35D-F) were analyzed with confocal microscopy. Co-culture and mono-culture of the HUVECs were done in EGM-2 Medium. It was not expected to see a morphological difference in the HUVECs due to culture medium composition. Cells were seen to grow on the hydrogel microchannels. There were more cells in microchannels of the mono-culture on both Day 7 and 14 (Fig. 35D, E) than the co-culture of the HUVECs (Fig. 35A, B).

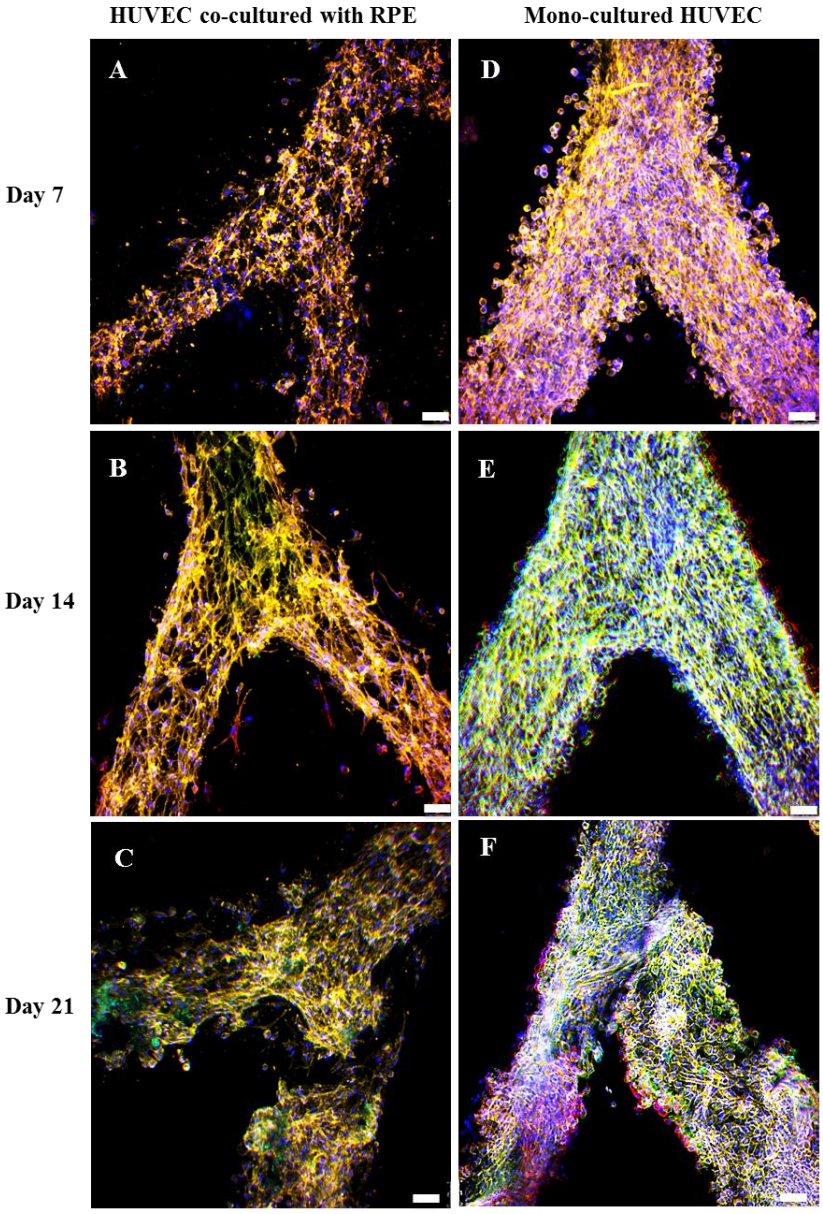

Figure 35. Confocal micrographs of HUVEC on ColMA modified microchannel in HAMA hydrogel membrane in both mono-culture and co-culture. (A, B, C) HUVEC in noncontact co-culture with RPE cells and, (D, E, F) mono-culture of HUVEC on Day 7, 14, 21, respectively. (G) Tube-like structure generated by mono-culture of HUVEC in the ColMA modified microchannel of HAMA hydrogel was shown also as z-stack image. Alexa Fluor® 488 anti-human CD31 Antibody (green) for CD31, Alexa Fluor® 532- Phalloidin for actin (red) and DRAQ5 (blue) for nucleus. Scale bar: 100 µm. Cells were cultured in EGM-2 Medium. Cell seeding density: 3×10^4.

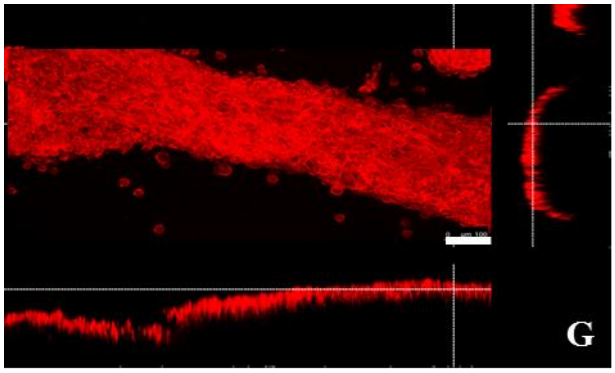

Figure 35. (continued)

Mono-cultured HUVECs filled the whole microchannel spaces while co-cultured counterpart presented non-confluent but homogenously distributed cells on the gel. In addition, mono-cultured HUVEC formed tube-like structures (Fig. 3.23G) whereas co-cultured HUVECs generated incomplete tubular structure. On day 21, organization of HUVEC in both mono-culture and co-culture could not be maintained due to excessive cell growth. At some regions of the tubular structures, detachment of cell sheet was observed. Especially, at the tip of the branches, cell detachment was seen clearly. Hydrogel degradation or release of ColMA at late culture periods could be a reason for this regional cell layer detachment from microchannel.

The decreased cell number and stretched morphology of co-cultured HUVECs was probably due to the anti-angiogenic effects of PEDF (pigment epithelium-derived factor) that may have been secreted by RPE cells. When HUVECs secrete VEGF (vascular endothelial growth factor), an angiogenic agent, RPE secrete the angiogenesis inhibitor PEDF as negative feedback as a control mechanism in the control of angiogenesis in the retina (Tong and Yao, 2006). Wang et al. (2010) studied the antiangiogenic effects of PEDF on angiogenesis of retina in terms of proliferation of endothelial cells and tubular network formation. They co-cultured HUVEC with fibroblasts to create an angiogenesis model to examine number of tubular structure, branching points, and length of tubules. They found that PEDF

decreased the number of tubule formation and branching points and the average length of tubules. Antiangiogenic mechanism of PEDF is unclear, but it was known that PEDF inhibits the endothelial cell migration that is a critical step in the process of angiogenesis (Wang et al., 2010). In addition, antiangiogenic effect of PEDF is selective and it affects newly generating vascular structures while sparing the earlier vessels (Ren et al., 2005).

In the literature, there are also contradicting results about the effects of RPE on vascularization of HUVEC. Dardik et al. constructed the co-culture of Human RPE cells (ARPE-19 cell line) and Human dermal microvascular endothelial cells (ECs) with contact and noncontact approach to study changes in the angiogenic potential of ECs. They showed increased tube formation by ECs on Matrigel in contact co-culture mode with RPE. VEGF levels increased by 36-fold. However, VEGF levels in the noncontact mode did not change at all. In addition, when solo ECs were exposed to hypoxia, 39 fold up regulation was seen in the VEGF level while it did not significantly change the VEGF level in the contact RPE-EC co-culture. Zhang and coworkers (2006) also showed that PEDF inhibited hypoxia-induced increases in VEGF promoter activity at the transcriptional level. Moreover, switching of cell type from RPE to fibroblast and testing in contact mode did not change the VEGF level. This was supported by Dardik et al., 2010, too. Similarly, in our model, when endothelial cells were co-cultured with RPE in noncontact mode no significant vascular-like structures were observed.

Confocal micrographs of co-cultured HUVECs on ColMA modified microchannels were shown in Fig. 36. Inset micrographs show higher magnifications of micrographs to examine the difference between cellular interaction and morphology clearly. On the 3rd day, the cells on the ColMA modified region of hydrogel showed typical flat, cobblestone like shape which elongated and stretched through the microchannel and extending filopodia (Fig. 36A). On day 7, less extended cell morphology was seen when compared with day 3 cell culture (Fig. 36B). It was probably due to antiangiogenic effects of RPE cells on HUVECs. Spindle like shape

of HUVEC was lost and they were showed more round. On day 14 again cell extension through the microchannel were seen (Fig. 36C). 3D cellular interaction was observed in the form of vascular structure. Although the tube-like structures were not formed in all microchannels, 3D organization of cells within the microchannels could be observed. On the 14th day culture, antiangiogenic effect of RPE was not observed since their proliferation decreased after 7 day culture as shown by Fig. 20. Their number decreased dramatically on day 14 implying that secretion of PEDF was decreased. On day 21, cells could not be seen separately; and they organized and completed the tube-like structure (Fig. 36D).

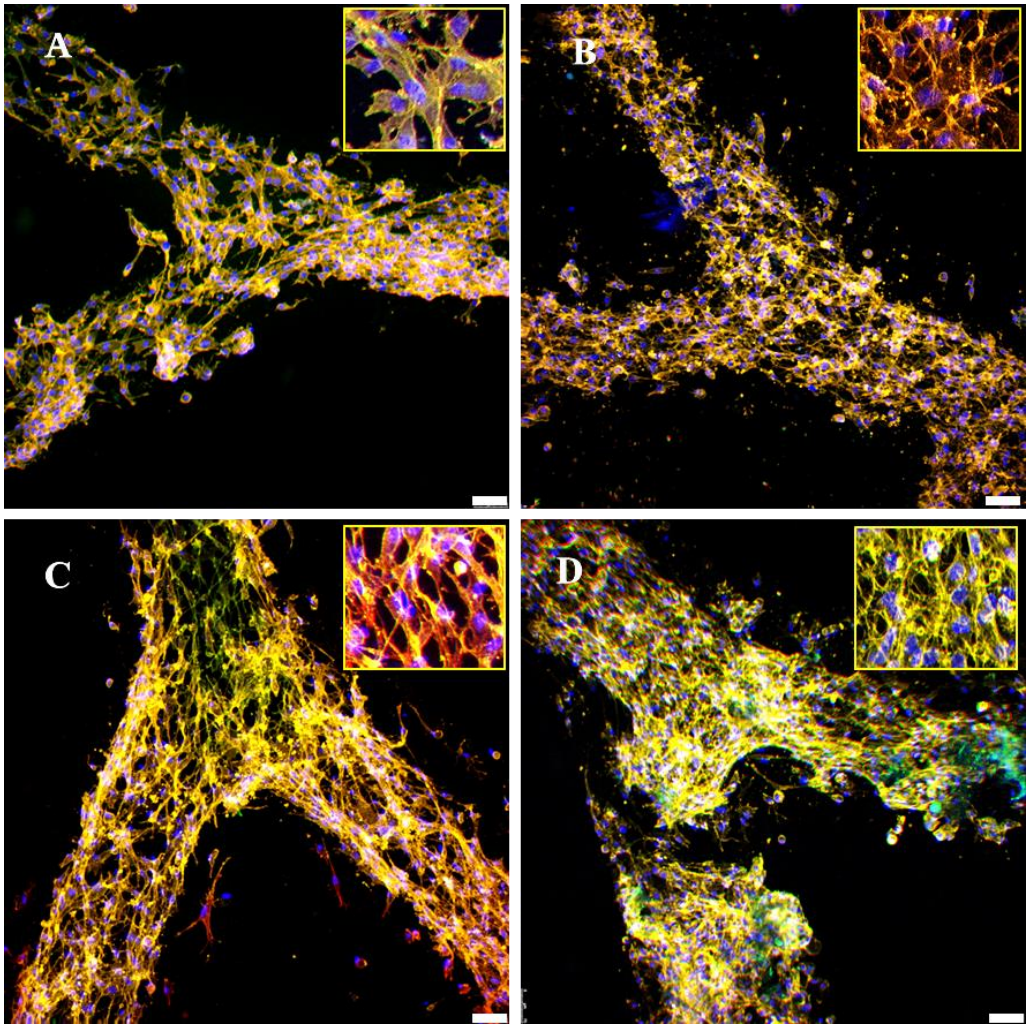

Figure 36. Confocal micrographs of co-cultured HUVECs on ColMA immobilized microchannels in HAMA hydrogel on (A) Day 3, (B) Day 7 (C) Day 14 and (D) Day 21 in EGM-2 medium. x100 (Inset: Higher magnification (x200) images). Alexa Fluor® 488 anti-human CD31 Antibody (green) for CD31, Alexa Fluor® 532-Phalloidin for actin (red) and DRAQ5 (blue) for nucleus. Scale bar: 75 μm. Cell seeding density: 3×10^4.

The effect of culture medium on the morphology and proliferation in the RPE-HUVEC co-culture was studied by using DMEM High and EGM-2 Medium (Fig. 37). HUVECs cultured in EGM-2 were more crowded in the microchannel than those cultured in DMEM. This could be because EGM-2 increases the proliferation rate of these cells with its content of growth factors like hEGF (human endothelial growth

factor), VEGF (vascular endothelial growth factor), hFGF (human fibroblast growth factor) and IGF-1 (insulin-like growth factor). It was also shown in a study that EGM-2 medium was increased proliferation of HUVEC approximately two folds when compared to M199 medium containing 20% FBS and EGF (Bala et al., 2011). In our study, as DMEM medium was not supplemented with growth factors, it was expected to see a higher difference in the proliferation of cells in DMEM and EGM-2 in relation to than between M199 and EGM-2. While cells show spindle-like shape in EGM-2, they resemble like typical cobblestone in DMEM. In general, while cells spread well through the microchannel and showed extensions between them, they preserved their cobblestone shapes in DMEM. Although the spindle like shape of cells in EGM-2 was not clearly seen in Fig. 37A because of confluence, their spindle like morphology can be observed distinctly in Fig. 36C. On the 21st day of culture HUVEC, detachment in tubular like structure was observed (Fig. 37A, B arrows). It was probably due to cell confluence. They started to gradually detach from the surface after two weeks of culture and progressed in the third week of HUVEC mono-culture, which is more crowded than the co-culture.

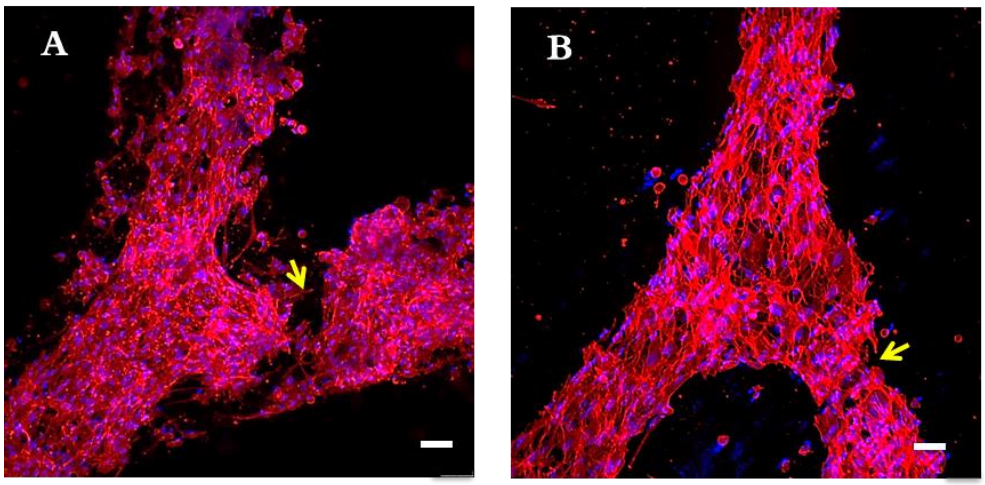

Figure 37. The effects of cell culture medium on the morphology and proliferation of HUVEC co-cultured with RPE. Confocal micrograph of HUVEC cultured in (A) EGM-2 Medium, (B) DMEM High Medium on Day 21. Alexa Fluor® 532-Phalloidin for actin (red) and DRAQ5 (blue) for nucleus. Scale bar: 75 µm. Magnification: x100. Arrows show the crack of tubular structure formed by HUVECs. Cell seeding density: 3×10^4.

Attachment and morphology of the RPE cells co-cultured with HUVEC were also examined with microscopy for the impact of HUVECs on RPE cells (Fig. 38). RPE cells were cultured without or with HUVEC cells in EGM-2 and DMEM-high glucose medium to study the influence of medium composition and co-culture on cell morphology. On Days 3 and 7, cell adhesion and morphologies were similar. In the first week of the culture, no significant differences between the cell numbers were detected. In the literature, there is no known negative effect of HUVECs on RPE cell proliferation but the medium have had an influence. Since the cell culture medium was specific for HUVEC, RPE may not have shown higher cellular activity. On day 14, cell extensions were more apparent and the number of cells was decreased. Decrease in the cell number on day 14 had also been demonstrated previously with Alamar Blue Assay (Fig. 20). On day 21, cell protrusions increased and more cells had spindle-like shape. The morphological change of RPE during culture may be a result of the effect of the medium and co-culture with HUVEC.

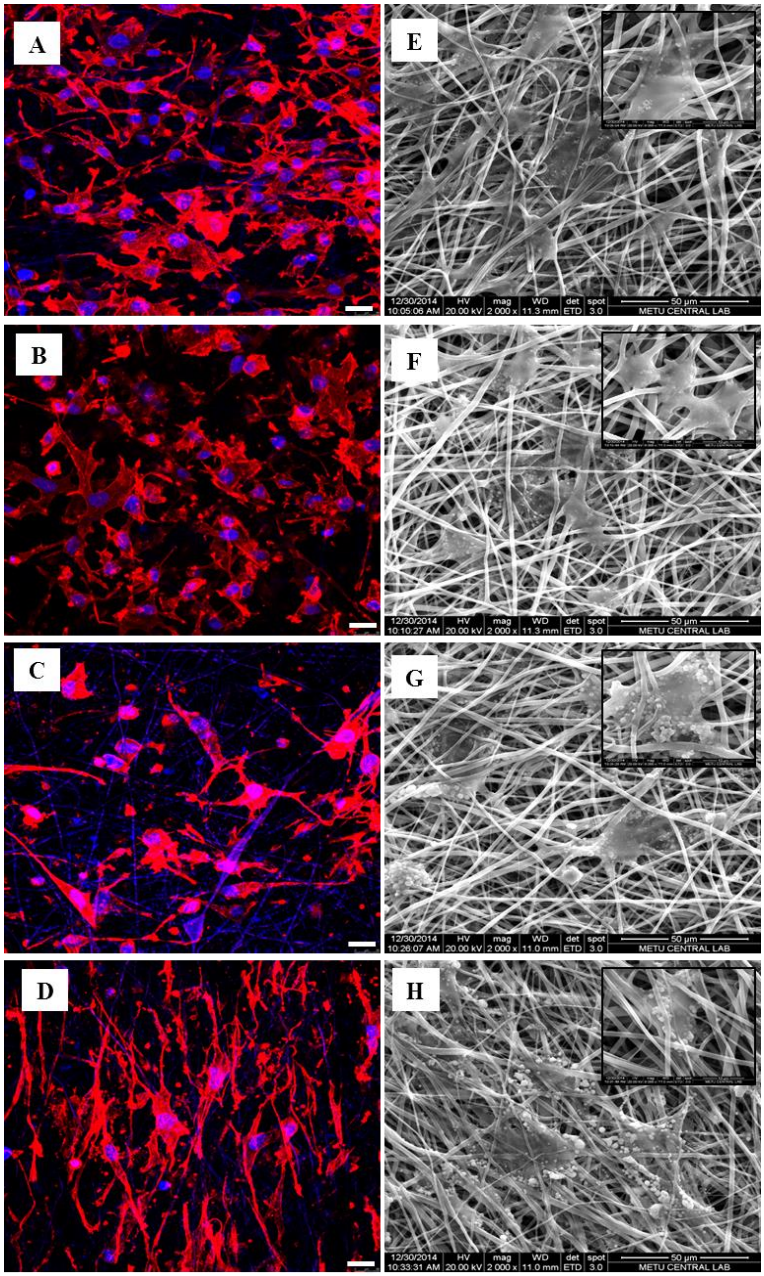

Figure 38. Confocal and SEM micrographs of RPE cells on from co-culture with HUVECs in EGM-2 medium. (A-D) Confocal micrographs and, (E-H) SEM micrographs on Days 3, 7, 14 and 21, respectively. AlexaFluor® 532- Phalloidin was used to stain actin (red) and DRAQ5 for nucleus (blue). Confocal micrographs: scale bar: 25 µm, magnification (x100). SEM micrographs: scale bar: 50 µm, magnification (x2000). Inset: Higher magnification (x8000) of SEM micrographs. RPE seeding density: 3×10^4.

Basically, confocal micrographs of RPE cells co-cultured with HUVEC in DMEM high medium and in EGM-2 Medium and mono-cultured RPE in DMEM high medium on day 21 are shown in Fig. 39. When co-cultured with HUVEC cell, RPE extensions are more distinct in EGM-2 medium compared to the cells that were cultured in DMEM-high glucose medium. On the other hand, there is no apparent cell extension in the mono-culture of RPE that was maintained in DMEM high glucose medium. It is expected that medium composition and co-culturing with HUVEC would have a significant effect on the formation of RPE cell extensions. Since the highest number of RPE extensions was detected when co-cultured with RPE in EGM-2, it can be concluded that EGM-2 somehow promotes cellular extensions. EGM-2 is a medium specific for HUVEC and it promotes vascularization when supplemented with growth factors such as human endothelial growth factor (hEGF), vascular endothelial growth factor (VEGF), human fibroblast growth factor (hFGF) and insulin-like growth factor (IGF-1). In a relevant study, Mitsuda et al. (2005) co-cultured isolated RPE sheet with choroid layer and examined the role of choroid on the transdifferentiation of RPE cells. They separated the two layers with a membrane filter to specify whether RPE-choroid interaction was contact dependent or mediated by soluble agents. They observed that co-cultured RPE cells showed depigmentation, neuritic processes and positive staining for acetylated tubulin. In addition, the number of co-cultured RPE was higher than the mono-cultured as analyzed with BrdU (5-bromo-2V-deoxyuridine) labeling. The results demonstrated that some soluble factors are involved in the RPE-choroid communication. These could be FGF-2 and IGF-1, which are two soluble agents important in the transdifferentiation of RPE because it was reported that the co-administration of FGF-2 and IGF-1 stimulates the proliferation and expression of differentiation marker (acetylated tubulin) of RPE (Mitsuda et al., 2005).

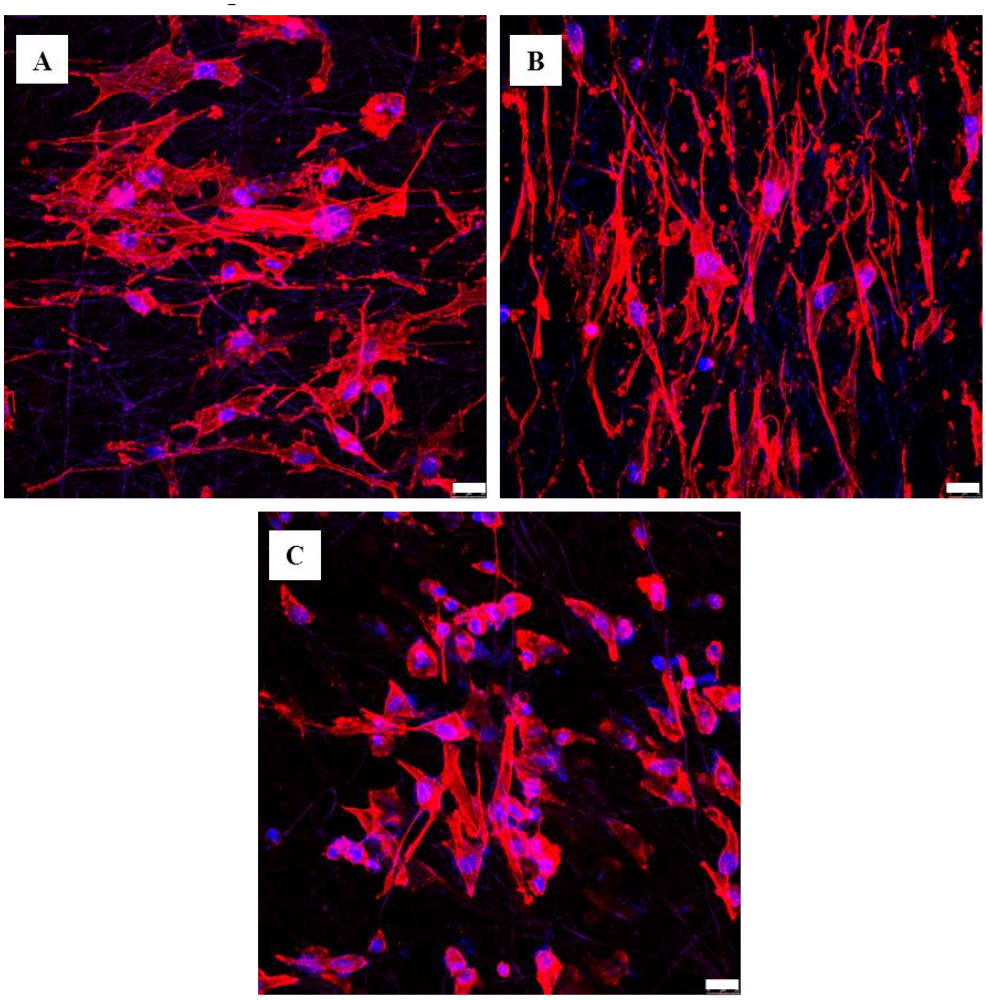

Figure 39. The effects of co-culture and culture medium on the morphology of RPE cells. Confocal micrographs of RPE cells were shown when (A) co-cultured with HUVEC in DMEM high glucose medium, (B) co-cultured with HUVEC in EGM-2 medium and (C) mono-cultured in DMEM high glucose medium on Day 21. Alexa Fluor® 532- Phalloidin for actin (red) and DRAQ5 (blue) for nucleus staining. Scale bar: 25 µm, magnification: x100. Cell seeding density: 3×10^4.

Aspect ratio (AR) of RPEs was measured to determine the differences in cells morphology caused by the co-culture with HUVEC and also by medium composition (Fig. 40). As expected, AR of mono-cultured RPE cells grown in DMEM high medium was lower than the AR determined by co-cultured RPE cells in the same medium. This difference can be explained with the influence of HUVECs on RPE

cells. In addition, the AR of co-cultured RPE cells in DMEM high glucose medium is higher than that observed with co-cultured RPE cells grown in EGM-2 medium. As explained previously, this increase in the AR of RPE can be due to the growth factors in the EGM-2 medium that promoted the formation of long cellular extensions.

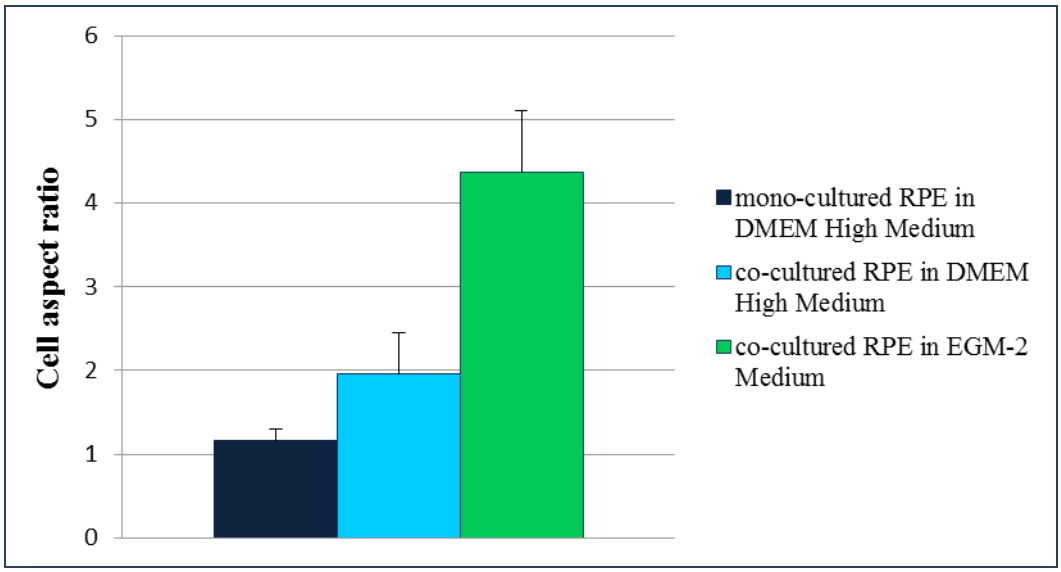

Figure 40. The aspect ratio (AR) of RPE cells as measured at different culture conditions; RPE co-cultured with HUVEC in EGM-2 medium, RPE co-cultured with HUVEC in DMEM-high glucose medium and mono-cultured RPE in DMEM-high glucose medium. AR measured by using image analysis software (ImageJ).

CHAPTER 4

CONCLUSION

In this study, a retinal substitute was constructed by mimicking the Bruch's membrane seeded with RPE and choroid structure of the eye. The Bruch's membrane was created successfully by electrospinning of silk fibroin as a fibrous mat (ESF) Choroid layer was fabricated by micropatterning methacrylated hyaluronic acid (HAMA) hydrogel with a fractal tree pattern and modifying microchannels with methacrylated collagen (ColMA) and methacrylated gelatin to increase cell adhesion and formation of a vascular network. While microchannels in the hydrogel provided a physical cue, modification with ColMA created a chemical cue to guide HUVECs to form tubular structures.

It was shown that ESF supported RPE cell attachment and proliferation. In late culture period RPE cells made a cell layer and cells could show normal physiological function like phagocytosis. HUVEC adhered spatially onto ColMA modified microchannels and could cover microchannel surface. Confocal micrographs showed that HUVECs formed tubular structures in the microchannels of HAMA hydrogel when cultured for sufficiently long periods in the angiogenic medium. Co-culture studies showed that RPE cells adversely affected the proliferation of HUVECs and decreased the formation of the tubular structures. It was deduced that by combining the RPE cell layer on the highly permeable Bruch's membrane and the choroid layer constituted of HUVECs, a retinal substitute could be constructed which has a potential to treat retinal diseases. In addition to application in tissue engineering, this substitute can also be used as an in vitro model system to study various diseases of

the retina and to investigate the effect of drugs and various biomolecules on the RPE and endothelial cells.

REFERENCES

Ahmad, I., Tang, L., & Pham, H. (2000). Identification of neural progenitors in the adult mammalian eye. *Biochemical and Biophysical Research Communications*, *270*(2), 517–21. doi:10.1006/bbrc.2000.2473

Ahsan, H. (2014). Diabetic retinopathy - Biomolecules and multiple pathophysiology. *Diabetes & Metabolic Syndrome*, *9*(1), 51–54. doi:10.1016/j.dsx.2014.09.011

Altman, G. H., Diaz, F., Jakuba, C., Calabro, T., Horan, R. L., Chen, J., Kaplan, D. L. (2003). Silk-based biomaterials. *Biomaterials*, *24*(3), 401–416. doi:10.1016/S0142-9612(02)00353-8

Amemiya, K., Haruta, M., Takahashi, M., Kosaka, M., & Eguchi, G. (2004). Adult human retinal pigment epithelial cells capable of differentiating into neurons. *Biochemical and Biophysical Research Communications*, *316*(1), 1–5. doi:10.1016/j.bbrc.2004.01.172

Atala, A. (2012). Tissue engineering of reproductive tissues and organs. *Fertility and Sterility*, *98*(1), 21–9. doi:10.1016/j.fertnstert.2012.05.038

Bala, K., Ambwani, K., & Gohil, N. K. (2011). Effect of different mitogens and serum concentration on HUVEC morphology and characteristics: implication on use of higher passage cells. *Tissue & Cell*, *43*(4), 216–22. doi:10.1016/j.tice.2011.03.004

Bi, Y.-Y., Feng, D.-F., & Pan, D.-C. (2009). Stem/progenitor cells: a potential source of retina-specific cells for retinal repair. *Neuroscience Research*, *65*(3), 215–21. doi:10.1016/j.neures.2009.07.008

Binder, S., Stanzel, B. V, Krebs, I., & Glittenberg, C. (2007). Transplantation of the RPE in AMD. *Progress in Retinal and Eye Research*, *26*(5), 516–54. doi:10.1016/j.preteyeres.2007.02.002

Bonnel, S., Mohand-Said, S., & Sahel, J.-A. (2003). The aging of the retina. *Experimental Gerontology*, *38*(8), 825–831. doi:10.1016/S0531-5565(03)00093-7

Booij, J. C., Baas, D. C., Beisekeeva, J., Gorgels, T. G. M. F., & Bergen, a a B. (2010). The dynamic nature of Bruch's membrane. *Progress in Retinal and Eye Research*, *29*(1), 1–18. doi:10.1016/j.preteyeres.2009.08.003

Brantley, M. A., & Sternberg, P. (2013). *Retina*. *Retina* (pp. 517–528). Elsevier. doi:10.1016/B978-1-4557-0737-9.00022-9

Bretillon, L., Simon, E., Acar, N., Berdeaux, O., Bron, A., & Creuzot-Garcher, C. (2011). Needs in omega 3 and ocular pathologies. *Oléagineux, Corps Gras, Lipides*, *18*(5), 279–283. doi:10.1051/ocl.2011.0407

Camci-Unal, G., Cuttica, D., Annabi, N., Demarchi, D., & Khademhosseini, A. (2013). Synthesis and characterization of hybrid hyaluronic acid-gelatin hydrogels. *Biomacromolecules*, *14*(4), 1085–92. doi:10.1021/bm3019856

Cao, X., Liu, M., Tuo, J., Shen, D., & Chan, C.-C. (2010). The effects of quercetin in cultured human RPE cells under oxidative stress and in Ccl2/Cx3cr1 double deficient mice. *Experimental Eye Research*, *91*(1), 15–25. doi:10.1016/j.exer.2010.03.016

Chen, H., Fan, X., Xia, J., Chen, P., Zhou, X., Huang, J., Gu, P. (2011). Electrospun chitosan-graft-poly (ε-caprolactone)/poly (ε-caprolactone) nanofibrous scaffolds for retinal tissue engineering. *International Journal of Nanomedicine*, *6*, 453–61. doi:10.2147/IJN.S17057

Chen, K., Zhang, Q., Wang, J., Liu, F., Mi, M., Xu, H., Chen, F., Zeng, K. (2009). Taurine protects transformed rat retinal ganglion cells from hypoxia-induced apoptosis by preventing mitochondrial dysfunction. *Brain Research*, *1279*, 131–8. doi:10.1016/j.brainres.2009.04.054

Chong, N. H. V., Keonin, J., Luthert, P. J., Frennesson, C. I., Weingeist, D. M., Wolf, R. L., Mullin, R. F., Hageman, G. S. (2005). Decreased thickness and integrity of the macular elastic layer of Bruch's membrane correspond to the distribution of lesions associated with age-related macular degeneration. *The American Journal of Pathology*, *166*(1), 241–51. doi:10.1016/S0002-9440(10)62248-1

Collins, M. N., & Birkinshaw, C. (2013). Hyaluronic acid based scaffolds for tissue engineering--a review. *Carbohydrate Polymers*, *92*(2), 1262–79. doi:10.1016/j.carbpol.2012.10.028

Coombes, A. G. A., Rizzi, S. C., Williamson, M., Barralet, J. E., Downes, S., & Wallace, W. A. (2004). Precipitation casting of polycaprolactone for applications in tissue engineering and drug delivery. *Biomaterials*, *25*(2), 315–25.

Coutinho, D. F., Sant, S. V, Shin, H., Oliveira, J. T., Gomes, M. E., Neves, N. M., Reis, R. L. (2010). Modified Gellan Gum hydrogels with tunable physical and mechanical properties. *Biomaterials*, *31*(29), 7494–502. doi:10.1016/j.biomaterials.2010.06.035

Cuenca, N., Fernández-Sánchez, L., Campello, L., Maneu, V., De la Villa, P., Lax, P., & Pinilla, I. (2014). Cellular responses following retinal injuries and therapeutic approaches for neurodegenerative diseases. *Progress in Retinal and Eye Research*, *43*, 17–75. doi:10.1016/j.preteyeres.2014.07.001

Dardik, R., Livnat, T., Nisgav, Y., & Weinberger, D. (2010). Enhancement of angiogenic potential of endothelial cells by contact with retinal pigment epithelial cells in a model simulating pathological conditions. *Investigative Ophthalmology & Visual Science*, *51*(12), 6188–95. doi:10.1167/iovs.09-5095

Deng, C., Li, F., Hackett, J. M., Chaudhry, S. H., Toll, F. N., Toye, B., Griffith, M. (2010). Collagen and glycopolymer based hydrogel for potential corneal application. *Acta Biomaterialia*, *6*(1), 187–94. doi:10.1016/j.actbio.2009.07.027

Falconnet, D., Csucs, G., Grandin, H. M., & Textor, M. (2006). Surface engineering approaches to micropattern surfaces for cell-based assays. *Biomaterials*, *27*(16), 3044–63. doi:10.1016/j.biomaterials.2005.12.024

Froger, N., Cadetti, L., Lorach, H., Martins, J., Bemelmans, A.-P., Dubus, E., Picaud, S. (2012). Taurine provides neuroprotection against retinal ganglion cell degeneration. *PloS One*, *7*(10), e42017. doi:10.1371/journal.pone.0042017

Froger, N., Jammoul, F., Gaucher, D., Cadetti, L., Lorach, H., Degardin, J., Picaud, S. (2013). Taurine is a crucial factor to preserve retinal ganglion cell survival. *Advances in Experimental Medicine and Biology*, *775*, 69–83. doi:10.1007/978-1-4614-6130-2_6

Genasetti, A., Vigetti, D., Viola, M., Karousou, E., Moretto, P., Rizzi, M., Passi, A. (2008). Hyaluronan and human endothelial cell behavior. *Connective Tissue Research*, *49*(3), 120–3. doi:10.1080/03008200802148462

Gregg, R. G., McCall, M. A., & Massey, S. C. (2013). *Retina*. *Retina* (pp. 360–400). Elsevier. doi:10.1016/B978-1-4557-0737-9.00015-1

Gunatillake, P., Mayadunne, R., & Adhikari, R. (2006). Recent developments in biodegradable synthetic polymers. *Biotechnology Annual Review*, *12*, 301–47. doi:10.1016/S1387-2656(06)12009-8

Hamel, C. (2006). Retinitis pigmentosa. *Orphanet Journal of Rare Diseases*, *1*, 40. doi:10.1186/1750-1172-1-40

Hamilton, R. D., Foss, A. J., & Leach, L. (2007). Establishment of a human in vitro model of the outer blood-retinal barrier. *Journal of Anatomy*, *211*(6), 707–16. doi:10.1111/j.1469-7580.2007.00812.x

Harkin, D. G., George, K. A., Madden, P. W., Schwab, I. R., Hutmacher, D. W., & Chirila, T. V. (2011). Silk fibroin in ocular tissue reconstruction. *Biomaterials*, *32*(10), 2445–58. doi:10.1016/j.biomaterials.2010.12.041

Haurigot, V., Villacampa, P., Ribera, A., Bosch, A., Ramos, D., Ruberte, J., & Bosch, F. (2012). Long-term retinal PEDF overexpression prevents neovascularization in a murine adult model of retinopathy. *PloS One*, *7*(7), e41511. doi:10.1371/journal.pone.0041511

Hogan, M. J. (1961). Ultrastructure of the choroid. Its role in the pathogenesis of chorioretinal disease. *Transactions of the Pacific Coast Oto-Ophthalmological Society Annual Meeting*, *42*, 61–87.

Hoon, M., Okawa, H., Della Santina, L., & Wong, R. O. L. (2014). Functional architecture of the retina: Development and disease. *Progress in Retinal and Eye Research*, *42C*, 44–84. doi:10.1016/j.preteyeres.2014.06.003

Hutson, C. B., Nichol, J. W., Aubin, H., Bae, H., Yamanlar, S., Al-Haque, S.,Khademhosseini, A. (2011). Synthesis and characterization of tunable poly(ethylene glycol): gelatin methacrylate composite hydrogels. *Tissue Engineering. Part A*, *17*(13-14), 1713–23. doi:10.1089/ten.TEA.2010.0666

Hynes, S. R., & Lavik, E. B. (2010). A tissue-engineered approach towards retinal repair: scaffolds for cell transplantation to the subretinal space. *Graefe's Archive for Clinical and Experimental Ophthalmology = Albrecht von Graefes Archiv Für Klinische Und Experimentelle Ophthalmologie*, *248*(6), 763–78. doi:10.1007/s00417-009-1263-7

Ito, A., Hibino, E., Kobayashi, C., Terasaki, H., Kagami, H., Ueda, M., Kobayashi, T., Honda, H. (2005). Construction and delivery of tissue-engineered human retinal pigment epithelial cell sheets, using magnetite nanoparticles and magnetic force. *Tissue Engineering*, *11*(3-4), 489–96. doi:10.1089/ten.2005.11.489

Ramírez, J. M., Salazar, J. J., Hoz, R., Rojas, B., Gallego, B. I., Ramírez, A. I., Triviño, A. (2012). *Current Basic and Pathological Approaches to the Function of Muscle Cells and Tissues - From Molecules to Humans*. (H. Sugi, Ed.). InTech. doi:10.5772/3003

Johnsen, E. O., Frøen, R. C., Albert, R., Omdal, B. K., Sarang, Z., Berta, A., Moe, M. C. (2012). Activation of neural progenitor cells in human eyes with proliferative vitreoretinopathy. *Experimental Eye Research*, *98*, 28–36. doi:10.1016/j.exer.2012.03.008

Kane, F. E., Burdan, J., Cutino, A., & Green, K. E. (2008). Iluvien: a new sustained delivery technology for posterior eye disease. *Expert Opinion on Drug Delivery*, *5*(9), 1039–46. doi:10.1517/17425247.5.9.1039

Lai, J.-Y., & Li, Y.-T. (2010). Evaluation of cross-linked gelatin membranes as delivery carriers for retinal sheets. *Materials Science and Engineering: C*, *30*(5), 677–685. doi:10.1016/j.msec.2010.02.024

Lamba, D. A., Gust, J., & Reh, T. A. (2009). Transplantation of human embryonic stem cell-derived photoreceptors restores some visual function in Crx-deficient mice. *Cell Stem Cell*, *4*(1), 73–9. doi:10.1016/j.stem.2008.10.015

Lavik, E. B., Klassen, H., Warfvinge, K., Langer, R., & Young, M. J. (2005). Fabrication of degradable polymer scaffolds to direct the integration and differentiation of retinal progenitors. *Biomaterials*, *26*(16), 3187–96. doi:10.1016/j.biomaterials.2004.08.022

Lawrence, J. M., Singhal, S., Bhatia, B., Keegan, D. J., Reh, T. A., Luthert, P. J., Limb, G. A. (2007). MIO-M1 cells and similar muller glial cell lines derived from adult human retina exhibit neural stem cell characteristics. *Stem Cells (Dayton, Ohio)*, *25*(8), 2033–43. doi:10.1634/stemcells.2006-0724

Leach, J. B., Bivens, K. A., Collins, C. N., & Schmidt, C. E. (2004). Development of photocrosslinkable hyaluronic acid-polyethylene glycol-peptide composite hydrogels for soft tissue engineering. *Journal of Biomedical Materials Research. Part A*, *70*(1), 74–82. doi:10.1002/jbm.a.30063

Lee, C. H., Singla, A., & Lee, Y. (2001). Biomedical applications of collagen. *International Journal of Pharmaceutics*, *221*(1-2), 1–22. doi:10.1016/S0378-5173(01)00691-3

Lei, Y., Gojgini, S., Lam, J., & Segura, T. (2011). The spreading, migration and proliferation of mouse mesenchymal stem cells cultured inside hyaluronic acid hydrogels. *Biomaterials*, *32*(1), 39–47. doi:10.1016/j.biomaterials.2010.08.103

Li, Y., Tao, W., Luo, L., Huang, D., Kauper, K., Stabila, P., Wen, R. (2010). CNTF induces regeneration of cone outer segments in a rat model of retinal degeneration. *PloS One*, *5*(3), e9495. doi:10.1371/journal.pone.0009495

Lin, T.-C., Hsu, C.-C., Chien, K.-H., Hung, K.-H., Peng, C.-H., & Chen, S.-J. (2014). Retinal stem cells and potential cell transplantation treatments. *Journal of the Chinese Medical Association : JCMA*, *77*(11), 556–561. doi:10.1016/j.jcma.2014.08.001

Liu, C., Xia, Z., & Czernuszka, J. T. (2007). Design and Development of Three-Dimensional Scaffolds for Tissue Engineering. *Chemical Engineering Research and Design*, *85*(7), 1051–1064. doi:10.1205/cherd06196

Liu, Z., Yu, N., Holz, F. G., Yang, F., & Stanzel, B. V. (2014). Enhancement of retinal pigment epithelial culture characteristics and subretinal space tolerance of scaffolds with 200 nm fiber topography. *Biomaterials*, *35*(9), 2837–50. doi:10.1016/j.biomaterials.2013.12.069

Lu, J. T., Lee, C. J., Bent, S. F., Fishman, H. A., & Sabelman, E. E. (2007). Thin collagen film scaffolds for retinal epithelial cell culture. *Biomaterials*, *28*(8), 1486–94. doi:10.1016/j.biomaterials.2006.11.023

Mason, C., & Dunnill, P. (2008). A brief definition of regenerative medicine. *Regenerative Medicine*, *3*(1), 1–5. doi:10.2217/17460751.3.1.1

Mitsuda, S., Yoshii, C., Ikegami, Y., & Araki, M. (2005). Tissue interaction between the retinal pigment epithelium and the choroid triggers retinal regeneration of the newt Cynops pyrrhogaster. *Developmental Biology*, *280*(1), 122–32. doi:10.1016/j.ydbio.2005.01.009

Nag, T. C., & Wadhwa, S. (2012). Ultrastructure of the human retina in aging and various pathological states. *Micron (Oxford, England : 1993)*, *43*(7), 759–81. doi:10.1016/j.micron.2012.01.011

Neeley, W. L., Redenti, S., Klassen, H., Tao, S., Desai, T., Young, M. J., & Langer, R. (2008). A microfabricated scaffold for retinal progenitor cell grafting. *Biomaterials*, *29*(4), 418–26. doi:10.1016/j.biomaterials.2007.10.007

Nickla, D. L., & Wallman, J. (2010). The multifunctional choroid. *Progress in Retinal and Eye Research*, *29*(2), 144–68. doi:10.1016/j.preteyeres.2009.12.002

Ozdemir, H., Karacorlu, M., & Karacorlu, S. (2005). Serous macular detachment in central retinal vein occlusion. *Retina (Philadelphia, Pa.)*, *25*(5), 561–3.

Page, W. J., Manchak, J., & Rudy, B. (1992). Formation of poly(hydroxybutyrate-co-hydroxyvalerate) by Azotobacter vinelandii UWD. *Applied and Environmental Microbiology*, *58*(9), 2866–73.

Park, Y. D., Tirelli, N., & Hubbell, J. A. (2003). Photopolymerized hyaluronic acid-based hydrogels and interpenetrating networks. *Biomaterials*, *24*(6), 893–900. doi:10.1016/S0142-9612(02)00420-9

Pearson, R. A. (2014). Advances in repairing the degenerate retina by rod photoreceptor transplantation. *Biotechnology Advances*, *32*(2), 485–91. doi:10.1016/j.biotechadv.2014.01.001

Pikuleva, I. A., & Curcio, C. A. (2014). Cholesterol in the retina: the best is yet to come. *Progress in Retinal and Eye Research*, *41*, 64–89. doi:10.1016/j.preteyeres.2014.03.002

Ramsden, C. M., Powner, M. B., Carr, A.-J. F., Smart, M. J. K., da Cruz, L., & Coffey, P. J. (2013). Stem cells in retinal regeneration: past, present and future. *Development (Cambridge, England)*, *140*(12), 2576–85. doi:10.1242/dev.092270

Redenti, S., Neeley, W. L., Rompani, S., Saigal, S., Yang, J., Klassen, H., Saigal, S., Desai, T., Young, M. J. (2009). Engineering retinal progenitor cell and scrollable poly(glycerol-sebacate) composites for expansion and subretinal transplantation. *Biomaterials*, *30*(20), 3405–14. doi:10.1016/j.biomaterials.2009.02.046

Remington, L. A. (2012). *Clinical Anatomy and Physiology of the Visual System*. *Clinical Anatomy and Physiology of the Visual System* (pp. 233–252). Elsevier. doi:10.1016/B978-1-4377-1926-0.10013-X

Ren, J.-G., Jie, C., & Talbot, C. (2005). How PEDF prevents angiogenesis: a hypothesized pathway. *Medical Hypotheses*, *64*(1), 74–8. doi:10.1016/j.mehy.2004.05.016

Roozafzoon, R., Lashay, A., Vasei, M., Ai, J., Khoshzaban, A., Keshel, S. H., & Bahrami, H. (2014). Dental pulp stem cells differentiation into retinal ganglion-like cells in a three dimensional network. *Biochemical and Biophysical Research Communications*. doi:10.1016/j.bbrc.2014.12.069

Sarks, J., Arnold, J., Ho, I.-V., Sarks, S., & Killingsworth, M. (2011). Evolution of reticular pseudodrusen. *The British Journal of Ophthalmology*, *95*(7), 979–85. doi:10.1136/bjo.2010.194977

Seidlits, S. K., Drinnan, C. T., Petersen, R. R., Shear, J. B., Suggs, L. J., & Schmidt, C. E. (2011). Fibronectin-hyaluronic acid composite hydrogels for three-dimensional endothelial cell culture. *Acta Biomaterialia*, *7*(6), 2401–9. doi:10.1016/j.actbio.2011.03.024

Shadforth, A. M. A., George, K. A., Kwan, A. S., Chirila, T. V, & Harkin, D. G. (2012). The cultivation of human retinal pigment epithelial cells on Bombyx mori silk fibroin. *Biomaterials*, *33*(16), 4110–7. doi:10.1016/j.biomaterials.2012.02.040

Subrizi, A., Hiidenmaa, H., Ilmarinen, T., Nymark, S., Dubruel, P., Uusitalo, H., Skottman, H. (2012). Generation of hESC-derived retinal pigment epithelium on biopolymer coated polyimide membranes. *Biomaterials*, *33*(32), 8047–54. doi:10.1016/j.biomaterials.2012.07.033

Suri, S., & Schmidt, C. E. (2009). Photopatterned collagen-hyaluronic acid interpenetrating polymer network hydrogels. *Acta Biomaterialia*, *5*(7), 2385–97. doi:10.1016/j.actbio.2009.05.004

Susaki, K., & Chiba, C. (2007). MEK mediates in vitro neural transdifferentiation of the adult newt retinal pigment epithelium cells: Is FGF2 an induction factor? *Pigment Cell Research / Sponsored by the European Society for Pigment Cell Research and the International Pigment Cell Society*, *20*(5), 364–79. doi:10.1111/j.1600-0749.2007.00407.x

Tezcaner, A., Bugra, K., & Hasirci, V. (2003). Retinal pigment epithelium cell culture on surface modified poly(hydroxybutyrate-co-hydroxyvalerate) thin films. *Biomaterials*, *24*(25), 4573–83.

Tong, J.-P., & Yao, Y.-F. (2006). Contribution of VEGF and PEDF to choroidal angiogenesis: a need for balanced expressions. *Clinical Biochemistry*, *39*(3), 267–76. doi:10.1016/j.clinbiochem.2005.11.013

Treharne, A. J., Thomson, H. A. J., Grossel, M. C., & Lotery, A. J. (2012). Developing methacrylate-based copolymers as an artificial Bruch's membrane substitute. *Journal of Biomedical Materials Research. Part A*, *100*(9), 2358–64. doi:10.1002/jbm.a.34178

Trese, M., Regatieri, C., & Young, M. (2012). Advances in Retinal Tissue Engineering. *Materials*, 108–120. doi:10.3390/ma4010108

Truskett, V. N., & Watts, M. P. C. (2006). Trends in imprint lithography for biological applications. *Trends in Biotechnology*, *24*(7), 312–7. doi:10.1016/j.tibtech.2006.05.005

Tsujikawa, A., Sakamoto, A., Ota, M., Kotera, Y., Oh, H., Miyamoto, K., Kita, M., Yoshimura, N. (2010). Serous retinal detachment associated with retinal vein occlusion. *American Journal of Ophthalmology*, *149*(2), 291–301.e5. doi:10.1016/j.ajo.2009.09.007

Usuelli, V., & La Rocca, E. (2014). Novel therapeutic approaches for diabetic nephropathy and retinopathy. *Pharmacological Research : The Official Journal of the Italian Pharmacological Society*. doi:10.1016/j.phrs.2014.10.003

Verhulsel, M., Vignes, M., Descroix, S., Malaquin, L., Vignjevic, D. M., & Viovy, J.-L. (2014). A review of microfabrication and hydrogel engineering for micro-organs on chips. *Biomaterials*, *35*(6), 1816–32. doi:10.1016/j.biomaterials.2013.11.021

Voleti, V. B., & Hubschman, J.-P. (2013). Age-related eye disease. *Maturitas*, *75*(1), 29–33. doi:10.1016/j.maturitas.2013.01.018

Wang, B., Atherton, P., Patel, R., Manning, G., & Donnelly, R. (2010). Antiangiogenic effects and transcriptional regulation of pigment epithelium-derived factor in diabetic retinopathy. *Microvascular Research*, *80*(1), 31–6. doi:10.1016/j.mvr.2010.02.012

Wang, Y., Ameer, G. A., Sheppard, B. J., & Langer, R. (2002). A tough biodegradable elastomer. *Nature Biotechnology*, *20*(6), 602–6. doi:10.1038/nbt0602-602

Xiang, P., Wu, K.-C., Zhu, Y., Xiang, L., Li, C., Chen, D.-L.,Jin, Z.-B. (2014). A novel Bruch's membrane-mimetic electrospun substrate scaffold for human retinal pigment epithelium cells. *Biomaterials*, *35*(37), 9777–88. doi:10.1016/j.biomaterials.2014.08.040

Yamaguchi, Y., Otani, T., & Kishi, S. (2006). Serous macular detachment in branch retinal vein occlusion. *Retina (Philadelphia, Pa.)*, *26*(9), 1029–33. doi:10.1097/01.iae.0000254893.94013.16

Yuan, X., Gu, X., Crabb, J. S., Yue, X., Shadrach, K., Hollyfield, J. G., & Crabb, J. W. (2010). Quantitative proteomics: comparison of the macular Bruch membrane/choroid complex from age-related macular degeneration and normal eyes. *Molecular & Cellular Proteomics : MCP*, *9*(6), 1031–46. doi:10.1074/mcp.M900523-MCP200

Zawko, S. A., Suri, S., Truong, Q., & Schmidt, C. E. (2009). Photopatterned anisotropic swelling of dual-crosslinked hyaluronic acid hydrogels. *Acta Biomaterialia*, *5*(1), 14–22. doi:10.1016/j.actbio.2008.09.012

Zhang, H., Li, L.-L., Dai, F.-Y., Zhang, H.-H., Ni, B., Zhou, W., Wu, Y.-Z. (2012). Preparation and characterization of silk fibroin as a biomaterial with potential for drug delivery. *Journal of Translational Medicine*, *10*(1), 117. doi:10.1186/1479-5876-10-117

Zhou, J., Cao, C., Ma, X., & Lin, J. (2010). Electrospinning of silk fibroin and collagen for vascular tissue engineering. *International Journal of Biological Macromolecules*, *47*(4), 514–9. doi:10.1016/j.ijbiomac.2010.07.010

Zweifel, S. A., Spaide, R. F., Curcio, C. A., Malek, G., & Imamura, Y. (2010). Reticular pseudodrusen are subretinal drusenoid deposits. *Ophthalmology*, *117*(2), 303–12.e1. doi:10.1016/j.ophtha.2009.07.014

APPENDIX A

ALAMAR BLUE CALIBRATION CURVE

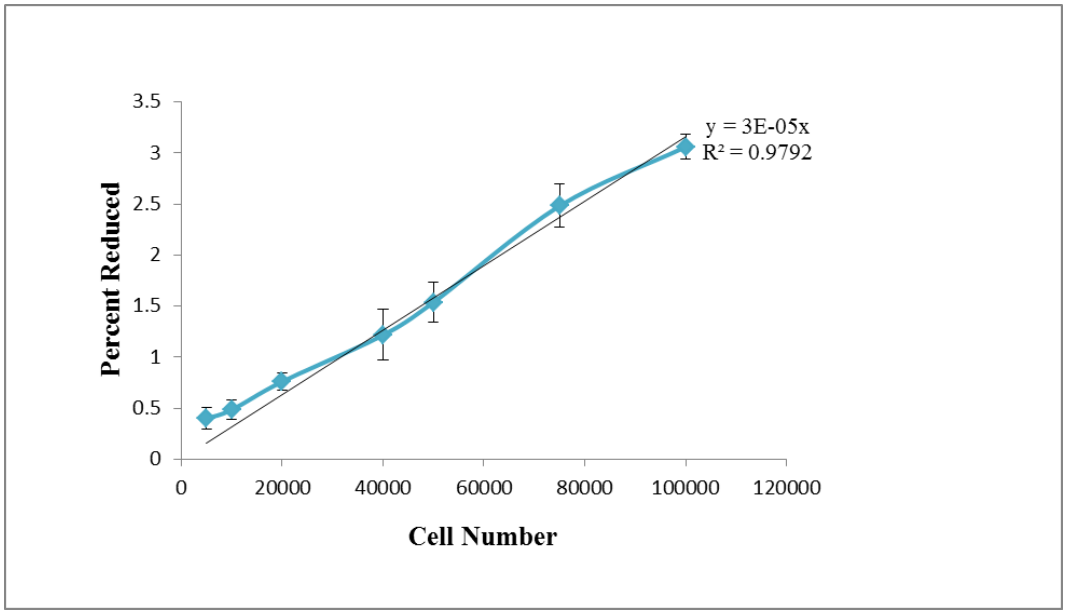

Figure 41. Alamar blue assay calibration curve for D407 cells.